

Investigating structures and optical
properties of monolayer films
prepared from a photo-polymerizable
surfactant in 2D

A Thesis Submitted to the
College of Graduate Studies and Research
In Partial Fulfillment of the Requirements
For the Degree of Doctor of Philosophy
In the Department of Chemistry
University of Saskatchewan
Saskatoon, Saskatchewan

By

Hessamaddin Younesi Araghi

PERMISSION TO USE

In presenting this thesis in partial fulfillment of the requirements for a postgraduate degree from the University of Saskatchewan, I agree that the Libraries of this University may make it freely available for inspection. I further agree that permission for copying of this thesis in any manner, in whole or in part, for scholarly purposes may be granted by the professor or professors who supervised my thesis work or, in their absence, by the Head of the Department or the Dean of the College in which my thesis work was done. It is understood that any copying or publication or use of this thesis or parts thereof for financial gain shall not be allowed without my written permission. It is also understood that due recognition shall be given to me and to the University of Saskatchewan in any scholarly use which may be made of any material in my thesis.

Requests for permission to copy or to make other use of material in this thesis in whole or part should be addressed to:

Head of the Department of Chemistry

University of Saskatchewan

110 Science Place

Saskatoon, Saskatchewan (S7N 5C9)

Abstract

The overall objective of this PhD thesis research is to characterize, understand and ultimately control phase-separated structures in mixed films consisting of a perfluorinated fatty acid and a photopolymerizable surfactant. In these systems, film morphology, mechanical properties and spectroscopic properties are inter-related and this thesis explores these relationships. In this context the interaction between perfluorotetradecanoic acid ($C_{13}F_{27}COOH$, referred to as PF in this dissertation), and 10,12-pentacosadynoic acid ($CH_3(CH_2)_{11}-C\equiv C-C\equiv C-(CH_2)_8COOH$, referred to as PCDA in this dissertation) has been studied in monolayers using a combination of surface and spectroscopic characterization techniques. To investigate the inter-relationship of the properties described above, film behavior under a variety of conditions, including behavior at different interfaces (solid-liquid, air-liquid), different film compositions and under different conditions of photoillumination and mechanical stress were explored.

Thermodynamic and morphological studies of mixed monolayer surfactant films of PF and the photo-polymerizable diacetylene molecule, PCDA, were carried out. The films were prepared at the air-water interface and transferred onto solid supports such as a glass slides via Langmuir-Blodgett (LB) deposition technique. The presence of the perfluoroacid helped to stabilize the diacetylene surfactant monolayer in comparison with the diacetylene alone, allowing film transfer onto solid substrates without needing to add cations to the sub-phase or photo-polymerize the components prior to deposition. Addition of the perfluorocarbon to PCDA resulted in films with the photopolymer strands oriented perpendicular to the direction of the film compression in a Langmuir trough.

This is in contrast with film structures formed from pure PCDA. Formation of these features could be explained by a two-step process that happened sequentially: first, the compression of monolayer with trough barriers while trying to maintain the surface pressure constant induces stress on the film surface; second, additional film buckling which was enhanced by the strong cohesion between PF and PCDA. Film compression data, supported by *in situ* fluorescence spectrophotometry, Brewster angle microscope imaging and atomic force microscope images of deposited films, supported this mechanism. Factors that controlled the orientation of the photopolymer fibers were also investigated. Fibers were found to consist of multiple strands, with each strand having a different orientation. Our investigation also revealed there was a preferred orientation for fibers in the film as a whole. The angle of approximately 60° to the direction of film compression during deposition from a Langmuir trough has been calculated with the help of dual-view, polarized fluorescence microscopy. This orientation was attributed to the mechanical stress exerted by the trough compression barriers coupled with rotation of the polymer fibers during film draining. The combination of Atomic Force Microscope (AFM) and fluorescence microscopy (FM) provided a thorough and comprehensive mapping of fundamental properties of mixed monolayer system, and enabled a quantitative determination of the degree of selectivity of the polymerization process.

ACKNOWLEDGMENTS

I would like to express my deep appreciation to my supervisor Dr. Matthew Paige for his priceless support and encouragement throughout the program. I would also like to thank my committee members, Dr. Ian Burgess, Dr. Steve Reid and Dr. Ildiko Badea for their guidance during my PhD program.

I would like to acknowledge the Department of Chemistry for financial support, the former and the present staff of the Department of Chemistry as well as the members of Dr. Paige's research group.

I am most grateful to my parents, Nasser my father and Azam my mother, and to my brothers, Ehssan, Iman and Mohammad for their support and encouragement throughout the hard times.

Last but not least, all of this wouldn't be possible without my wife support since the beginning of my PhD program. I am so grateful to you, Souzan, my love.

TO LOVE OF MY LIFE SOUZAN

TABLE OF CONTENTS

1. CHAPTER 1: INTRODUCTION	1
1.1 Polydiacetylenes	1
1.1.1 Fluorogenic properties of Polydiacetylenes	2
1.1.2 Polydiacetylene Chemosensors	4
1.2 Interfaces	5
1.2.1 Surface Tension	5
1.3 Langmuir Monolayers	6
1.3.1 Phases of Monolayer Films	7
1.3.2 Mixed Monolayers	9
1.3.3 Langmuir Trough	11
1.3.4 Langmuir-Blodgett Films	13
1.4 Perfluorinated Surfactants	15
1.5 Monolayer Characterization Techniques	16
1.5.1 Brewster Angle Microscopy	17
1.5.2 Atomic Force Microscopy	18
1.6 Research Objectives	21
1.7 References	22
2. CHAPTER 2: DEPOSITION AND PHOTOPOLYMERIZATION OF PHASE- SEPARATED PERFLUOROTETRADECANOIC ACID 10,12-PENTACOSADIYNOIC ACID LANGMUIR BLODGETT MONOLAYER FILMS	29
2.1 Description	29
2.2 Description of Candidate's Contribution	30
2.3 Relation of Contribution to Research Objectives	30
2.4 Reprint of Contribution	31
2.5 Abstract	31

2.6	Introduction	32
2.7	Experimental section	35
	2.7.1 Chemicals	35
	2.7.2 Surface pressure isotherms and Langmuir-Blodgett film preparation.	36
	2.7.3 Atomic force microscope and fluorescence microscope measurements.	37
2.8	Results and Discussion	38
2.9	Conclusions	54
2.10	Acknowledgments	55
2.11	References	55
3.	CHAPTER 3: THE EFFECT OF PERFLUOROTETRADECANOIC ACID ON THE STRUCTURE OF PHOTOPOLYMERIZED 10,12-PENTACOSADIYNOIC ACID FILMS AT THE AIR-WATER INTERFACE	62
3.1	Description	62
3.2	Description of Candidate's Contribution	63
3.3	Relation of Contribution to Research Objectives	63
3.4	Reprint of Contribution	64
3.5	Abstract	64
3.6	Introduction	65
3.7	Experimental section	69
	3.7.1 Chemicals	69
	3.7.2 Surface pressure isotherms and Langmuir-Blodgett film preparation	70
	3.7.3 Atomic force microscope and Brewster angle microscope measurements	71
	3.7.4 In-situ fluorescence spectrophotometry	71
3.8	Results and Discussion	72
3.9	Conclusions	90
3.10	Supporting Information	91
3.11	Acknowledgments	93
3.12	References	93

4. CHAPTER 4: POLARIZED FLUORESCENCE MICROSCOPY OF PATTERNED, POLYMERIZED PERFLUOROTETRADECANOIC ACID – PENTACOSADIYNOIC ACID THIN FILMS	98
4.1 Description	98
4.2 Description of Candidate’s Contribution	99
4.3 Relation of Contribution to Research Objectives	99
4.4 Reprint of Contribution	100
4.5 Abstract	100
4.6 Introduction	101
4.7 Materials and Methods	104
4.7.1 Sample Preparation	104
4.7.2 Polarized fluorescence microscopy	105
4.7.3 Atomic Force and Brewster angle microscope imaging	106
4.7.4 Bulk polarization measurements	107
4.8 Results and Discussion	108
4.9 Conclusions	117
4.10 Acknowledgements	118
4.11 Supplemental Figures	118
4.12 References	118
5. CHAPTER 5: SIMULTANEOUS ATOMIC FORCE MICROSCOPY AND FLUORESCENCE MICROSCOPY IMAGING OF POLYMERIZED PERFLUOROTETRADECANOIC ACID – 10, 12- PENTACOSADIYNOIC ACID LANGMUIR-BLODGETT FILMS	122
5.1 Description	122
5.2 Description of the Candidate’s contribution	123
5.3 Relation of Contribution to Research Objectives	123
5.4 Introduction	124
5.5 Materials and Methods	127

5.5.1	Sample Preparation	127
5.5.2	Instrumentation	128
5.6	Results and Discussion	138
5.7	Conclusions	145
5.8	Acknowledgments	145
5.9	References	146
6.	CHAPTER 6: DISCUSSION, CONCLUSIONS AND FUTURE WORK	151
6.1	Discussion	151
6.2	Future Work	155
6.3	References	157

LIST OF TABLES

Table 2-1. Table showing the total calculated perfluorotetradecanoic acid content (mol%) of the mixed surfactant solutions and the resultant measured percent total surface area occupied by the higher domains as determined by AFM image analysis.	46
Table 3-1. Table of BAM images comparing film structures of 1PF:4PCDA and pure PCDA monolayers as a function of illumination time. Inset BAM images are 520 μm x 380 μm in size. Contrast and brightness in the BAM images was kept fixed throughout the experiment and differences between images are caused by reflectivity differences in the films.	80
Table 5-1. Summary of results collected from photopolymerization of 2:1 PF:PCDA sample with two different light sources.	142

LIST OF FIGURES

Figure 1-1. Photopolymerization of 10, 12 pentacosadiynoic acid.	2
Figure 1-2. Fluorescence emission spectra of PDAs in blue and red phases, excited by 532 nm laser beam.	3
Figure 1-3. Schematic illustration of Gibbs and Langmuir monolayers (adapted from reference ³⁶).	7
Figure 1-4. Schematic illustration of Langmuir monolayer isotherm phases. Surfactants may exhibit some or all phases (adapted from reference ⁴⁰).	8
Figure 1-5. Schematic illustration of a Langmuir trough (adapted from reference ⁴⁵).	13
Figure 1-6. Physical principle of Brewster angle microscopy (adapted from reference ⁴⁰).	18
Figure 1-7. AFM components and working principles.	20
Figure 2-1. Schematic illustration of the photopolymerization of 10,12-pentacosadiynoic acid surfactant monolayer. Photopolymerization proceeds via 1-4 addition of adjacent monomer units to produce the final conjugated polymer product.	34
Figure 2-2. Surface pressure-area isotherms of pure and mixed Langmuir monolayers of PF and PCDA at the air–water interface with a sub-phase temperature of 22 + 1°C. The inset legend describes the PF to PCDA mole ratio.	39
Figure 2-3. Schematic illustration of the syn-periplanar conformation of the PCDA Langmuir monolayer film proposed by Ogawa et al. ³⁶ to occur at a film compression of 28Å ² per molecule.	40

- Figure 2-4. Plot showing mean molecular area as a function of mole fraction of PF for the mixed surfactant films. The dashed lines represent the ideal behavior predicted by the additivity relationship (equation (2.1)) whereas solid lines are included as a guide to the eyes..... 42
- Figure 2-5. AFM height mode image ($10\ \mu\text{m} \times 10\ \mu\text{m}$) and corresponding cross-sectional analysis of a 2:1 PF:PCDA mixed LB film deposited on cover glass using water as a sub-phase. The difference in heights between the smooth continuous domain (light yellow) and the lower domains (dark) was typically $\sim 0.8\text{-}1.0\ \text{nm}$ 43
- Figure 2-6. AFM height mode images ($10\ \mu\text{m} \times 10\ \mu\text{m}$) of 2:1 PF:PCDA mixed films before and after UV light illumination (illumination time ~ 5 minutes, with the lamp mounted $\sim 10\ \text{cm}$ above the film-covered substrate). A cross-sectional analysis of both polymerized and unpolymerized regions of the film is included. 44
- Figure 2-7. AFM height mode image ($2\ \mu\text{m} \times 2\ \mu\text{m}$) of a 2:1 PF:PCDA mixed film after exposure to UV light. The cross-section line crosses three different domains. The height difference between domain ‘A’ and ‘B’ is $\sim 1.8\ \text{nm}$, which is equal to the estimated length of a PF molecule, whereas the height difference between domain ‘B’ and ‘C’ (the photopolymer) is $\sim 5.0\ \text{nm}$, which is equal to the estimated thickness of a polymerized PCDA bilayer..... 48
- Figure 2-8. Schematic illustration of the mixed surfactant film morphology after photopolymerization. The surfactant molecules with the grey head-group are PF molecules, while the molecules with the red head-group are photopolymerized

PCDA molecules. To aid clarity, surfactant have been drawn adsorbed normal to the surface, though under the deposition conditions used here, a slight tilt angle to the normal may occur..... 50

Figure 2-9. Fluorescence emission spectrum of a 2:1 PF:PCDA mixed monolayer on a glass substrate after photopolymerization with a 532 nm, 30 mW laser for ~ 1 minute. 52

Figure 2-10. Fluorescence signal versus illumination time for a 2:1 PF:PCDA monolayer sample deposited on micro cover glass to the 532 nm green laser beam. The illumination intensity at the focal plane was 10 W / cm^2 . The image to the right is a false-color fluorescence image of a typical 2:1 mixed monolayer sample after completion of a photopolymerization experiment. 54

Figure 3-1. π -A compression isotherms for a 1PF:4PCDA mixed monolayer before (blue) and after (red) UV illumination (photopolymerization) on a pure water subphase..... 73

Figure 3-2. Photograph of the experimental apparatus and the air-water interface after ~ 60 minutes of UV illumination. The red PDA photoproduct is readily visible in the image..... 73

Figure 3-3. Plots showing mean molecular area as a function of illumination time at constant surface pressure for 1PF:4PCDA mixed monolayers at various surface pressures and a pure PCDA monolayer (measured at $\pi = 15 \text{ mN/m}$)..... 75

Figure 3-4. Plots showing MMA as a function of time for a 1PF:4PCDA mixed monolayer at the air-water interface. During the initial time period ($t = 0 - 600 \text{ s}$;

data from this region of the curve not shown) the spreading solvent was allowed to evaporate and the film was compressed to the desired pressure ($\pi = 15 \text{ mN/m}$). The black curve corresponds to a control experiment with no illumination, while the red curve corresponds to an experiment in which illumination commenced at $t = 1200 \text{ s}$ (indicated by an arrow). 77

Figure 3-5. A) Expanded view BAM image ($520 \mu\text{m} \times 380 \mu\text{m}$) of mixed film at the air-water interface after ~ 60 minutes of illumination time. The direction of film compression by the trough barriers is indicated by the black arrows. B) A zoom-in section of the image (corresponding region indicated by the red ellipse) has been included for closer inspection..... 82

Figure 3-6. Plot showing integrated fluorescence intensity (red; measured by *in situ* fluorescence spectrophotometry) and mean surface feature height (blue; measured by AFM) versus illumination time for the mixed monolayer at the air-water interface. Solid lines are a guide to the eye. 84

Figure 3-7. AFM height images ($20 \mu\text{m} \times 20 \mu\text{m}$) and corresponding cross sectional analysis for 1PF:4PCDA films deposited at A) $\pi = 5 \text{ mN/m}$; and B) $\pi = 10 \text{ mN/m}$ onto mica substrates after 1500 s of UV photopolymerization..... 87

Figure 3-8. Bulk anisotropy measurements for a mixed, photopolymerized 1PF:4PCDA film deposited onto a glass substrate. The black and red curves correspond to parallel and perpendicular orientation of the analyzer, respectively. 89

Figure 4-1. Schematic illustration of photopolymerization process of 10, 12 pentacosadiynoic acid films, and the resulting photopolymer film structure. 103

- Figure 4-2. Schematic diagram of the dual-view polarized fluorescence microscope (Laser: 532 nm cw diode laser, P1: linear polarizer, B: Berek variable waveplate, P2: linear polarizer (optional) L: focusing lens, D: dichroic mirror, O: objective lens, S: sample, W Wollaston prism, CCD: electron multiplying CCD detector). The orientation of a single emission transition dipole moment (μ) can be described in the x-y reference plane by using the angle ϕ . The y-axis projection of a variety of oriented transition dipoles are shown in green. 106
- Figure 4-3. AFM height mode images of a 2PF:1PCDA mixed surfactant film A) before, and B) after photopolymerization with a 532 nm diode laser. Samples are positioned such that the x-axis is the direction of film compression in the Langmuir trough. 109
- Figure 4-4. Dual-view polarized fluorescence microscope images of various 2PF:1PCDA samples imaged using circularly polarized incident light. Images are 30 μm x 12 μm in size. The top portion of the image is herein referred to as the x-polarization component of the image, and the bottom portion, the y-polarization component. Note the general tendency for the fibers to orient themselves at $\sim 60^\circ$ to the field of view. 110
- Figure 4-5. Polarized fluorescence emission spectra for mixed film after photopolymerization. Spectra were collected with various orientations of the excitation and emission polarizers as detailed in section 4.4.3. 113
- Figure 4-6. BAM images (520 μm x 380 μm) of mixed films at the air-water interface taken at several different surface pressures (A: $\pi = 1 \text{ mN}\cdot\text{m}^{-1}$, B: $8 \text{ mN}\cdot\text{m}^{-1}$, C: 15

mN·m⁻¹) before photopolymerization. The x-axis (long axis) of the images is the direction of film compression. 115

Figure 5-1. Photograph of the combined AFM-fluorescence microscope system; (a) laser diode (532 nm emission), (b) CCD camera, (c) AFM head, (d) microscope objective, (e) focusing lens, (f) neutral density filters, (g) vibration isolation table equipped with an air cushion underneath it. 128

Figure 5-2. Schematic illustration of combined AFM/fluorescence microscope system, Neutral density filters (ND), Lens (L). 130

Figure 5-3. Optical signals measured in the combined microscope. The black curve shows the laser output from the AFM laser diode (signal is cut off because of detector saturation); and the red curve shows the two 550 and 640 nm characteristic fluorescence emission peaks of red-PDA. 132

Figure 5-4. Optical signals in the combined microscope, showing the effect of adding optical filters. The filters that were added were a 540 Long Pass (LP), a 640 Short Pass (SP) and finally a 540-600 band pass filter. This resulted in the blue, black and red curves, cumulatively. 133

Figure 5-5. Images collected using the combined microscope. A) Fluorescence image of standard fluorophore spheres sample, viewed through the microscope eyepiece. Green emission is from the 532 nm excitation laser beam, and the red emission is fluorescence emission of the sample in combination with the scattered laser light from AFM red laser beam. The image was taken with a camera through the microscope eyepiece, and was intended to show the alignment of two lasers light.

Image size is approximately $100\ \mu\text{m} \times 100\ \mu\text{m}$, B) CCD camera perspective of the same sample. The red arrow indicates fluorescence emitted from sample because of the 532 nm laser illumination. For these measurements, the AFM noise canceling box was left open, and the background is due to ambient light. An out-of-focus outline of the triangular AFM cantilever is visible above the glass substrate. Image size is approximately $400\ \mu\text{m} \times 400\ \mu\text{m}$ 134

Figure 5-6. Optical image of USAF test target imaged using ambient light and the CCD detector. The out-of-focus rectangular object in the lower field of view is the AFM probe. Image size is $1000\ \mu\text{m} \times 1000\ \mu\text{m}$. To obtain the final image, the image was rotated 90 degrees clockwise and horizontally inverted (mirror image). 135

Figure 5-7. (A) Atomic force topography image (image size $113\ \mu\text{m} \times 113\ \mu\text{m}$) captured when all the additional equipment was powered off; (B) Atomic force topography image (image size $115\ \mu\text{m}$); (C) optical microscope image (reflected light) with $150\ \mu\text{m} \times 150\ \mu\text{m}$ size, (A) and (C) were collected simultaneously with the combined microscope. 136

Figure 5-8. Standard $1.0\ \mu\text{m}$ diameter fluorescent spheres. (A) AFM deflection image of standard fluorophore; (B) fluorescence image of standard fluorophore ($120\ \mu\text{m} \times 120\ \mu\text{m}$); the 532 nm excitation laser power density used here was $5.0\ \text{mW}\cdot\text{cm}^{-2}$ with 1.0 second integration time. A unique region of the sample has been highlighted in both images as a reference marker. 138

Figure 5-9. AFM image (A) and (B) is the binary image reproduced by ImageJ software from the AFM image (A) for ease of image analysis and (C) is the fluorescence image of 2:1 PF:PCDA film; Laser light $\lambda=532$ nm induced polymerization. (A) and (B) were collected simultaneously with microscopes setup of AFM-FM. .. 140

Scheme 3-1. Schematic illustration of photopolymerization of PCDA..... 66

LIST OF ABBREVIATIONS

AFM: Atomic Force Microscope

BAM: Brewster Angle Microscope

PF: Perfluorotetradecanoic, $C_{13}F_{27}COOH$

κ : Isothermal elasticity

FM : Fluorescence Microscope

C_s : Isothermal compressibility

LB: Langmuir Blodgett

LC: liquid-condensed

LE: liquid-expanded

PCDA: 10,12 Pentacosadiynoic Acid

PDA: Polydiacetylene

1 CHAPTER 1: INTRODUCTION

1.1 Polydiacetylenes

Conjugated polymer-based chemical sensors are an attractive research subject for scientists¹. Various properties of these materials, including their spectroscopic and electrochemical properties, can be altered by environmental stimuli, making them well-suited as signal transducers. Using conjugated polymers in chemical sensors offers the benefit of signal amplification compared to small molecule-based sensors. A variety of conjugated polymers have been investigated as sensing matrices, such as polythiophenes, polyanilines, polypyrroles, polyacetylenes, and polydiacetylenes²⁻⁴.

Polydiacetylene (PDA; monomer unit $R-C\equiv C-C\equiv C-R'$) is particularly well-suited for sensor applications because of the easy preparation of these materials, and its large output signal. PDA-based sensors can provide dual signals through color transitions (blue/red) and fluorescence emission. An example of a PDA monomer, and the one that will be studied in this thesis, is 10,12-pentacosadiynoic acid ($CH_3(CH_2)_{11}-C\equiv C-C\equiv C-(CH_2)_8COOH$, PCDA). Diacetylene molecules can be photopolymerized to produce PDA. Upon irradiation with 254 nm light, diacetylene molecules are polymerized via a 1,4-addition reaction; the result is an alternating ene-yne polymer chain⁵⁻¹¹. (Figure 1-1)

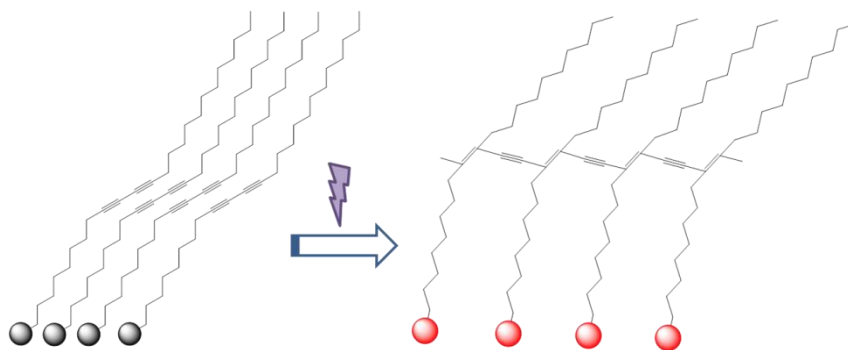


Figure 1-1. Photopolymerization of 10, 12 pentacosadiynoic acid.

The polymerization process needs neither initiators nor catalyst; the polymers are not contaminated with impurities and as a result no further purification process is necessary. Under optimized photochemical conditions the produced PDAs have a strong blue color. Blue PDAs are non-fluorescent. However, PDAs can also form different colors, most notable being the red form. Red PDAs are strongly fluorescent¹²⁻¹⁴. The color change of PDAs from blue to red is a unique property that has given rise to their application in sensors. This color change has been reported in response to heat (thermochromism)¹⁵, mechanical stress (mechanochromism)^{5, 13, 16}, and in response to the binding with various “target” molecules (affinochromism or biochromism)¹⁷⁻²¹. The optical properties of PDAs are discussed in detail in the following section.

1.1.1 Fluorogenic properties of Polydiacetylenes

PDAs undergo a distinctive blue-to-red color change upon stimulation. The importance of this fluorogenic property has been explored from the sensor application point of view²²⁻²⁴. This property has a number of attractive features. The most remarkable one, the generation of a fluorescent signal when PDAs undergo a phase transition from blue to red, is shown in Figure 1-2. The transition of PDAs from a non-fluorescent to a fluorescent form makes them well-suited for biosensing applications. The question why the blue phase of PDAs are non-fluorescent has

not yet been fully answered and understood. Fluorescence in these systems is due to radiative decay from the lowest excited energy level with B_u state^{5, 25} to the ground state, while it has been suggested the blue phase of PDAs have A_g symmetry and emission from its singlet excited state suffer from a dipole-forbidden transition and hence, is essentially non-fluorescent.

A key spectroscopic property of PDAs is the readily detectable fluorescence that arises from mechanically stressed PDA films that have been deposited on solid substrates. A number of conjugated polymers lose fluorescence intensity (quenching) when they are in solid form²⁶. It is concluded that quenching by intermolecular energy or electron transfer processes is not significant in PDAs, although an embedded quencher substitute in the vicinity of the PDA backbone can result in quenching processes²⁷.

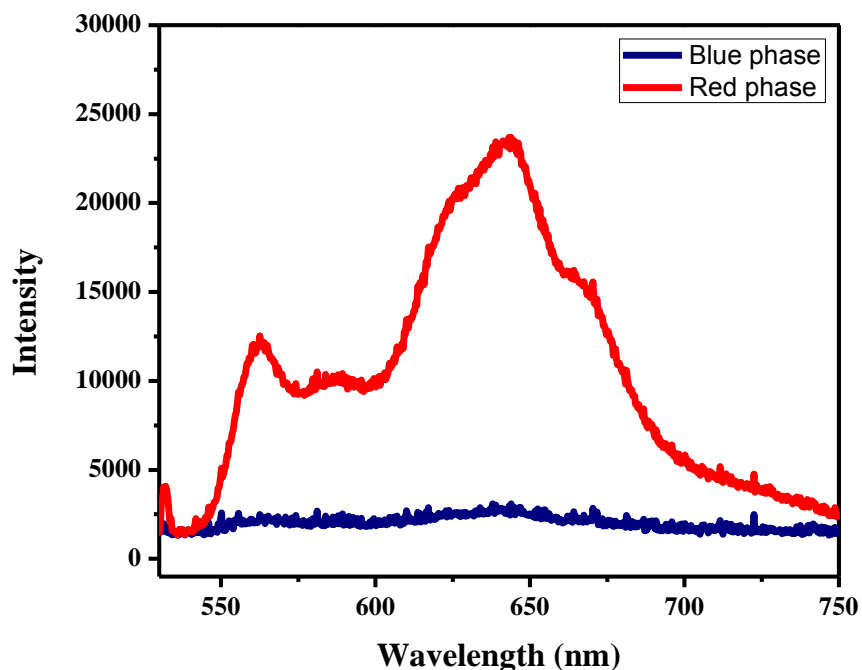


Figure 1-2. Fluorescence emission spectra of PDAs in blue and red phases, excited by 532 nm laser beam.

In terms of quantitative values, the fluorescence quantum yield of the red phase PDAs is reported to be 2×10^{-2} by Olmsted²⁸, while that of the blue-phase is 1×10^{-4} . Because of this, the fluorescence emission from the blue-phase PDAs can be disregarded. The stress-stimulated nonfluorescent-to-fluorescent transition is readily detectable under a fluorescence microscope even though the fluorescence quantum yield of the red PDA is relatively low.

1.1.2 Polydiacetylene Chemosensors

Pioneering works were carried out by Wegner, Ringsdorf, and Charych in the field of PDA sensors. PDAs were first reported by Wegner¹¹. Ringsdorf²⁹ advanced PDA vesicles and film preparation approaches. Charych established that PDAs could function as a sensor for the detection of a variety of target molecules of interest¹⁷. In a remarkably interesting early work, Charych prepared a PDA Langmuir–Blodgett (LB) film, functionalized with sialic acid, and revealed that binding of the influenza virus can stimulate blue-to-red color change in the film¹⁷.

Since the discovery of the influenza virus detection system, a variety of colorimetric PDA-based chemo/biosensors have been investigated. The influenza virus¹⁸, cholera toxin¹⁹, and *Escherichia coli*²⁰ were detected by PDA films and vesicles, functionalized with carbohydrates. Another sophisticated application of PDA-based biosensing is colorimetric detection of glucose³⁰; a PDA monolayer functionalized with hexokinase goes through ligand induced conformational changes. The selective detection of metal ions by embedding an ionophore into a PDA liposome²¹ has been reported. Finally, there is a report on cyclodextrin-induced color changes of PDA vesicles and polymerized diacetylene Langmuir-Schaefer (LS) films³¹. In this system, the terminal anilide moiety-modified PDA film interacted with α -cyclodextrin, causing a color transition which was both time and concentration dependent. Among the cyclodextrins

studied, α -CD had the most noticeable effect, perturbing the ordered structures of the PDA vesicles. PDA vesicles in the presence of α -CD precipitate. It is proved later to be the result of a PDA- α -CD inclusion complex forming.

To incorporate PDAs into chemical sensors as sensing matrices, several techniques such as micropatterning^{24, 32}, micromolding³³, Langmuir-Blodgett (LB) deposition^{5, 17} and of course immobilizing vesicles^{24, 34} has been used. The Langmuir film-based approaches have great versatility and allow controlled preparation of PDA films. In the following section, the basic physical chemical properties of Langmuir and Langmuir Blodgett films will be reviewed.

1.2 Interfaces

Two different phases of matter such as solid/liquid, solid/gas or gas/liquid are separated by a region called an interface. At the interface, because of substantially different potential energy, molecules have different properties than those in the bulk. Due to the tendency of surface active molecules (surfactants) to adsorb to the interface (air/water), it is important to review the properties of liquids at interfaces³⁵.

1.2.1 Surface Tension

Molecules in bulk liquid experience attractive forces that are uniform in all directions. The energy of surface molecules is considerably higher than molecules in the bulk phase because the number of nearest neighbor molecules at the interface is smaller than in the bulk. Consequently, to make a surface (expand a liquid surface), work has to be done. This work is needed to overcome interactions between bulk molecules in order to bring them to the surface. It can be calculated by the following equation³⁵:

$$dw = \gamma \cdot dA \quad (1.1)$$

the amount of work required, dw , to change surface area, dA . The proportionality constant γ is called surface tension.

By adsorbing surfactant molecules to the air/water interface under certain conditions it is possible to minimize the positive free energy associated with the surface molecules. A surfactant consists of two portions, a hydrophobic or water (solvent) repelling part and a hydrophilic or water (solvent) attracting part. The interaction between the surfactants' hydrophobic portion and water (solvent) molecules is unfavorable which drives their adsorption to the interface, thus reducing the free energy of the system.

1.3 Langmuir Monolayers

To form a monolayer of surfactants at the air/water interface, two main approaches are commonly used: 1) the adsorption of water soluble amphiphiles to create a Gibbs monolayer, 2) spreading of insoluble amphiphiles directly to the interface to form a Langmuir monolayer³⁶. Figure 1-3 schematically illustrates the formation of both types of monolayers. Following the discussion in 1.2.1, this accumulation decreases the water surface tension which leads to a new definition named surface pressure (π). Surface pressure is the difference between surface tension of a pure water surface (γ_0) and a monolayer covered surface (γ)³⁷:

$$\pi = \gamma_0 - \gamma \quad (1.2)$$

Gibbs relates the decrease in the surface tension to the amount of surfactant adsorbed from the bulk solution for the adsorption process³⁸. In the Langmuir approach, the surface tension changes are described as a function of area occupied per molecule at the surface. It

means by compressing or expanding the monolayer, surface tension varies. At low film compression, Langmuir monolayers exhibit behavior similar to an ideal, 2D gas. Similar to an ideal gas, the surface pressure increases or decreases as a function of the area per molecule³⁸.

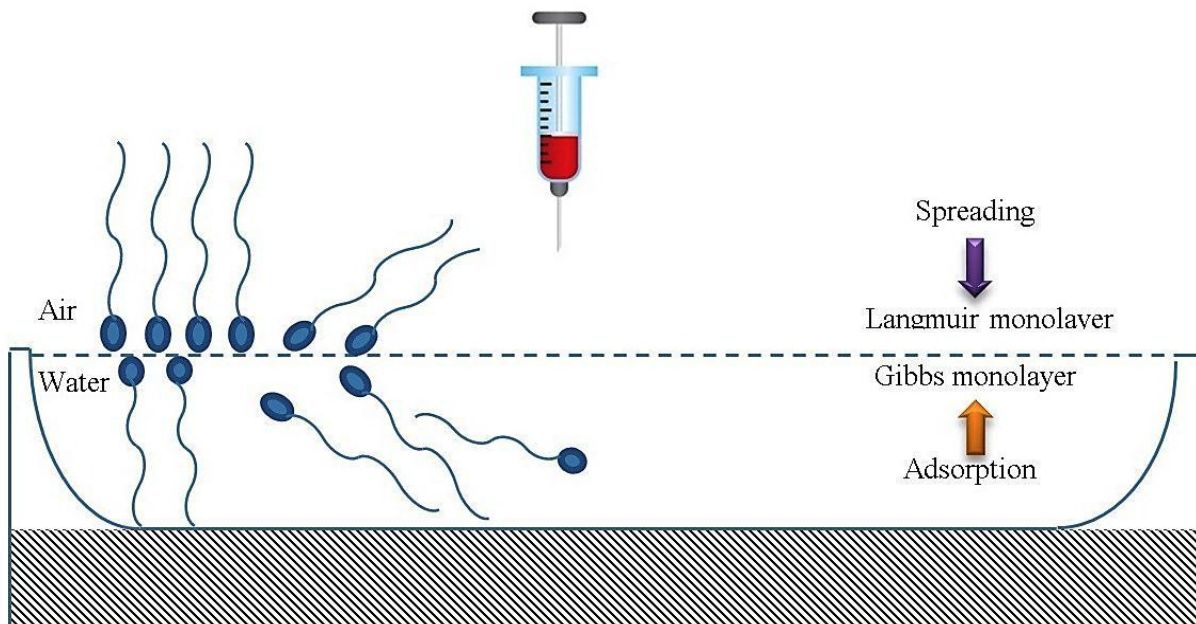


Figure 1-3. Schematic illustration of Gibbs and Langmuir monolayers (adapted from reference³⁶).

1.3.1 Phases of Monolayer Films

At the air/liquid interface, monomolecular insoluble films, often referred to as Langmuir monolayers, provide the opportunity to study interfacial behavior of surfactants under controlled conditions. Plots of surface pressure as a function of the area per molecule at constant temperature are called surface pressure-area isotherms. These plots are one of the most useful and common approaches to characterize monolayer films at the air/liquid interface. The collected information provides useful information about the system's thermodynamic properties³⁹. Figure 1-4 shows a scheme of general surface pressure-mean molecular area isotherm and the

corresponding surfactant film properties in a Langmuir monolayer in different stages of film compression.

Upon changes in surface pressure, monolayer films can exhibit different phases ranging from gaseous, liquid and solid which are analogous to conventional three dimensional systems. The gaseous phase is a result of low packing densities of surfactant molecules at the air/water interface, with an area per molecule in the range of hundreds square angstroms. In the gaseous phase, one can easily conclude that molecules are distant from each other. The molecules can move freely because of the minimal attraction between them^{35, 38}.

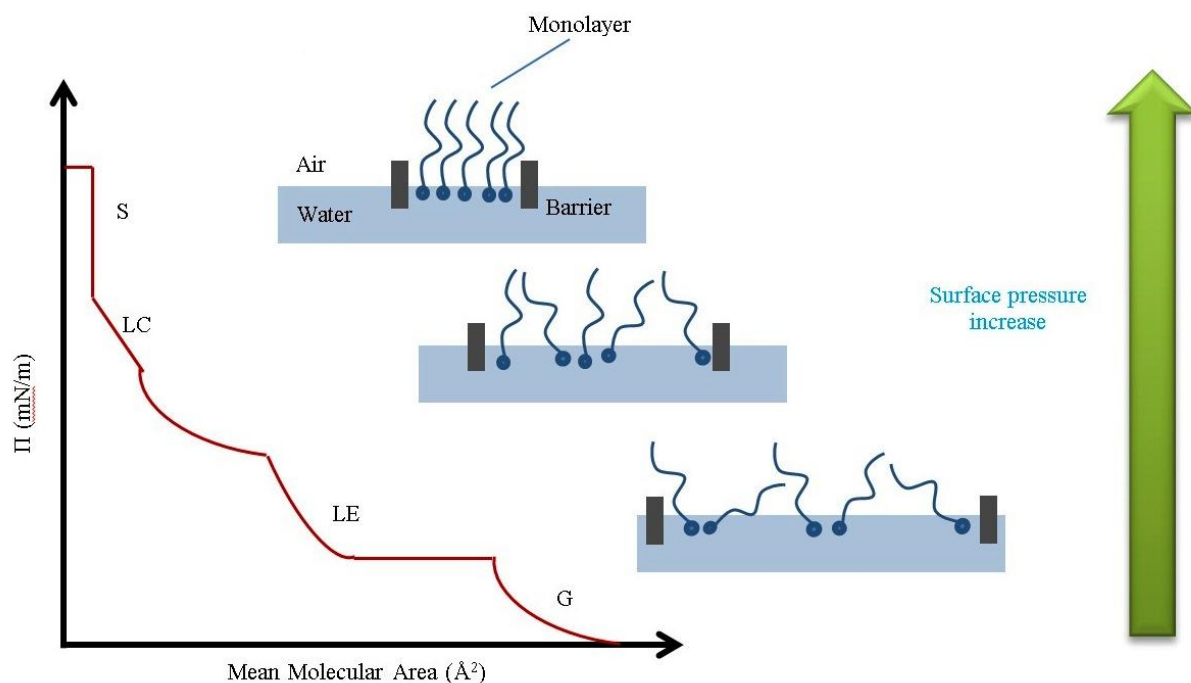


Figure 1-4. Schematic illustration of Langmuir monolayer isotherm phases. Surfactants may exhibit some or all phases (adapted from reference⁴⁰).

Addition of extra surfactant or compressing the monolayer increases the molecular density of the monolayer which will lead to an increase in surface pressure. This often gives rise to the formation of a liquid expanded (LE) phase. Even though the lateral interaction between the amphiphilic molecules in the LE phase is significant, they remain mobile and possess minimal lateral order. The liquid condensed (LC) phase is a result of further compression of the monolayer. It is apparent from the isotherm graph via a plateau (constant pressure) region that indicates the coexistence of two phases. At this point, molecules are more closely packed and exhibit a small tilt angle from the surface normal in comparison to those in the LE phase. As a result of closely packed surfactant molecules, the monolayer becomes less compressible than the LE phase^{35, 38}.

By further compression of the monolayer, the surfactant side chains align themselves normal to the surface and the cavities between the closely packed vertical molecules disappear to form a solid phase. Monolayers in this phase are much less compressible than the LC phase. The cross-sectional area of a molecule can be obtained by extrapolating the mean molecular area of the solid phase to zero surface pressure. This gives the cross-sectional area under close-packed conditions. Increasing the compression further causes the monolayer to collapse (called the collapse pressure^{35, 38}).

1.3.2 Mixed Monolayers

Mixed monolayer systems are useful and important variations of simple, single-component monolayers. The same thermodynamics that are used to describe mixed gases and liquids apply equally well to mixed monolayers. Considering the monolayer comprised of two components A and B, with intermolecular forces between A and B similar to A-A and B-B

molecules interactions, we can presume the mixture to be ideal. The following equation describes the Gibbs energy of mixing of a multicomponent ideal film³⁵:

$$\Delta G_{mix} = RT \sum_{i=1}^N x_i \ln x_i \quad (1.3)$$

where ΔG_{mix} is the Gibbs energy of mixing and x_i is the mole fraction of the i^{th} component. Consequently, the entropy of mixing, ΔS_{mix} is:

$$\Delta S_{mix} = -\left(\frac{\partial \Delta G_{mix}}{\partial T}\right)_{P, N_i} = -R \sum_{i=1}^N x_i \ln x_i \quad (1.4)$$

The enthalpy of mixing, ΔH_{mix} , is zero ($\Delta G = \Delta H - T\Delta S$) as a result of the above equations. This is anticipated for ideal systems where there are no additional interactions between A and B molecules. In conclusion, the spontaneous mixing is driven by the increase in the entropy of the system, because $\ln x_i$ has a negative value, which results in positive ΔS_{mix} for all compositions.

In the case of non-ideal mixtures, different interactions are observed for A-A, B-B and A-B. To address the phenomena from a thermodynamic point of view, thermodynamic excess functions are defined. The excess function is equal to the difference between the observed thermodynamic function of mixing and the function of the ideal system. This is a convenient way to describe the properties of non-ideal mixtures. As a result, calculated positive values of excess Gibbs energy of mixing indicate that the immiscibility of film constituents or are at least partially miscible while negative values supports strong association between the film components^{37, 41}.

Formation of domains with various shapes and sizes seen in phase-separated mixed monolayers are the result of competition between line tension and dipole-dipole interactions between the phase-separated regions^{42, 43}. Line tension is defined as the excess free energy per unit length of a contact line where three distinct phases coexist. Polar repulsions take place between dipole components that are perpendicular to the plane of monolayer. These countering forces minimize overall free energy for a particular system; monolayers tend to reduce the boundary length between isolated domains through formation of compact, often circular domains, which help to decrease high edge energies. This is the opposite result of dipolar repulsion that favors formation of domains particularly with extended shapes^{37, 42}.

1.3.3 Langmuir Trough

The Langmuir trough is a useful tool for measuring properties of insoluble surfactant monolayers at the air/water interface. In addition to measuring compression isotherms, it can also be coupled with other characterization techniques such as Brewster angle microscopy (BAM) and fluorescence microscopy to measure film structure and domain formation at the air/water interface. Figure 1-5 shows a schematic diagram of a typical Langmuir trough. It is constructed of a polytetrafluoroethylene (Teflon) coated trough and two barriers in contact with the top of an aqueous subphase³⁸.

The process for preparing a Langmuir monolayer is dispensing an exact volume of dilute surfactant solution, dissolved in volatile organic solvent or solvent mixtures, with well-known concentration onto the subphase (water) surface. Mean molecular area, the area occupied by each molecule at the surface, is calculated using the following expression³⁸:

$$MMA = \frac{AM}{cN_A V} \quad (1.5)$$

Where MMA is the surfactant mean molecular area, A is trough area, M is surfactant molecular weight, c is surfactant concentration (g/L), N_A is Avogadro's number and V is the volume of surfactant solution that spreads on the liquid surface.

After spreading the solution, the solvent is allowed to evaporate for several minutes, and film compression can be used to control the film area through the movable barrier(s). Applying compression or expansion to the film affects the surface tension (and surface pressure). Changes in surface tension can be measured by a technique called the Wilhelmy electro-balance which is a balance equipped with a Wilhelmy plate (usually made from absorbent paper or platinum) that is in contact with the subphase.

It is important that the Wilhelmy plate is wetted by the subphase to make sure the contact angle between the plate and the water is zero. Roughening the plate helps to overcome this issue. The major benefit of using a Wilhelmy plate for measurement is low cost maintenance and ease of use³⁵. The barriers used to compress or expand the area of the film over the subphase in Langmuir trough are made of hydrophilic or hydrophobic materials. Although hydrophilic barriers prevent the leakage of aqueous subphase and consequently the spread of surfactants beyond the barriers they potentially enable adsorption of the film materials. Hydrophobic (often Teflon) barriers can help to avoid adsorption⁴⁴. These issues need to be considered as they restrict the capability to reach high surface pressure even for a highly compressed monolayer.

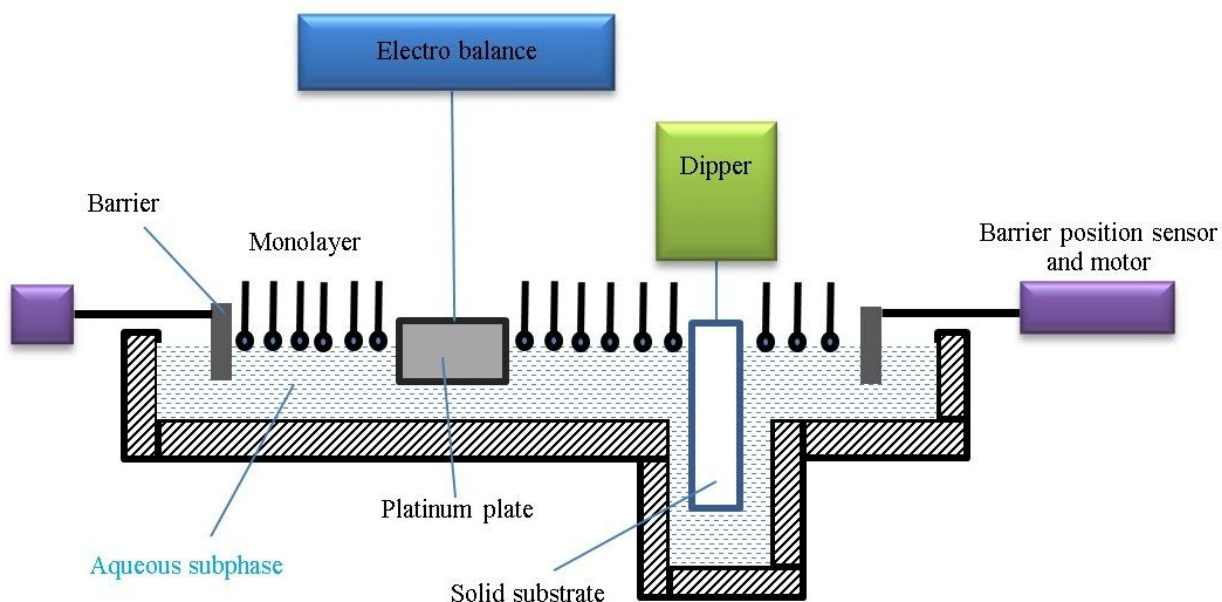


Figure 1-5. Schematic illustration of a Langmuir trough (adapted from reference⁴⁵).

1.3.4 Langmuir-Blodgett Films

It is possible to transfer the Langmuir monolayer to a solid substrate using a technique called Langmuir-Blodgett (LB) deposition. A solid substrate is pulled through the monolayer which transfers it from the air/water interface onto the air/solid interface. For deposition purposes the Langmuir trough comes equipped with a dipping well to provide enough space for the solid substrate below the surface of the aqueous subphase. The deposition procedure starts with preparing the Langmuir film and then compressing it to desired surface pressure, followed by an upward movement of a substrate through the film. Using a hydrophilic substrate results in hydrophilic head groups oriented towards the solid substrate and the tails exposed to the air⁴⁶. A subsequent immersion and emersion of the substrate can be used to deposit multilayers in a head-to-head fashion, known as Y-type films. Upstrokes yield deposited molecules with heads oriented towards the substrate while those deposited on the down stroke orient their tails facing

the substrate³⁸. Depending on substrate hydrophilicity or stroke direction, other configurations such as head-to-tail or tail-to-head structure are possible. The pH and temperature of the subphase may also affect the deposition configuration⁴⁷.

Transfer ratio is a semi-quantitative value to assess the quality of film deposition. This parameter is a ratio of changes in occupied area of the film at constant surface pressure to the area of the substrate which is covered by the monolayer at the end of deposition process. An ideal transfer ratio for a perfect deposition trial would be 1.00. Films deposited with the ratio deviation more than ± 0.05 will be discarded³⁵.

This technique offers easy construction of supported lipid monolayers with a controlled molecular density. Furthermore, the variety of the film characterization techniques with a range of different spatial resolution and mechanism of contrast makes LB films attractive to investigate structure, orientation, domain formation and topography of mixed film systems. Nonetheless, attention must also be paid to ensure that the LB deposition process itself does not change the surfactant film structure, as has been reported for a number of surfactant systems⁴⁸.

A range of solid substrates are available to prepare LB films. Substrate selection is often based upon requirements for subsequent characterization methods. To be specific, most optical techniques demand high optical transparency. Some basic properties which make a good substrate include: 1) optical transparency, 2) flatness, 3) ease of cleaning and 4) doesn't perturb film morphology. In this PhD thesis, microscope cover glass slides have been used to prepare LB films. They are compatible for use with atomic force microscopy and fluorescence microscopy. For most optical measurements in this thesis, glass slides had negligible absorbance above 400

nm. The glass slides were cleaned extensively by a plasma-cleaner to remove production impurities, and results in a negatively charged surface^{37, 38}.

1.4 Perfluorinated Surfactants

The other surfactant which has been used in this thesis is perfluorotetradecanoic acid, $\text{CF}_3\text{-(CF}_2\text{)}_{12}\text{-COOH}$, which plays an important role in mixtures with PCDA. It belongs to the fluorinated surfactant family. These are synthetic amphiphiles and are analogous to hydrogenated surfactants except all the hydrogen atoms of the carbon backbone of the hydrophobic tail have been replaced with fluorine atoms. In comparison with hydrogenated surfactants, these compounds have unique thermal resistance (stability) and are chemically inert. This makes them suitable for multiple applications in material science such as cookware, clothing and firefighting foams⁴⁹.

The large electronegativity and size of the fluorine atom provide fluorinated surfactants with unique properties. A comparison of some basic properties between fluorinated and hydrogenated compounds indicates that fluorinated chains are more bulky than their hydrogenated counterparts. The cross sectional area of fluorinated chain is $27\text{-}30 \text{ \AA}^2$ and $18\text{-}21 \text{ \AA}^2$ for the hydrogenated⁵⁰, which leads to the chain conformation of fluorinated surfactants to be helical rather than zigzag seen in hydrogenated chains. This help to reduce the steric hindrance between the CF_2 groups along the carbon chain. In a simple way, the $\text{CF}_2\text{:CF}_2$ interaction is being reduced by the helical conformation. Moreover, the weaker intermolecular interactions between the fluoroalkyl chains in comparison with aliphatic chains is the result of the lower polarizability of fluorine atoms compared with hydrogens. Altogether this results in

fluorinated surfactants having greater volatility and lower cohesive and surface energies than the analogous hydrocarbon surfactants.

PF was selected because its well-documented tendency to form patterned films when mixed with hydrogenated surfactants⁵¹. Mixing of fluorinated surfactants, particularly perfluorinated (fully fluorinated) surfactants, with hydrocarbon surfactants may yield mixed films that are miscible, partially miscible or fully immiscible. The miscibility/immiscibility of mixed hydrogenated-fluorinated surfactants Langmuir monolayer rises from the reorganization of these surfactants at the air/water interface due to compression⁵². Head group interactions and any factor that may modulate it (pH of subphase⁵³, divalent cation such as Cd^{+2} or even monovalent cation such as Na^+ presence in subphase^{53, 54}) should be carefully explored as the head group interactions play and contribute comprehensively to the overall miscibility of the system⁵⁰.

1.5 Monolayer Characterization Techniques

Throughout this research project, several different surface microscopy techniques, including atomic force microscopy, confocal fluorescence microscopy and Brewster angle microscopy, have been used to study the morphology, composition and molecular organization of mixed lipid monolayers. None of these techniques alone can deliver all of the information required to describe the surfactant system morphology and composition thoroughly. In the following sections, the mechanism of operation, benefits and limitations of these approaches for characterizing mixed films is discussed.

1.5.1 Brewster Angle Microscopy

One of the useful techniques to study Langmuir monolayers at the air/water interface in real-time is Brewster angle microscopy (BAM). It is a technique based on reflectance. Brewster Angle Microscopy uses the fact that when light is directed towards an air/water interface, no reflection of parallel polarized light happens at a certain incident angle. This angle, the Brewster angle, is calculated by Snell's law and is governed by the refractive indices of the two media, according to the following equation⁵⁵:

$$\frac{\sin \theta_1}{\sin \theta_2} = \frac{n_2}{n_1} \quad (1.6)$$

where \sin of angle of incidence θ_1 and angle of refraction θ_2 ratio is inversely related to ratio of n_1 and n_2 the refractive indexes of the media. If $n_2 > n_1$ and light is initially passing through medium 1 (the lower refractive index medium), then the refracted ray, the light travelling within medium 2 (the higher refractive index medium), will bend toward the surface normal. The refraction law shows that the refracted ray and incident ray both lie in the same plane.

Figure 1-6 demonstrates the principles of BAM schematically. The air/water interface on a Langmuir trough is illuminated with parallel polarized light at the Brewster angle ($\sim 53^\circ$), no reflection happens and the surface appears dark. In the presence of a floating object with a refractive index that is different from water (i.e. surfactant film) at the interface, the light will be reflected and an image is produced.

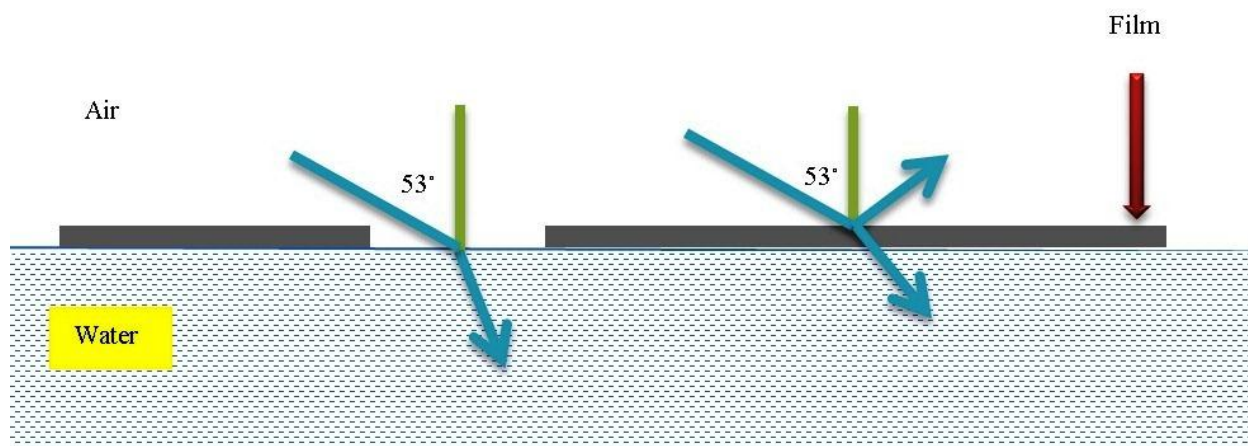


Figure 1-6. Physical principle of Brewster angle microscopy (adapted from reference⁴⁰).

Typically, a Brewster angle microscope and a Langmuir trough are coupled together with a CCD camera. This facilitates capturing images of monolayer film structure at different molecular densities directly at the air-water interface. This method enables monolayer imaging with micrometer spatial resolution. The advantage of using BAM over other methods such as fluorescence microscopy is its response to a wide variety of molecules without the necessity of adding probe molecules to the surfactant film to generate a signal⁴⁰.

1.5.2 Atomic Force Microscopy

Atomic force microscopy (AFM) produces a topographic image of the sample surface. It belongs to the scanning probe microscopy (SPM) microscope family and generates information by measuring interactions between a probe tip and sample surface. It can image numerous types of samples, ranging from soft biological materials to hard surfaces with nanometer scale resolution and provide morphological information about them. This flexibility in AFM makes it well-suited to study LB films⁵⁶.

AFM operates by scanning a sharp tip over the surface of a sample. As a result of tip interaction with surface features, a cantilever deflects which causes displacement in a laser beam reflected off the back of the cantilever. This displacement is associated with surface morphology (Figure 1-7). There are several modes of AFM operation; the two common ones are contact and tapping mode. When the AFM tip is kept in contact with the sample while scanning across the surface, it is called contact mode. In contact mode AFM, a feedback loop that adjusts the z position of the tip helps to maintain the deflection of the cantilever. In tapping mode AFM, the tip doesn't continuously touch the sample while scanning. It "taps" the surface for short time intervals, which is achieved by oscillating the cantilever at its resonance frequency. Tapping mode is much more useful for soft samples to minimize any destruction or dislocation of adsorbed molecules. A complex electronic controller is used to run feedback loops and keep imaging stable.

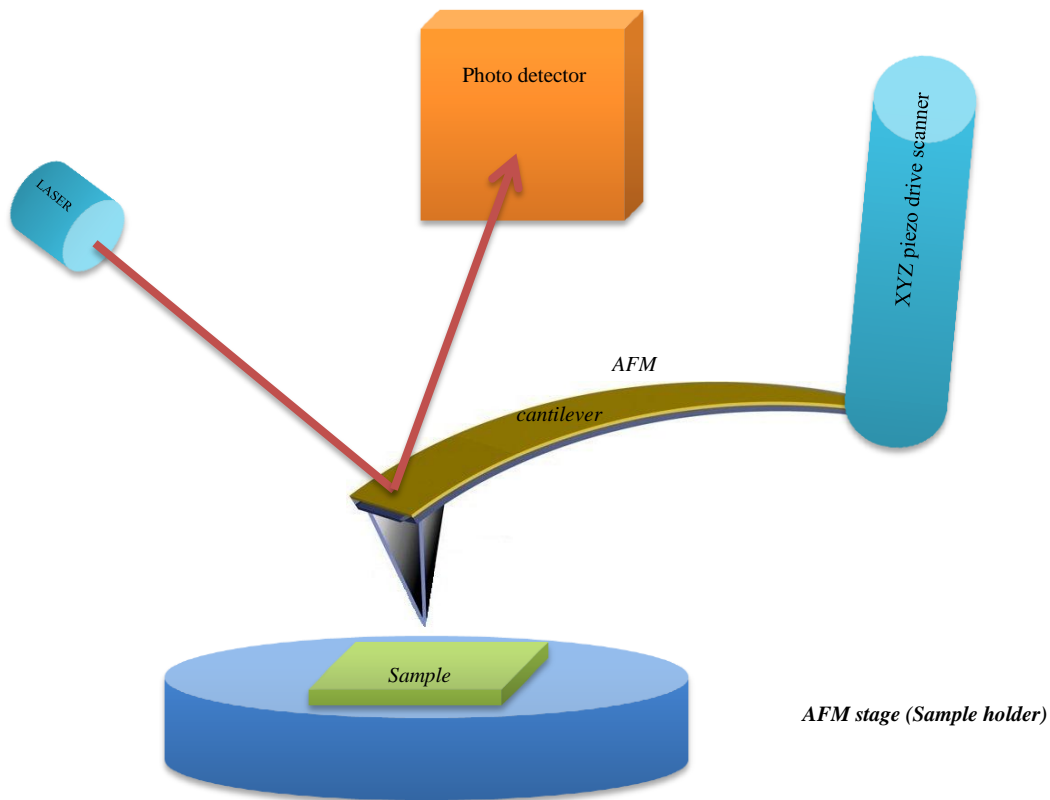


Figure 1-7. AFM components and working principles.

The spatial resolution of AFM imaging is excellent. AFM can obtain lateral resolution of several nanometers and less than a nanometer vertically. These are constrained predominantly by convolution of surface topographies with the tip and by electronic or vibrational noise. However, AFM images fundamentally do not provide chemical information, and combined morphological/compositional imaging with the microscope can be challenging. It is important to note that AFM can only image solid supported samples and as explained, the deposition process and/or solid substrate might distort the monolayer structure during deposition⁵⁶.

1.6 Research Objectives

The ultimate objective of this PhD project is to understand the relationships that exist between structures, mechanical and spectroscopic properties of photopolymers in mixed surfactant films. In this context the interaction between perfluorotetradecanoic acid (PF) and 10,12-pentacosadynoic acid (PCDA), the photopolymerizable surfactant, have been explored in Langmuir monolayers and Langmuir–Blodgett films, with an outlook on controlling film composition, morphology and opto-mechanical properties. As PCDA has shown promising applications as a chemo- and bio-sensor, the knowledge gained in this thesis has significant potential for application in these sensing tools. In order to achieve the overall objectives, the influence of the perfluorinated fatty acid PF on the structure of films of the photopolymerizable surfactant PCDA has been explored at the air-water interface through a combination of surface pressure-area compression measurements and Brewster angle microscopy imaging during polymerization. Next, the spatial orientation of polymer fibers prepared from the photopolymerization of mixed films was investigated by dual-view polarized fluorescence microscopy. Efforts were made to pattern samples of this polymer by taking advantage of miscibility, and as part of trying to pattern samples, an approach for characterizing orientation in these systems was developed. Finally, the possibility that the AFM images were showing both blue and red photopolymerization products were resolved by performing correlated fluorescence – AFM measurements. It has been used to correlate images to try and understand relationships between film structure and fluorescence.

1.7 References

1. Younesi Araghi, H.; Paige, M. F., Deposition and photopolymerization of phase-separated perfluorotetradecanoic acid-10,12-pentacosadiynoic acid Langmuir-Blodgett monolayer films. *Langmuir* **2011**, 27, (17), 10657-10665.
2. Rose, A.; Zhu, Z. G.; Madigan, C. F.; Swager, T. M.; Bulovic, V., Sensitivity gains in chemosensing by lasing action in organic polymers. *Nature* **2005**, 434, (7035), 876-879.
3. Thomas, S. W.; Joly, G. D.; Swager, T. M., Chemical sensors based on amplifying fluorescent conjugated polymers. *Chemical Reviews* **2007**, 107, (4), 1339-1386.
4. Pun, C. C.; Lee, K.; Kim, H. J.; Kim, J., Signal amplifying conjugated polymer-based solid-state DNA sensors. *Macromolecules* **2006**, 39, (22), 7461-7463.
5. Carpick, R. W.; Sasaki, D. Y.; Marcus, M. S.; Eriksson, M. A.; Burns, A. R., Polydiacetylene films: a review of recent investigations into chromogenic transitions and nanomechanical properties. *Journal of Physics: Condensed Matter* **2004**, 16, R679-R697.
6. Mueller, A.; O'Brien, D. F., Supramolecular materials via polymerization of mesophases of hydrated amphiphiles. *Chemical Reviews* **2002**, 102, (3), 727-757.
7. Jelinek, R.; Kolusheva, S., Polymerized lipid vesicles as colorimetric biosensors for biotechnological applications. *Biotechnology Advances* **2001**, 19, (2), 109-118.
8. Okada, S.; Peng, S.; Spevak, W.; Charych, D., Color and chromism of polydiacetylene vesicles. *Accounts of Chemical Research* **1998**, 31, (5), 229-239.
9. Sarkar, A.; Okada, S.; Matsuzawa, H.; Matsuda, H.; Nakanishi, H., Novel polydiacetylenes for optical materials: beyond the conventional polydiacetylenes. *Journal of Materials Chemistry* **2000**, 10, (4), 819-828.

10. Wegner, G., Solid-State Polymerization Mechanisms. *Pure and Applied Chemistry* **1977**, 49, (4), 443-454.
11. Wegner, G., Topochemical Reactions Of Monomers With Conjugated Triple Bonds .6. Topochemical Polymerization Of Monomers With Conjugated Triple Bonds. *Makromolekulare Chemie* **1972**, 154, (NAPR), 35.
12. Baughman, R. H.; Chance, R. R., Comments On Optical-Properties Of Fully Conjugated Polymers - Analogy Between Polyenes And Polydiacetylenes. *Journal of Polymer Science Part B-Polymer Physics* **1976**, 14, (11), 2037-2045.
13. Carpick, R. W.; Sasaki, D. Y.; Burns, A. R., First observation of mechanochromism at the nanometer scale. *Langmuir* **2000**, 16, (3), 1270-1278.
14. Sheth, S. R.; Leckband, D. E., Direct force measurements of polymerization-dependent changes in the properties of diacetylene films. *Langmuir* **1997**, 13, (21), 5652-5662.
15. Ahn, D. J.; Chae, E. H.; Lee, G. S.; Shim, H. Y.; Chang, T. E.; Ahn, K. D.; Kim, J. M., Colorimetric reversibility of polydiacetylene supramolecules having enhanced hydrogen-bonding under thermal and pH stimuli. *Journal of the American Chemical Society* **2003**, 125, (30), 8976-8977.
16. Nallicheri, R. A.; Rubner, M. F., Investigations Of The Mechanochromic Behavior Of Poly(urethane diacetylene) Segmented Copolymers. *Macromolecules* **1991**, 24, (2), 517-525.
17. Charych, D. H.; Nagy, J. O.; Spevak, W.; Bednarski, M. D., Direct Colorimetric Detection Of A Receptor-ligand Interaction By A Polymerized Bilayer Assembly. *Science* **1993**, 261, (5121), 585-588.

18. Reichert, A.; Nagy, J. O.; Spevak, W.; Charych, D., Polydiacetylene Liposomes Functionalized With Sialic-Acid Bind And Colorimetrically Detect Influenza-Virus. *Journal of the American Chemical Society* **1995**, 117, (2), 829-830.
19. Pan, J. J.; Charych, D., Molecular recognition and colorimetric detection of cholera toxin by poly(diacetylene) liposomes incorporating G(m1) ganglioside. *Langmuir* **1997**, 13, (6), 1365-1367.
20. Ma, Z. F.; Li, J. R.; Liu, M. H.; Cao, J.; Zou, Z. Y.; Tu, J.; Jiang, L., Colorimetric detection of Escherichia coli by polydiacetylene vesicles functionalized with glycolipid. *Journal of the American Chemical Society* **1998**, 120, (48), 12678-12679.
21. Kolusheva, S.; Shahal, T.; Jelinek, R., Cation-selective color sensors composed of ionophore-phospholipid-polydiacetylene mixed vesicles. *Journal of the American Chemical Society* **2000**, 122, (5), 776-780.
22. Kolusheva, S.; Molt, O.; Herm, M.; Schrader, T.; Jelinek, R., Selective detection of catecholamines by synthetic receptors embedded in chromatic polydiacetylene vesicles. *Journal of the American Chemical Society* **2005**, 127, (28), 10000-10001.
23. Li, X.; McCarroll, M.; Kohli, P., Modulating Fluorescence Resonance Energy Transfer in Conjugated Liposomes. *Langmuir* **2006**, 22, 8615-8617.
24. Ahn, D. J.; Kim, J. M., Fluorogenic polydiacetylene supramolecules: Immobilization, micropatterning, and application to label-free chemosensors. *Accounts of Chemical Research* **2008**, 41, (7), 805-816.
25. Soos, Z. G.; Galvao, D. S.; Etemad, S., Fluorescence And Excited-State Structure Of Conjugated Polymers. *Advanced Materials* **1994**, 6, (4), 280-287.

26. Friend, R. H.; Gymer, R. W.; Holmes, A. B.; Burroughes, J. H.; Marks, R. N.; Taliani, C.; Bradley, D. D. C.; Dos Santos, D. A.; Bredas, J. L.; Logdlund, M.; Salaneck, W. R., Electroluminescence in conjugated polymers. *Nature* **1999**, 397, (6715), 121-128.
27. Kim, I. B.; Dunkhorst, A.; Bunz, U. H. F., Nonspecific interactions of a carboxylate-substituted PPE with proteins. A cautionary tale for biosensor applications. *Langmuir* **2005**, 21, (17), 7985-7989.
28. Olmsted, J.; Strand, M., Fluorescence Of Polymerized Diacetylene Bilayer Films. *Journal of Physical Chemistry* **1983**, 87, (24), 4790-4792.
29. Ringsdorf, H.; Schlarb, B.; Venzmer, J., Molecular Architecture And Function Of Polymeric Oriented Systems - Models For The Study Of Organization, Surface Recognition, And Dynamics Of Biomembranes. *Angewandte Chemie-International Edition* **1988**, 27, (1), 113-158.
30. Cheng, Q.; Stevens, R. C., Coupling of an induced fit enzyme to polydiacetylene thin films: Colorimetric detection of glucose. *Advanced Materials* **1997**, 9, (6), 481-&.
31. Cho, J. T.; Woo, S. M.; Ahn, D. J.; Ahn, K. D.; Lee, H.; Kim, J. M., Cyclodextrin-induced color changes in polymerized diacetylene Langmuir-Schaefer films. *Chemistry Letters* **2003**, 32, (3), 282-283.
32. Baek, J. H.; Ahn, H.; Yoon, J.; Kim, J.-M., Micro-patterning of polydiacetylene supramolecules using micromolding in capillaries (MIMIC). *Macromolecular Rapid Communications* **2008**, 29, 117-122.
33. Kim, E.; Xia, Y. N.; Whitesides, G. M., Micromolding in capillaries: Applications in materials science. *Journal of the American Chemical Society* **1996**, 118, (24), 5722-5731.

34. Lee, C. H.; Oh, E.-H.; Kim, J.-M.; Ahn, D. J., Immobilization of polydiacetylene vesicles on cellulose acetate butyrate (CAB)-coated substrates for self-assembled supramolecular sensor arrays. *Colloids and Surfaces A: Physicochemical and Engineering Aspects* **2008**, 313, 500-503.
35. Adamson, A. W.; Gast, A. P., *Physical chemistry of surfaces*. 6 ed.; Wiley: New York, 1997.
36. Vollhardt, D.; Fainerman, V. B., Characterisation of phase transition in adsorbed monolayers at the air/water interface. *Advances in Colloid and Interface Science* **2010**, 154, (1-2), 1-19.
37. Israelachvili, J. N., *Intermolecular and Surface Forces, 3rd Edition*. Elsevier Academic Press Inc: San Diego, 2003.
38. Petty, M. C., *Langmuir-Blodgett Films: An Introduction*. Cambridge University Press: Cambridge, 1996.
39. Kaganer, V. M.; Mohwald, H.; Dutta, P., Structure and phase transitions in Langmuir monolayers. *Reviews of Modern Physics* **1999**, 71, (3), 779-819.
40. KSV-NIMA, Biolin Scientific Brewster Angle Microscope. <http://www.ksvnima.com/brewster-angle-microscope> **2014**.
41. Goodrich, F. C., Molecular interaction in mixed monolayers. *Proceedings of the Second International Congress of Surface Activity* **1957**, 1, 85-91.
42. McConnell, H. M., Structures and Transitions in Lipid Monolayers at the Air-Water-Interface. *Annual Review of Physical Chemistry* **1991**, 42, 171-195.
43. Sriram, I.; Schwartz, D. K., Line tension between coexisting phases in monolayers and bilayers of amphiphilic molecules. *Surface Science Reports* **2012**, 67, (6), 143-159.

44. Nakahara, H.; Lee, S.; Sugihara, G.; Shibata, O., Mode of interaction of hydrophobic amphiphilic alpha-helical peptide/dipalmitoylphosphatidylcholine with phosphatidylglycerol or palmitic acid at the air-water interface. *Langmuir* **2006**, 22, (13), 5792-5803.
45. Oliveira Jr, O., Langmuir-Blodgett Films - Properties and Possible Applications. *Brazilian Journal of Physics* **1992**, 22, (2), 60.
46. Matsumoto, M.; Tanaka, M.; Azumi, R.; Manda, E.; Tachibana, H.; Kondo, Y.; Yoshino, N., Component exchange in phase-separated LB films of a long-chain silane-coupling agent mixed with conventional amphiphiles. *Molecular Crystals and Liquid Crystals Science and Technology Section a-Molecular Crystals and Liquid Crystals* **1997**, 294, 31-34.
47. Blodgett, K. B., Films built by depositing successive monomolecular layers on a solid surface. *Journal of the American Chemical Society* **1935**, 57, (1), 1007-1022.
48. Gleiche, M.; Chi, L. F.; Fuchs, H., Nanoscopic channel lattices with controlled anisotropic wetting. *Nature* **2000**, 403, (6766), 173-175.
49. Farn, R. J., *Chemistry and technology of surfactants*. Blackwell Publishing: Oxford, UK, 2006.
50. Krafft, M. P.; Riess, J. G., Chemistry, physical chemistry, and uses of molecular fluorocarbon--hydrocarbon diblocks, triblocks, and related compounds--unique "apolar" components for self-assembled colloid and interface engineering. *Chemical Reviews* **2009**, 109, (5), 1714-1792.
51. Qaqish, S. E.; Paige, M. F., Rippled domain formation in phase-separated mixed Langmuir-Blodgett films. *Langmuir* **2008**, 24, (12), 6146-6153.

52. Nakahara, H.; Lee, S.; Krafft, M. P.; Shibata, O., Fluorocarbon-hybrid pulmonary surfactants for replacement therapy - A Langmuir monolayer study. *Langmuir* **2010**, 26, (23), 18256-18265.
53. Eftaiha, A. F.; Paige, M. F., The influence of salinity on surfactant miscibility in mixed dipalmitoylphosphatidylcholine - perfluorooctadecanoic acid monolayer films. *Journal of Colloid and Interface Science* **2011**, 353, (1), 210-219.
54. Deckert, A. A.; Fallon, L.; Kiernan, L.; Cashin, C.; Perrone, A.; Encalade, T., Kinetics of the Reversible Thermochromism in Langmuir-Blodgett Films of Cd²⁺ Salts of Polydiacetylenes Studied Using UV-Vis Spectroscopy. *Langmuir* **1994**, 10, (6), 1948-1954.
55. Eftaiha, A. F., ; Brunet, S.,; Paige, M. F., Eds Méndez-Vilas, A, A Comparison of Atomic Force Microscopy, Confocal Fluorescence Microscopy and Brewster Angle Microscopy for Characterizing Mixed Monolayer Surfactant Films. *Current Microscopy Contributions to Advances in Science and Technology* **2012**, 2.
56. Binnig, G.; Gerber, C.; Stoll, E.; Albrecht, T. R.; Quate, C. F., Atomic resolution with atomic force microscope. *Europhys. Lett.* **1987**, 3, (12), 1281-6.

2 CHAPTER 2: DEPOSITION AND PHOTOPOLYMERIZATION OF PHASE-SEPARATED PERFLUOROTETRADECANOIC ACID 10,12-PENTACOSADIYNOIC ACID LANGMUIR BLODGETT MONOLAYER FILMS

2.1 Description

This chapter is a copy of a paper published in the journal *Langmuir* [Reproduced with permission from *Langmuir*, **2011**, 27 (17), pp 10657–10665].

In this work, the isotherms of different mixtures of 10,12-pentacosadiynoic acid and perfluorotetradecanoic acid were measured on a pure water subphase at room temperature without any extra salt addition. A stable monolayer was formed which allowed the film to be transferred onto solid substrates for further structural imaging, spectroscopic characterization and polymerization studies. UV polymerization of mixed diacetylene-perfluorocarbon Langmuir-Blodgett monolayer films were carried out at the solid-air interface followed by measurement of the emission spectrum and fluorescent images of the red-phase polymer. The thermodynamics of surfactant miscibility was investigated, and film morphology and spectroscopic characterization of the mixed films was carried out. There was no evidence of blue product formation upon solid phase illumination.

The experimental section for this study is provided in the paper. A detailed overview of the experimental techniques used is provided in Chapter 1.

2.2 Description of Candidate's Contribution

For this contribution, I carried out all experimental measurements, played a major role in interpreting the results, prepared an early draft of the work and participated in the revision of the manuscript upon receiving reviews. Dr. Matthew Paige provided extensive guidance throughout the experimental work and was greatly involved in results interpretation, writing and editing the paper.

2.3 Relation of Contribution to Research Objectives

This contribution was exclusively performed towards the objectives of the thesis research. In this chapter the basic thermodynamic, structural and spectroscopic characterization of mixed monolayers of PCDA – PF was performed. Despite having potential application in biosensors, little is known about the morphology and phase behavior of PCDA in mixed films. Determining these basic physical chemical properties was an important first step in understanding and controlling PCDA behavior in monolayers. Mixing PCDA with PF played the ultimate role of stabilizing the monolayer on the air/water interface. The importance of the perfluorocarbon for monolayer stabilization was also discussed in further detail in the following chapter. A full discussion of the results as part of the whole study is provided in Chapter 6.

2.4 Reprint of Contribution

Deposition and photopolymerization of phase-separated perfluorotetradecanoic acid – 10,12-pentacosadiynoic acid Langmuir-Blodgett monolayer films

Hessamaddin Younesi Araghi and Matthew F. Paige

Department of Chemistry, University of Saskatchewan, 110 Science Place,
Saskatoon, SK. S7N 5C9
Canada

2.5 Abstract

Mixed monolayer surfactant films of perfluorotetradecanoic acid and the photopolymerizable diacetylene molecule 10, 12-pentacosadiynoic acid were prepared at the air-water interface and transferred onto solid supports via Langmuir-Blodgett (LB) deposition. The addition of the perfluoroacid to the diacetylene surfactant results in enhanced stabilization of the monolayer in comparison with the pure diacetylene alone, allowing film transfer onto a solid substrate without resorting to addition of cations in the sub-phase or photopolymerization prior to deposition. The resulting LB films consisted of well-defined phase-separated domains of the two film components, and the films were characterized by a combination of atomic force microscope (AFM) imaging and fluorescence emission microscopy both before and after photopolymerization into the highly emissive “red form” of the polydiacetylene. Photopolymerization of the monolayer films resulted in the formation of diacetylene polymer bilayers, which were highly fluorescent, with the apparent rate of photopolymerization and the fluorescence emission of the films being largely unaffected by the presence of the perfluoroacid.

2.6 Introduction

The micron and sub-micron scale spatial patterning of organic molecules in solid-state thin films is a desirable goal for a variety of important technological applications, including the development of organic optoelectronic devices, surface coatings and for a number of novel biosensing platforms.¹⁻¹¹ While there are a variety of approaches for controlled spatial patterning of molecules in organic systems, ranging from lithography to chemical self-assembly, a particularly elegant method that has come to the forefront of research of late is the use of Langmuir-Blodgett (LB) monolayer deposition of phase-separated amphiphiles.¹²⁻¹⁵ In this approach, mutually immiscible (or partially miscible) surfactants are combined at the air-water interface and transferred onto solid substrates via Langmuir-Blodgett deposition. For carefully selected amphiphiles that are deposited under an appropriate set of mixing conditions, the surfactants will undergo phase-separation and form well-defined, regular surface structures that can be transferred onto a variety of solid substrates. Of particular interest to workers in this field are surfactant systems that are comprised of mixtures of perfluorinated (or partially fluorinated) amphiphiles with aliphatic amphiphiles as these systems are often highly immiscible and give rise to structurally and chemically well-defined films.^{14, 16-22} While these approaches are useful, it should be noted that the factors that regulate surfactant miscibility and surface structures that are formed are complex, and often involve a combination of thermodynamic (line tension effects, dipole-dipole headgroup repulsions), kinetic (domain growth) and surfactant-substrate interaction effects.

A family of surfactant molecules that has found widespread use in biosensing applications, and hence is a potentially important target for solid surface patterning via LB deposition, is that based on the diacetylene functional group (monomer unit $R-C\equiv C-C\equiv C-R'$) and

their resulting polymerization products, the polydiacetylenes (the product of 1,4 addition of the diacetylene units typically induced by UV-illumination; schematic illustration of this process for 10,12-pentacosadiynoic acid shown in Figure 2-1).²³ Polydiacetylenes exhibit a number of novel, useful properties, the most notable and commonly exploited of which is a strong optical absorption and fluorescence in the visible region of the spectrum. After polymerization polydiacetylenes are typically blue and non-fluorescent, but under appropriate environmental conditions can undergo a transition to a red, highly-fluorescent form (emission peak maxima typically at 560 nm and 640 nm). The optical properties of the polydiacetylenes are strongly affected by local perturbations to environmental conditions, with the polymer showing *mechanochromism* (optical response to mechanical stress), *thermochromism* (optical response to thermal stress) as well as optical changes that result from the binding of various “target” molecules, the latter of which has been heavily exploited as a signal transduction mechanism for biosensing and diagnostic applications.^{8, 24-27} Changes in the optical properties of the polydiacetylene system as a function of environmental conditions have generally been correlated with perturbations to the highly-conjugated polydiacetylene backbone.²⁷ Polydiacetylenes with various chemically-modified side-groups to promote analyte binding have been synthesized and are often incorporated into vesicles or films for application purposes; biosensors which use this approach have been developed for numerous analytes including influenza virus²⁸, cholera toxin²⁹, bacterial cells^{30, 31} and others. Readers are referred to a number of recent review articles available on this topic.^{23, 32, 33}

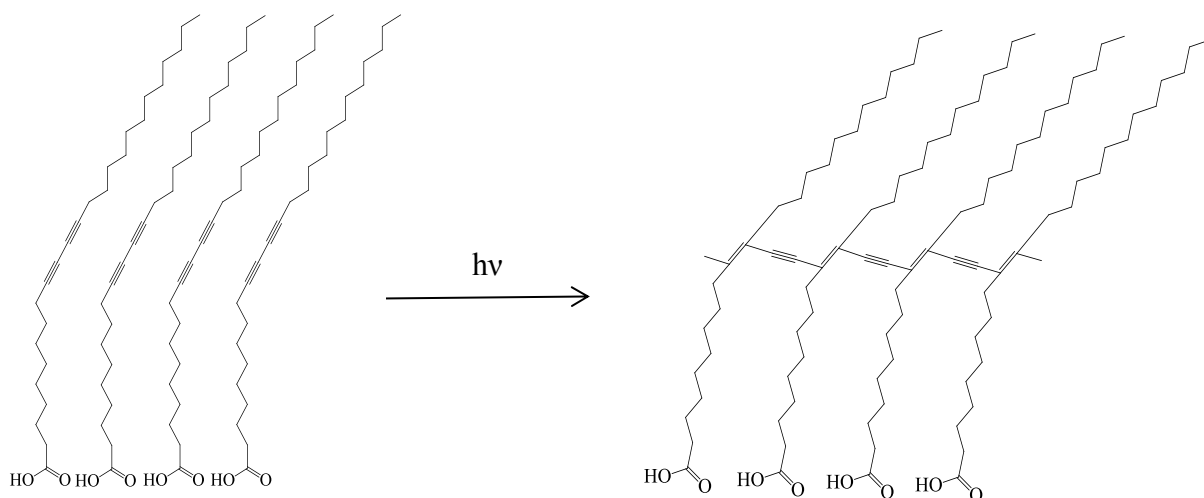


Figure 2-1. Schematic illustration of the photopolymerization of 10,12-pentacosadiynoic acid surfactant monolayer. Photopolymerization proceeds via 1-4 addition of adjacent monomer units to produce the final conjugated polymer product.

While polydiacetylenes have great potential for biosensing and optoelectronic thin-film applications, patterning molecules of this type via LB miscibility approaches is not trivial, as the transfer of these surfactants from the air-water interface to a solid-air interface can be problematic. For example, one of the more commonly used diacetylene surfactant monomers used in this field, 10,12-pentacosadiynoic acid ($C_{24}H_{41}COOH$; PCDA), will form Langmuir monolayers (or stable ‘Y-type’ trilayers upon higher surface pressure compression) on pure aqueous sub-phases (see Carpick et al. 24, for example) but the films are not sufficiently stable to allow quantitative transfer onto solid substrates. Polymerization of the monomer is generally done on the aqueous sub-phase prior to (Langmuir-Schaeffer) deposition in order to further stabilize the film structure. This is the case for many of the closely-related diacetylene-based surfactants described in the literature. Sub-phase additives (typically inorganic cations with +2 or +3 oxidation numbers) can enhance film stability³⁴, though in some surfactant film systems, these additives can strongly affect the deposited film morphology. As phase-separation of

immiscible components in mixed LB films takes place at the air-water interface, and because the dynamics / kinetics of the phase-separation process is of crucial importance in regulating film morphology, we believe that the maximum degree of control over surface morphology can be obtained by allowing the film components to exist as a freely mobile monolayer at the air-water interface, then deposit the film onto a solid substrate and finally photopolymerize the monolayer film directly on the solid substrate. A key factor to enable such an approach to film patterning is to sufficiently enhance stability of the diacetylene mixture at the air-water interface such that monolayer deposition (preferably quantitative) can be achieved.

In this study, we demonstrate that mixtures of PCDA and the perfluorinated surfactant perfluorotetradecanoic acid (PF; selected because its well-documented tendency to form patterned films when mixed with hydrogenated surfactants; *vide infra*) form stable monolayers at the air-water interface and that these unpolymerized monolayer films can be transferred with high efficiency onto solid glass substrates. The film morphology can be altered by adjusting the relative PF:PCDA mixing ratio, and the LB monolayers on glass can be photopolymerized by UV or visible laser light, resulting in the formation of multimolecular polymer aggregates. The optical properties, including the fluorescence emission spectrum and photopolymerization rate, of these mixed films are comparable with those reported for pure polymerized PCDA films in the literature.

2.7 Experimental section

2.7.1 Chemicals

Perfluorotetradecanoic acid (97%) was purchased from Sigma-Aldrich Corp., and 10,12-pentacosadiynoic acid (98%) was purchased from Alfa Aesar. The solvents hexanes and tetrahydrofuran (HPLC grade) were purchased from EMD and Merck EM Science, respectively.

All reagents were used as received. Microscope cover glass (VWR International) was rinsed with absolute ethanol and cleaned in a commercial plasma cleaner (Harrick Plasma, PDC-32G) for ~20 minutes at high power prior to use. Because of the light-sensitive nature of the PCDA, films and solutions were prepared and stored in the dark whenever possible in order to minimize exposure to ambient room light.

2.7.2 Surface pressure isotherms and Langmuir-Blodgett film preparation.

LB experiments were performed on a KSV 2000 Langmuir trough system (KSV Instruments), at room temperature (22 ± 1 °C) with ultrapure water (Millipore, resistivity 18.2M Ω -cm) as a sub-phase. Before each measurement, the water surface was cleaned thoroughly by suction. Blank runs (compression of the clean water surface) showed no appreciable change in surface pressure with compression. Stock solutions of PF and PCDA were prepared by dissolving the appropriate solid in a 9:1 volume ratio of hexanes:THF to give final solution concentrations of 1×10^{-3} M. Surface pressure-area isotherms were collected for pure PF, PCDA, and mixtures of the two in well-defined stoichiometric ratios. The stock solutions were mixed to give a range of PF:PCDA mole ratios (1:0, 3:1, 2:1, 1:1, 1:3, 1:2 and 0:1). For isotherm and deposition experiments, a 100 μ l aliquot of the surfactant solution was placed on the sub-phase surface and the solvent was allowed to evaporate for at least 10 min prior to compression. During isotherm measurements, a barrier compression rate of 20 mm \cdot min $^{-1}$ was used. For film deposition, a compression rate of 10 mm \cdot min $^{-1}$ was used until a deposition pressure of 15 mN \cdot m $^{-1}$ was reached. After the target deposition pressure was reached, the film was allowed to stabilize for ~20 minutes before the cover glass substrate (oriented perpendicular to the sub-phase surface) was pulled upward through the water-air interface in a single stroke. The film was left to dry at room temperature in a clean environmental chamber before measurement in the AFM. Unless

otherwise stated, measurements of solid films were carried out on 2:1 mole ratio mixtures, though results for other compositions were comparable.

2.7.3 Atomic force microscope and fluorescence microscope measurements.

AFM measurements were carried out in contact mode in air on a Dimension Hybrid Nanoscope system (Veeco Metrology Group). Commercial Si_3N_4 AFM probes (Veeco Metrology Group), with nominal spring constant of 0.12 N/m were used, and samples could be imaged repeatedly in air without causing detectable damage to the film structure. For photopolymerization experiments, a short wavelength UV pen lamp (primary emission output at 254 nm, output power density of $4.5 \text{ mW}\cdot\text{cm}^{-2}$, Edmund Optics) was held ~ 10 cm above the film-covered substrate and the sample was illuminated for ~ 5 minutes prior to imaging in the AFM.

Fluorescence emission spectra of the polymerized monolayer films were collected using a modified epifluorescence microscope (Nikon Diaphot 200) with laser illumination. The output from a solid-state laser (532 nm, 30 mW, World Star Tech Inc.) was directed onto a film-covered cover glass sample via a microscope objective lens (10X) to induce photopolymerization, and after ~ 1 minute of exposure, the fluorescence emission from the polymerized film (“red form”) was collected through the same objective, passed through appropriate optical emission filters (540LP; Omega Filters) and directed onto a miniature fibre-optic-based spectrometer (USB-2000, Ocean Optics).

The rate of film photopolymerization was measured using an epifluorescence microscope setup that has been described previously.³⁵ Briefly, film samples were illuminated with the attenuated output ($20 \mu\text{W}$ at the sample focal plane) of a solid-state laser (532 nm, 100 mW output power, Dragon Lasers Inc.), with fluorescence emission collected through a 100X,

1.4NA objective lens, passed through two long pass emission filters (540LP; Omega Filters) and directed onto a back-illuminated, electron-multiplying CCD (Cascade 512F, Photometrics). Images were collected continuously with a 1 second per frame integration period and the emission intensity of each frame was calculated as the sum of image pixel intensities corrected for the detector offset, background and dark counts.

2.8 Results and Discussion

Surface pressure – area (π -A) isotherms for monolayer films of PF, PCDA and their mixtures on a pure water sub-phase were collected and are shown in Figure 2-2. Isotherms for both PF and PCDA consisted of a slowly-increasing disordered phase at low film compression, followed by a steep increase in surface pressure at higher compressions. At a surface pressure of $\pi = 15 \text{ mN}\cdot\text{m}^{-1}$ (the surface pressure at which deposition onto solid substrates was carried out), PF occupied $\sim 28 \text{ \AA}^2$ per molecule and PCDA $\sim 29 \text{ \AA}^2$ per molecule. The value of the mean molecular area for PCDA during deposition is of particular importance, as Ogawa et al.³⁶ have reported that the photopolymerization of PCDA monolayers proceeds optimally at this degree of film packing. It has been proposed that under these conditions, PCDA adopts a *syn-periplanar* configuration about the C14-C15 bond (illustrated schematically in Figure 2-3) in which the distance between alkyne-bonds in adjacent PCDA molecules is optimal for photopolymerization; subsequent AFM imaging described later in this manuscript provides support for this configuration. Neither of the pure films underwent phase-transitions to liquid-like states, which is consistent with other isotherms reported in the literature for these surfactants.^{15, 27, 37} The films exhibited collapse pressures of $\sim 55 \text{ mN}\cdot\text{m}^{-1}$ for PF and $\sim 20 \text{ mN}\cdot\text{m}^{-1}$ for PCDA, respectively, which again, is in agreement with previous literature reports. For the mixed films, the π -A isotherms were generally shifted to lower mean molecular areas compared to the pure individual

components, which is indicative of deviations from ideal mixing behavior.³⁸ The film collapse pressures for the mixtures decreased as a function of the PCDA content, which is expected because of the substantial difference in the collapse pressure values for the pure individual components.

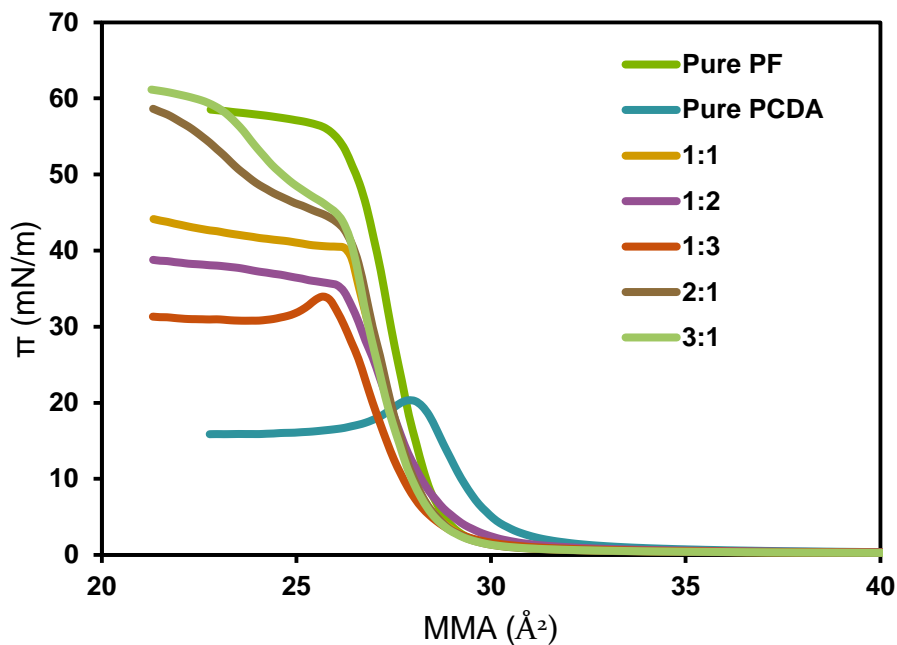


Figure 2-2. Surface pressure-area isotherms of pure and mixed Langmuir monolayers of PF and PCDA at the air–water interface with a sub-phase temperature of $22 \pm 1^\circ\text{C}$. The inset legend describes the PF to PCDA mole ratio.

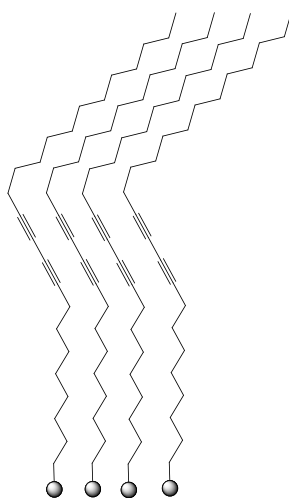


Figure 2-3. Schematic illustration of the syn-periplanar conformation of the PCDA Langmuir monolayer film proposed by Ogawa et al.³⁶ to occur at a film compression of 28\AA^2 per molecule.

To further investigate the mixing behavior of the two surfactants, plots showing the mean molecular area for the mixed films as a function of the mole fraction of PF have been generated (Figure 2-4) for two different surface pressures. For a binary surfactant system in which the two film components behave ideally (i.e. no net difference in average interaction energies for A-A, B-B and A-B interaction pairs, where A, B are the individual film components), the additivity relationship shown in equation (2.1) applies:

$$A_{12} = A_1\chi_1 + A_2\chi_2 \quad (2.1)$$

where A_{12} is the mean molecular area for the mixed film, A_i is the mean molecular area for the i^{th} -component and χ_i is the mole fraction of the i^{th} -component. Net attractive or repulsive interactions between different film components manifest themselves as deviations (below the line predicted from equation (2.1) for attractive interactions and above the line for repulsive

interactions) from additivity. For reference purposes, Figure 2-4 includes the behavior predicted by equation (2.1) with values for A_1 , A_2 taken from the film measurements for the pure components. All of the mixtures investigated showed negative deviations from ideality at both surface pressures, indicating that there are significant attractive interactions between the film components, and hence the surfactant molecules occupy a smaller mean molecular area in the mixed film than in the pure films. This result differs significantly for those we have reported previously with simple fatty acids and perfluorocarboxylic acid mixtures under comparable sub-phase conditions, including mixtures of PF with arachidic acid ($C_{19}H_{39}COOH$) and with stearic acid ($C_{17}H_{35}COOH$), in which the additivity rule was rigorously followed.^{15, 21} In the case of PCDA, it appears that the larger hydrocarbon chain length (and consequently higher net molecular weight) in conjunction with the polarizable carbon-carbon triple bonds give rise to larger net dispersion attractions between the hydrocarbon and perfluorocarbon as compared to the shorter-chain fatty acids examined previously.

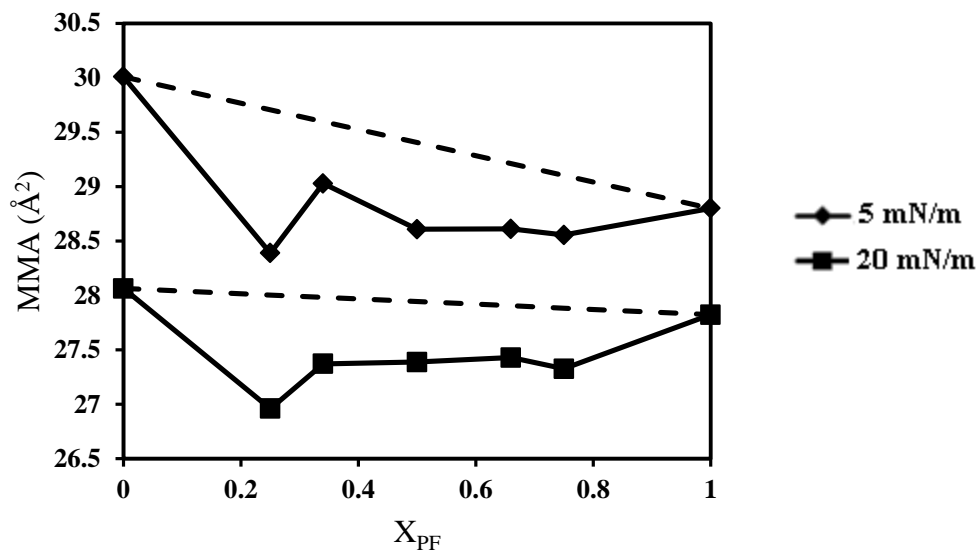


Figure 2-4. Plot showing mean molecular area as a function of mole fraction of PF for the mixed surfactant films. The dashed lines represent the ideal behavior predicted by the additivity relationship (equation (2.1)) whereas solid lines are included as a guide to the eyes.

It has been observed that for a number of different perfluorocarbon-fatty acid surfactant pairs, a chain-length difference of two or more carbons gives rise to highly-structured surfactant films.^{15, 39, 40} Based on these results, one might reasonably predict that the PF-PCDA mixtures studied here should also give rise to structured films. To explore this prediction, PF-PCDA mixtures of varying composition were deposited onto solid glass substrates and imaged in the AFM. As observed by others, we were unable to transfer pure PCDA monolayers from the air-water interface onto solid substrates. However, the mixed PF-PCDA films were stable for all mixing ratios that were investigated, and the films deposited onto glass with transfer ratios of ~ 1 . To our knowledge, this is the first report of the deposition of stable, unpolymerized PCDA monolayers onto solid glass substrates via simple LB-deposition and in the absence of stabilizing cations in the sub-phase.

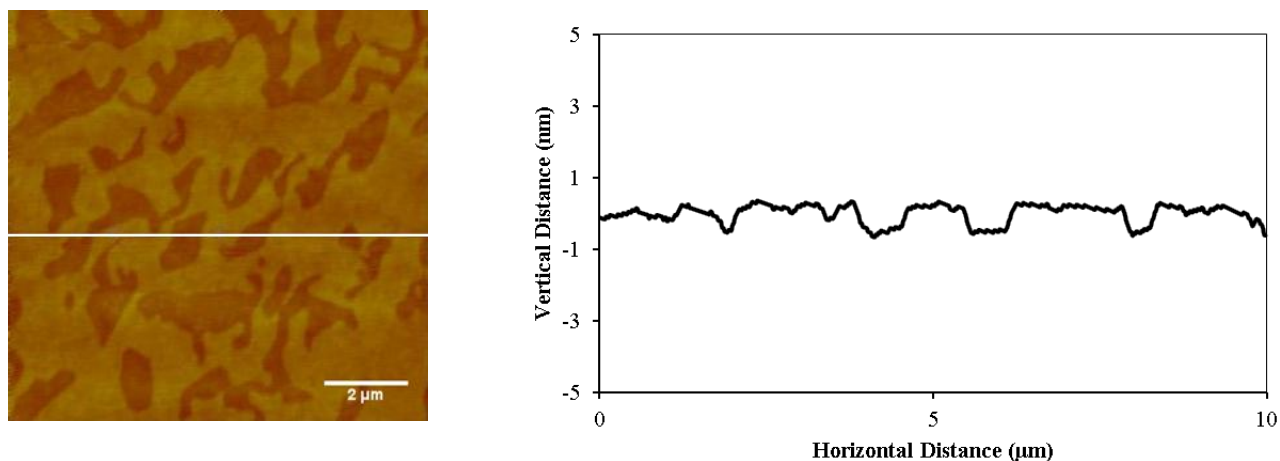


Figure 2-5. AFM height mode image ($10\ \mu\text{m} \times 10\ \mu\text{m}$) and corresponding cross-sectional analysis of a 2:1 PF:PCDA mixed LB film deposited on cover glass using water as a sub-phase. The difference in heights between the smooth continuous domain (light yellow) and the lower domains (dark) was typically $\sim 0.8\text{-}1.0\ \text{nm}$.

A typical image of a 2PF:1PCDA monolayer is shown in Figure 2-5, along with a cross-sectional analysis. As an aside, we note that the solid films were surprisingly resistant to mechanical damage via the AFM probe. All attempts to scratch the samples with the AFM tip failed, and in general, samples could be imaged at the highest operating force of our AFM for extended periods of time without causing detectable damage. Films consisted of a continuous, smooth (at the noise level of our instrument) layer that contained occasional irregularly-shaped domains. The height difference between the continuous smooth layer and the bottom of the irregularly-shaped domains had an average value of 0.8 nm. For reference, we note that the approximate molecular length (calculated for molecules in vacuum using MMFF calculations in Spartan '08, V1.2.0) for PF is 1.8 nm, 3.2 nm for the fully extended conformation of PCDA, and 1.0 nm for the PCDA conformation (taken as the length of the molecule from headgroup to the C14-C15 bond) predicted by Ogawa et al. to be the likely conformation under the deposition conditions used in these studies.³⁶ The height difference measured by AFM is consistent with the difference in length between vertically adsorbed PF and the *syn-periplanar* conformation of

PCDA, which suggests the film consists of phase-separated regions of PF (the smooth continuous film) and PCDA (the lower, irregularly shaped domains). However, we also note that definitive chemical identification cannot be made using this approach alone, and further information is needed for identity assignment of these domains.

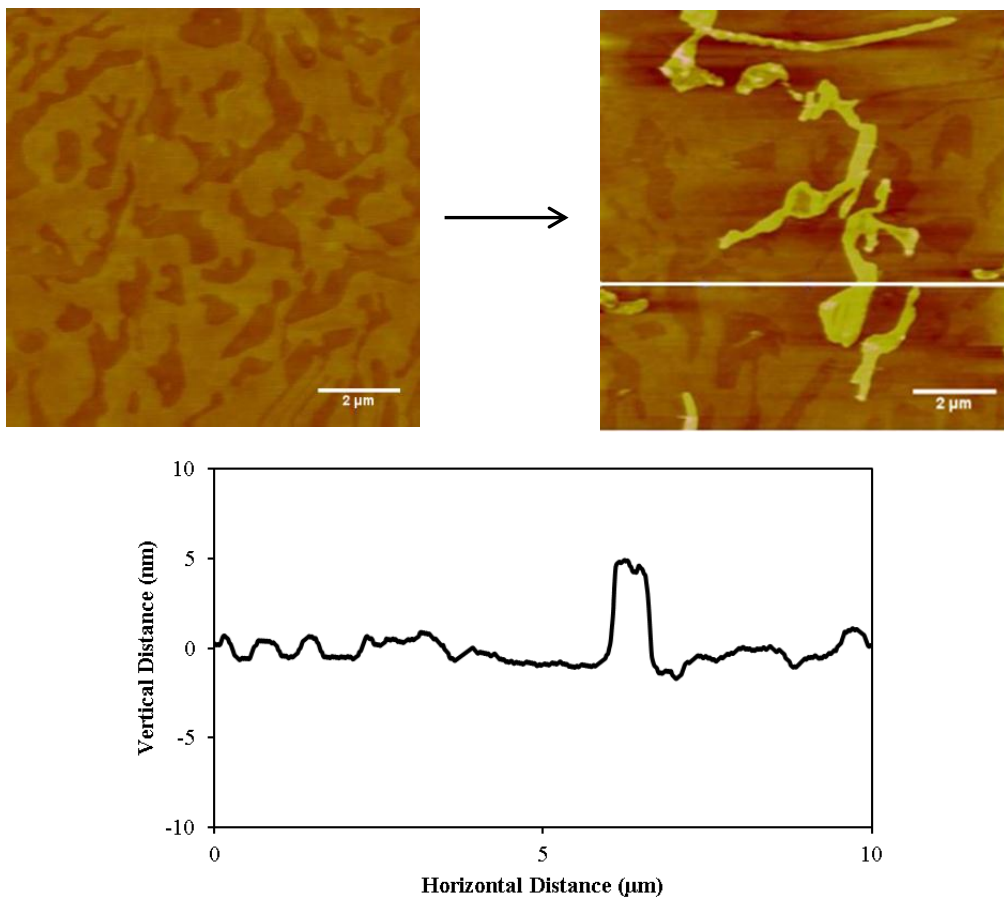


Figure 2-6. AFM height mode images ($10\ \mu\text{m} \times 10\ \mu\text{m}$) of 2:1 PF:PCDA mixed films before and after UV light illumination (illumination time ~ 5 minutes, with the lamp mounted ~ 10 cm above the film-covered substrate). A cross-sectional analysis of both polymerized and unpolymerized regions of the film is included.

To confirm the chemical identity of these different film regions, we have used two additional approaches: first, we systematically surveyed the fractional surface area occupied by the lower domains (total number of image pixels in the lower domains divided by the total

number of pixels per image) as a function of the PF-PCDA mixing ratio, and second, we observed the effect of UV light exposure on film morphology. Results from the surface area analysis are shown in Table 2-1. It was found that as the ratio of PF to PCDA increased, the area of the smooth continuous film increased in comparison to that of the lower domains. The data in Table 2-1 shows good agreement between the mole percent of PF in the mixture and the calculated area of the smooth continuous film, providing supporting evidence that these regions indeed consisted of the perfluoroacid monomer. In the second approach, mixed LB films were exposed to a UV pen lamp for ~ 5 minutes, and the resulting film was measured in the AFM. Figure 2-6 shows a typical AFM image and cross-section from a 2PF:1PCDA mixed film after photopolymerization. Upon exposure to UV light, the film morphology changed considerably, with the appearance of a new, elevated region (sample heights were ~ 3.0 nm – 3.2 nm above the smooth continuous film surface), presumably consisting of photopolymerized PCDA. The photopolymer was not uniformly distributed over the film surface, but was rather located in discrete patches. Closer inspection of the AFM images revealed that the photopolymer patches correlated with the lower, irregular shaped domains that were proposed to consist of PCDA. On the basis of this cumulative evidence, we can definitively assign the identity of these lower regions as being PCDA, with the continuous smooth layer consisting primarily of PF.

Table 2-1. Table showing the total calculated perfluorotetradecanoic acid content (mol%) of the mixed surfactant solutions and the resultant measured percent total surface area occupied by the higher domains as determined by AFM image analysis.

PF:PCDA solution mole ratio	PF content (mol%)	% surface area occupied by higher domains
1:3	25	24.9
1:2	33	32.3
1:1	50	50.8
2:1	67	66.6
3:1	75	77.3

The nature of the photopolymerized film structure in the LB monolayer system bears further consideration. The heights of the photopolymer product above the underlying glass substrate was, for all conditions explored (different illumination times, different sample compositions; data not shown), considerably larger than the length of individual PCDA molecules (elevated regions were 3.2 nm above the PF layer, which, assuming normal adsorption to the surface (*vide infra*) is 1.8 nm thick, giving a total height of the polymerized material above the underlying substrate of ~ 5.0 nm). This suggests that the structures consisted of more than a single layer of PCDA. Carpick et al.²⁴ have estimated the thickness of a polydiacetylene bilayer oriented normal to the substrate surface as ~ 5.5 nm (our estimates for film thickness via simple molecular modeling calculations are in reasonable agreement with this value), suggesting that the photopolymer formed in these experiments consists of a polymerized PCDA bilayer. On rare occasions, we have observed very thick polymerized films (domain heights of ~20 nm) indicating that it is possible, though unlikely, to form films which contain a greater number of layers (~4), though the bilayer is by far the most common structure formed using this approach. It is also worth considering the source of the material needed to generate the polymerized bilayer – that is, the before polymerization, the film is clearly a monolayer, but after exposure to UV

light, additional material is being added on top of the originally deposited PCDA. For PCDA multilayers deposited via Langmuir-Schaeffer approaches, Carpick et al. have shown that the shear force from scanning probe microscope tips can displace PCDA, leading to the buildup of thicker films in regions that have been scanned by a probe.²⁴ This effect can be ruled out for our system, however, as the monolayer films studied here can be imaged repeatedly at high operating force without affecting film structure, and the buildup of bilayers only occurs upon illumination. The most likely source of the additional material for bilayer formation is mass transport of PCDA monomers from the cover glass substrate. Assuming this is the case, then the photopolymerization process should not only result in the formation of bilayers in parts of the sample, but it should also give rise to a simultaneous *loss* of PCDA from different regions of the sample, presumably immediately adjacent to the site of polymer buildup. Direct evidence of this comes in the form of higher magnification AFM images of the photopolymerized film morphology, an example of which is shown in Figure 2-7 along with the corresponding cross-section.

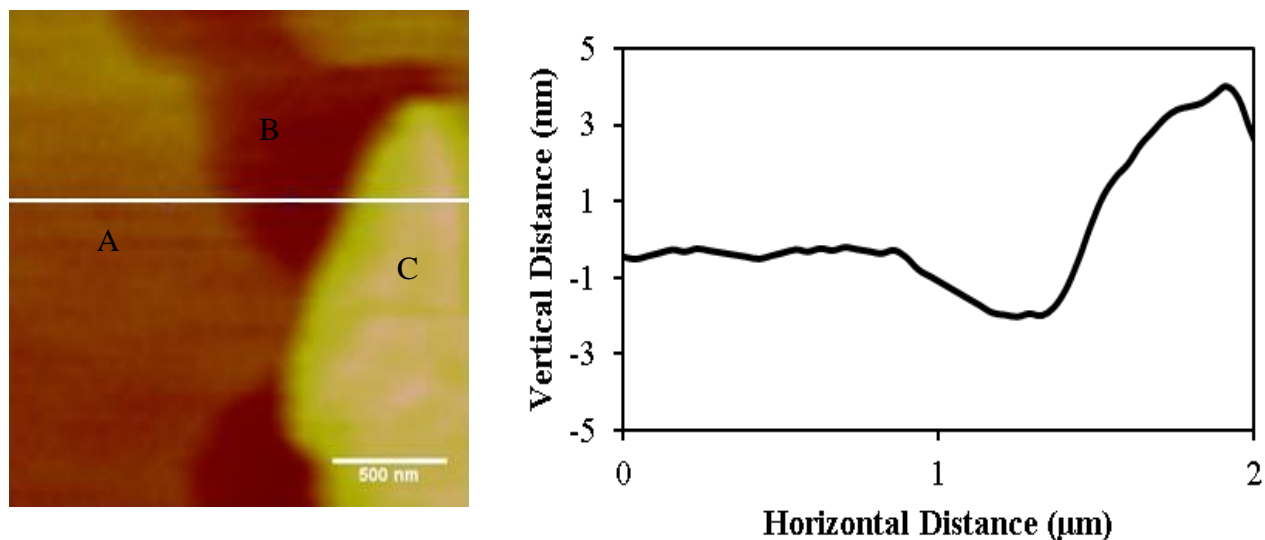


Figure 2-7. AFM height mode image ($2\ \mu\text{m} \times 2\ \mu\text{m}$) of a 2:1 PF:PCDA mixed film after exposure to UV light. The cross-section line crosses three different domains. The height difference between domain ‘A’ and ‘B’ is $\sim 1.8\ \text{nm}$, which is equal to the estimated length of a PF molecule, whereas the height difference between domain ‘B’ and ‘C’ (the photopolymer) is $\sim 5.0\ \text{nm}$, which is equal to the estimated thickness of a polymerized PCDA bilayer.

In this image, the interface between the smooth continuous domain and the photopolymerized bilayer has been scanned, and three regions (labeled A, B, C in Figure 2-7) with different, well-defined heights are observed. The height difference between region ‘A’ and ‘C’ ($\sim 4.8\ \text{nm}$) falls within the range of height differences seen between the smooth continuous domains (PF) and the photopolymerized bilayer in the larger-scale images. However, a third region (labeled ‘B’) can now be resolved at this level of magnification, and this region is lower in height than the smooth continuous domain by $\sim 1.8\ \text{nm}$. This distance corresponds to the length of an individual PF molecule which is adsorbed perpendicular to the underlying substrate, indicating that region ‘B’ is the bare glass substrate. The overall geometry of the situation is shown schematically in Figure 2-8. These results are the expected outcome of mass transport of PCDA molecules from the underlying glass substrate onto a monolayer of PCDA, resulting in the net formation of a polymerized bilayer and a void, bare glass region. Of course, many details

of this situation cannot be definitively determined by the approaches we have used here; for example, the schematic illustration in Figure 2-8 is drawn to show a head-to-tail bilayer, though a tail-to-tail bilayer (or both) might also be formed. Friction force images of the films give comparable tip-sample contrast for the polymerized PCDA and the unpolymerized PCDA monolayer, suggesting that the bilayer adopts a head-to-tail conformation, though we are cautious about this assignment at present. Another issue that remains unresolved is the exact mass transport mechanism, and it is not immediately obvious how photoillumination can drive a physisorbed (via the carboxylic acid headgroup) PCDA molecule to desorb from the substrate, attain the correct orientation and undergo photopolymerization. Mass transport of surfactants across fluid lipid bilayers (“flip flop” exchange) is certainly well-documented in the literature⁴¹, though this is entirely different from the dry LB monolayer used in these experiments. It is not immediately obvious how to gain further insight into the mechanism by which mass transport occurs, though a detailed kinetic investigation of the polymerization process might prove insightful and will be considered for future experiments.

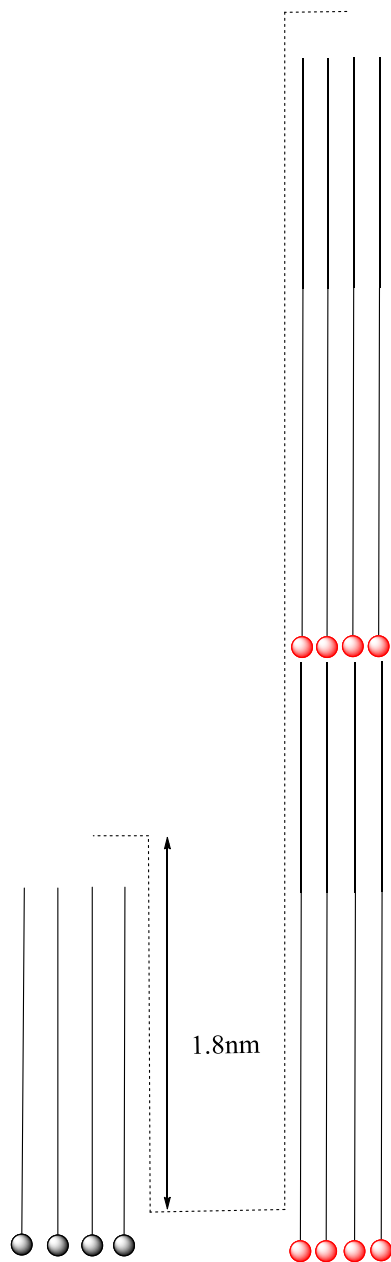


Figure 2-8. Schematic illustration of the mixed surfactant film morphology after photopolymerization. The surfactant molecules with the grey head-group are PF molecules, while the molecules with the red head-group are photopolymerized PCDA molecules. To aid clarity, surfactants have been drawn adsorbed normal to the surface, though under the deposition conditions used here, a slight tilt angle to the normal may occur.

In addition to the use of polydiacetylenes in sensing applications which exploit simple colorimetry (i.e. transitions between the red and blue forms), there has also been considerable recent interest in the use of polydiacetylene fluorescence for sensing applications. Particular interest has focused on fluorogenic enhancement of polydiacetylene emission upon binding to target molecules³² as well as in terms of modulating fluorescence emission through Forster-type energy exchange with lipophilic fluorophores.⁴² While the fluorescence emission of highly-aggregated conjugated polymers can be quenched⁴³, polydiacetylenes generally appear immune to this effect, making them well-suited probes for fluorescence-based measurements.³² In addition to morphological characterization, we have also performed a basic fluorescence spectroscopic characterization of the mixed PF:PCDA monolayer films (absorption spectroscopy is insufficiently sensitive for monolayer detection), and used the fluorescence emission of the polymerized monolayer to provide a simple estimate of the photopolymerization rate. To confirm the identity of the photopolymerization product in the mixed system, a fluorescence microscope-based experiment was performed. In these measurements, an unpolymerized mixed film (2:1 mole ratio) was placed in an epifluorescence microscope and illuminated with a 532 nm diode laser to induce photopolymerization. After a sufficient illumination period (several minutes), the emission spectrum of the resulting film (Figure 2-9) was collected as described in the Experimental section above. As an aside, we note that while photopolymerization in diacetylene systems is most commonly carried out with UV-lamps, the polymerization also takes place with high efficiency when using suitably intense visible light. This is an issue that should be carefully considered when diacetylene-based surfactants are measured at the air-water interface via optical techniques like Brewster Angle Microscopy, as the probe beam might inadvertently induce photopolymerization. As a control experiment, samples that had been

illuminated using this approach were imaged in the AFM, and the polymerized film structure was found to be comparable with that observed for the UV-based polymerization experiments.

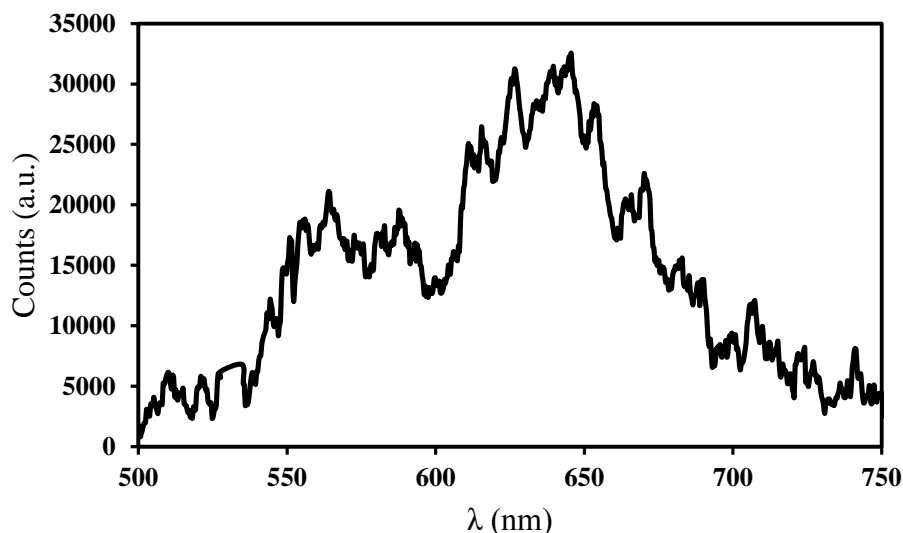


Figure 2-9. Fluorescence emission spectrum of a 2:1 PF:PCDA mixed monolayer on a glass substrate after photopolymerization with a 532 nm, 30 mW laser for \sim 1 minute.

The fluorescence emission spectrum of the photopolymerized film consisted of two broadly overlapped emission peaks centered at 560 nm and 640 nm, which is in agreement with reported spectra for the red form of PCDA multilayers.^{23, 24, 32} We note that while the signal-to-noise ratio of the spectrum in Figure 2-9 is not exceptional, this measurement was carried out for a *single monolayer*, and an acceptably large signal can still be measured using a modestly sensitive spectrometer. This further suggests that the presence of a significant mole fraction of perfluorocarbon surfactant (2:1 mole ratio) in the mixed film does not result in substantial quenching of fluorescence, or any major spectral perturbations of the polydiacetylene emission. There have been reports of in the literature (see the work of Choi et al.⁴⁴ for example) of perfluorocarbons that significantly quench fluorescence emission of some fluorophores, though

that does not appear to be the case here; this bodes well for potential applications of these structured films for fluorescence-based sensing purposes.

As a final, simple test of the ability of the mixed LB films to undergo photopolymerization, crude measurements of polymerization rates have been performed by measuring the rate of appearance of fluorescence upon continuous laser illumination (532 nm excitation) by epifluorescence microscopy. Unpolymerized mixed films were placed in the fluorescence microscope and illuminated while constantly monitoring the fluorescence emission of the film via a CCD camera detector. To track the rate and extent of polymerization, the total fluorescence emission signal for the illuminated area was determined and plotted as a function of time. Typical results from one set of illumination conditions (average of seven independent measurements) are shown in Figure 2-10. At the beginning of the illumination period, samples were essentially non-fluorescent, with the total emission signal coming from simple background scattering in the system. The overall signal increased in a sigmoidal fashion as a function of time, with the increase in signal due to the appearance of irregularly-shaped, luminescent domains (appearance was red through the eye-piece; false colour image included in Figure 2-10) in the microscope field of view. While we have not rigorously measured the rate of photopolymerization under a variety of illumination conditions, it was observed that the rate of appearance of fluorescence increased as a function of illumination intensity (measured in power per unit illumination area). For the conditions shown in Figure 2-10 (2:1 PF:PCDA film, illumination intensity of 10 W/cm^2), the sample reached a steady-state emission level after ~ 90 seconds, after which there was no further significant change in fluorescence emission. While difficult to compare quantitatively because of differences in illumination sources and intensities, substrate effects, temperature and other factors, this polymerization time is of the same order as

the value reported by Hofmann et al.⁴⁵ for the UV-based photopolymerization of ethyl morpholine pentacosadiynoic amide Langmuir monolayers on an aqueous sub-phase, and also comparable to the value measured by Deckert et al.³⁷ for the photopolymerization of 30 layer PCDA films on solid supports after performing reasonable corrections for film thickness and differences in illumination intensity. While we view this analysis as a qualitative assessment only, it appears that there are no gross differences in the ability and rate of the mixed PF-PCDA solid-phase films to undergo photopolymerization in comparison with their pure film counterparts at the solid-air and water-air interface.

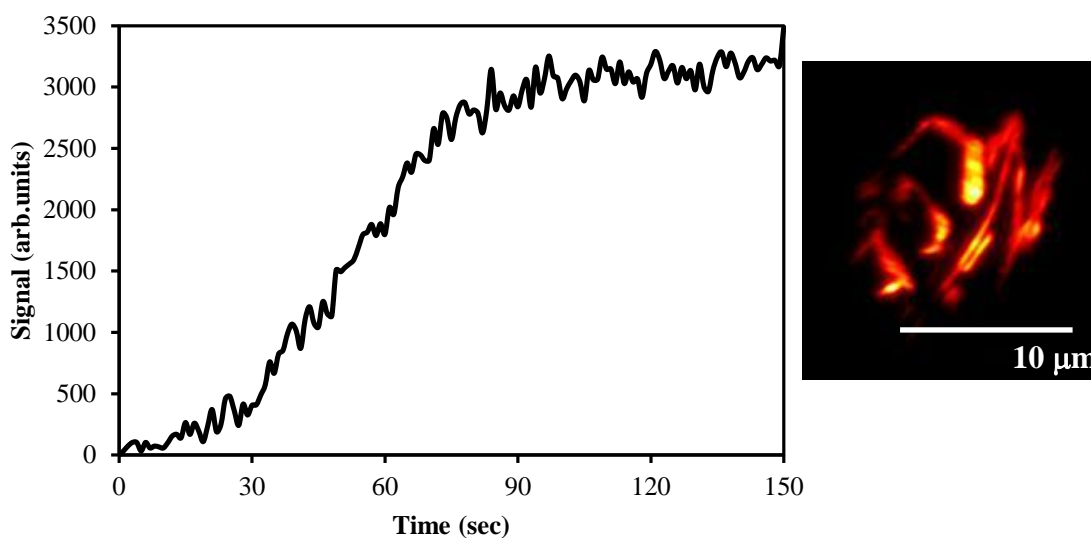


Figure 2-10. Fluorescence signal versus illumination time for a 2:1 PF:PCDA monolayer sample deposited on micro cover glass to the 532 nm green laser beam. The illumination intensity at the focal plane was $10 \text{ W} / \text{cm}^2$. The image to the right is a false-color fluorescence image of a typical 2:1 mixed monolayer sample after completion of a photopolymerization experiment.

2.9 Conclusions

Phase-separated mixed monolayer films of perfluorotetradecanoic acid and 10,12-pentacosadiynoic acid have been prepared on a salt-free, aqueous sub-phase in a variety of mole

ratio mixtures, and were deposited with high efficiency onto solid cover glass substrates. Mixing of the diacetylene surfactant with a perfluoroacid leads to substantial stabilization of the film in comparison with pure PCDA monolayers, allowing for the films to be deposited as monolayers without a pre-polymerization step. The two surfactants form phase-separated monolayer films, which consisted of two chemically distinct domains, one enriched in PF and the other enriched in PCDA. The LB monolayers could be photopolymerized via continuous UV or laser-light illumination, leading to the formation of polymerized “red” PCDA bilayers through the mass transport of PCDA from the glass substrate onto the remaining PCDA monolayer. The rate of photopolymerization and the fluorescence emission spectrum of the red polymerized PCDA were consistent with that reported for pure PCDA monolayers on solid and aqueous surfaces, indicating that the presence of the perfluorinated surfactant in the mixed film does not significantly decrease the rate of the polymerization process or quench the fluorescence of the red photoproduct.

2.10 Acknowledgments

Funding for this work was provided by the Natural Sciences and Engineering Research Council of Canada (NSERC), the Canada Foundation for Innovation (CFI), the Province of Saskatchewan and by the University of Saskatchewan.

2.11 References

1. Bratton, D.; Yang, D.; Dai, J. Y.; Ober, C. K., Recent progress in high resolution lithography. *Polymers for Advanced Technologies* **2006**, 17, (2), 94-103.

2. Gates, B. D.; Xu, Q. B.; Stewart, M.; Ryan, D.; Willson, C. G.; Whitesides, G. M., New approaches to nanofabrication: Molding, printing, and other techniques. *Chemical reviews* **2005**, 105, (4), 1171-1196.
3. Kim, J.; Swager, T. M., Control of conformational and interpolymer effects in conjugated polymers. *Nature* **2001**, 411, (6841), 1030-1034.
4. Nguyen, T. Q.; Wu, J. J.; Doan, V.; Schwartz, B. J.; Tolbert, S. H., Control of energy transfer in oriented conjugated polymer-mesoporous silica composites. *Science* **2000**, 288, (5466), 652-656.
5. Nie, Z. H.; Kumacheva, E., Patterning surfaces with functional polymers. *Nature Materials* **2008**, 7, (4), 277-290.
6. Sirringhaus, H.; Brown, P. J.; Friend, R. H.; Nielsen, M. M.; Bechgaard, K.; Langeveld-Voss, B. M. W.; Spiering, A. J. H.; Janssen, R. A. J.; Meijer, E. W.; Herwig, P.; de Leeuw, D. M., Two-dimensional charge transport in self-organized, high-mobility conjugated polymers. *Nature* **1999**, 401, (6754), 685-688.
7. Xia, Y. N.; Whitesides, G. M., Soft lithography. *Angewandte Chemie-International Edition* **1998**, 37, (5), 551-575.
8. Lee, J.; Yarimaga, O.; Lee, C. H.; Choi, Y.-K.; Kim, J.-M., Network Polydiacetylene Films: Preparation, Patterning, and Sensor Applications. *Advanced Functional Materials* **2011**, 21, (6), 1032-1039.
9. Mandal, S. K.; Okawa, Y.; Hasegawa, T.; Aono, M., Rate-Determining Factors in the Chain Polymerization of Molecules Initiated by Local Single-Molecule Excitation. *ACS Nano* **2011**, 5, (4), 2779-2786.

10. Sakamoto, A.; Mori, K.; Imura, K.; Okamoto, H., Nanoscale Two-Photon Induced Polymerization of Diacetylene Langmuir-Blodgett Film by Near-Field Photoirradiation. *J. Phys. Chem. C* **2011**, 115, (14), 6190-6194.
11. Shimogaki, T.; Matsumoto, A., Structural and Chromatic Changes of Host Polydiacetylene Crystals during Intercalation with Guest Alkylamines. *Macromolecules* **2011**, 44, (9), 3323-3327.
12. Imae, T.; Takeshita, T.; Kato, M., Phase separation in hybrid Langmuir-Blodgett films of perfluorinated and hydrogenated amphiphiles. Examination by atomic force microscopy. *Langmuir* **2000**, 16, (2), 612-621.
13. Kimura, H.; Watanabe, S.; Shibata, H.; Azumi, R.; Sakai, H.; Abe, M.; Matsumoto, M., Phase-Separated Structures of Mixed Langmuir-Blodgett Films of Fatty Acid and Hybrid Carboxylic Acid. *Journal of Physical Chemistry B* **2008**, 112, (48), 15313-15319.
14. Matsumoto, M.; Watanabe, S.; Tanaka, K.; Kimura, H.; Kasahara, M.; Shibata, H.; Azumi, R.; Sakai, H.; Abe, M.; Kondo, Y.; Yoshino, N., Control of two-dimensional nanopatterns by adjusting intermolecular interactions. *Advanced Materials* **2007**, 19, (21), 3668-3671.
15. Qaqish, S. E.; Paige, M. F., Rippled domain formation in phase-separated mixed Langmuir-Blodgett films. *Langmuir* **2008**, 24, (12), 6146-6153.
16. Krafft, M. P.; Goldmann, M., Monolayers made from fluorinated amphiphiles. *Current Opinion in Colloid and Interface Science* **2003**, 8, (3), 243-250.
17. Lehmler, H. J.; Bummer, P. M., Mixing of perfluorinated carboxylic acids with dipalmitoylphosphatidylcholine. *Biochimica et Biophysica Acta, Biomembranes* **2004**, 1664, (2), 141-149.

18. Matsumoto, Y.; Nakahara, H.; Moroi, Y.; Shibata, O., Langmuir monolayer properties of perfluorinated double long-chain salts with divalent counterions of separate electric charge at the air-water interface. *Langmuir* **2007**, *23*, (19), 9629-9640.
19. Nakamura, S.; Nakahara, H.; Krafft, M. P.; Shibata, O., Two-component Langmuir monolayers of single-chain partially fluorinated amphiphiles with dipalmitoylphosphatidylcholine (DPPC). *Langmuir* **2007**, *23*, (25), 12634-12644.
20. Qaqish, S. E.; Paige, M. F., Mechanistic insight into domain formation and growth in a phase-separated Langmuir-Blodgett monolayer. *Langmuir* **2007**, *23*, (20), 10088-10094.
21. Qaqish, S. E.; Paige, M. F., Structural and compositional mapping of a phase-separated Langmuir-Blodgett monolayer by atomic force microscopy. *Langmuir* **2007**, *23*, (5), 2582-2587.
22. Shibata, O.; Krafft, M. P., Mixed Langmuir monolayers made from single-chain perfluoroalkylated amphiphiles. *Langmuir* **2000**, *16*, (26), 10281-10286.
23. Carpick, R. W.; Sasaki, D. Y.; Marcus, M. S.; Eriksson, M. A.; Burns, A. R., Polydiacetylene films: a review of recent investigations into chromogenic transitions and nanomechanical properties. *Journal of Physics: Condensed Matter* **2004**, *16*, R679-R697.
24. Carpick, R. W.; Sasaki, D. Y.; Burns, A. R., First observation of mechanochromism at the nanometer scale. *Langmuir* **2000**, *16*, (3), 1270-1278.
25. Charych, D. H.; Nagy, J. O.; Spevak, W.; Bednarski, M. D., Direct Colorimetric Detection Of A Receptor-ligand Interaction By A Polymerized Bilayer Assembly. *Science* **1993**, *261*, (5121), 585-588.
26. Nallicheri, R. A.; Rubner, M. F., Investigations Of The Mechanochromic Behavior Of Poly(urethane diacetylene) Segmented Copolymers. *Macromolecules* **1991**, *24*, (2), 517-525.

27. Tomioka, Y.; Tanaka, N.; Imazeki, S., Surface-Pressure-Induced Reversible Color-Change Of A Polydiacetylene Monolayer At A Gas Water Interface. *Journal of Chemical Physics* **1989**, 91, (9), 5694-5700.
28. Reichert, A.; Nagy, J. O.; Spevak, W.; Charych, D., Polydiacetylene Liposomes Functionalized With Sialic-Acid Bind And Colorimetrically Detect Influenza-Virus. *Journal of the American Chemical Society* **1995**, 117, (2), 829-830.
29. Pan, J. J.; Charych, D., Molecular recognition and colorimetric detection of cholera toxin by poly(diacetylene) liposomes incorporating G(m1) ganglioside. *Langmuir* **1997**, 13, (6), 1365-1367.
30. Ma, Z. F.; Li, J. R.; Liu, M. H.; Cao, J.; Zou, Z. Y.; Tu, J.; Jiang, L., Colorimetric detection of Escherichia coli by polydiacetylene vesicles functionalized with glycolipid. *Journal of the American Chemical Society* **1998**, 120, (48), 12678-12679.
31. Scindia, Y.; Silbert, L.; Volinsky, R.; Kolusheva, S.; Jelinek, R., Colorimetric detection and fingerprinting of bacteria by glass-supported lipid/polydiacetylene films. *Langmuir* **2007**, 23, (8), 4682-4687.
32. Ahn, D. J.; Kim, J. M., Fluorogenic polydiacetylene supramolecules: Immobilization, micropatterning, and application to label-free chemosensors. *Accounts of Chemical Research* **2008**, 41, (7), 805-816.
33. Okada, S.; Peng, S.; Spevak, W.; Charych, D., Color and chromism of polydiacetylene vesicles. *Accounts of Chemical Research* **1998**, 31, (5), 229-239.
34. Petty, M. C., *Langmuir-Blodgett Films: An Introduction*. Cambridge University Press: Cambridge, 1996.

35. Bagh, S.; Paige, M. F., Construction and application of a single-molecule fluorescence microscope. *Canadian Journal of Chemistry-Revue Canadienne De Chimie* **2005**, 83, (5), 435-442.
36. Ogawa, K.; Tamura, H.; Hatada, M.; Ishihara, T., Study of Photoreaction Processes of PDA Langmuir Films. *Langmuir* **1988**, 4, (4), 903-906.
37. Deckert, A. A.; Fallon, L.; Kiernan, L.; Cashin, C.; Perrone, A.; Encalade, T., Kinetics of the Reversible Thermochromism in Langmuir-Blodgett Films of Cd²⁺ Salts of Polydiacetylenes Studied Using UV-Vis Spectroscopy. *Langmuir* **1994**, 10, (6), 1948-1954.
38. Gaines, G. L., *Insoluble Monolayers At Liquid - Gas Interfaces*. Interscience Publishers: New York, 1966.
39. Rontu, N.; Vaida, V., Miscibility of perfluorododecanoic acid with organic acids at the air-water interface. *Journal of Physical Chemistry C* **2007**, 111, (27), 9975-9980.
40. Shibata, O.; Yamamoto, S. K.; Lee, S.; Sugihara, G., Mixed monolayer properties of tetradecanoic acid with n-perfluorocarboxylic acids with 10, 12, 14, 16, and 18 carbon atoms. *Journal of Colloid and Interface Science* **1996**, 184, (1), 201-208.
41. Israelachvili, J., *Intermolecular and Surface Forces*. 2nd ed.; Academic Press: San Diego, 2002.
42. Li, X.; McCarroll, M.; Kohli, P., Modulating Fluorescence Resonance Energy Transfer in Conjugated Liposomes. *Langmuir* **2006**, 22, 8615-8617.
43. Friend, R. H.; Gymer, R. W.; Holmes, A. B.; Burroughes, J. H.; Marks, R. N.; Taliani, C.; Bradley, D. D. C.; Dos Santos, D. A.; Bredas, J. L.; Logdlund, M.; Salaneck, W. R., Electroluminescence in conjugated polymers. *Nature* **1999**, 397, (6715), 121-128.

44. Choi, H.; Lipsky, S., Effect of Perfluorocarbons on the Ultraviolet Absorption and Fluorescence Characteristics of Some Saturated Hydrocarbon Liquids. *Journal of Physical Chemistry* **1981**, 85, 4089-4099.
45. Hofmann, U. G.; Peltonen, J., Color transitions in monolayers of a polymerizable single-chain diacetylenic lipid. *Langmuir* **2001**, 17, (5), 1518-1524.

3 CHAPTER 3: THE EFFECT OF PERFLUOROTETRADECANOIC ACID ON THE STRUCTURE OF PHOTOPOLYMERIZED 10,12-PENTACOSADIYNOIC ACID FILMS AT THE AIR–WATER INTERFACE

3.1 Description

This chapter is a copy of a paper published in the *Canadian Journal of Chemistry* [Reproduced with permission from *Can.J.Chem* , **2013**, 91(11): 1130-1138].

In this work, an important new approach for patterning films of the technologically useful luminescent photopolymer PDA was presented. The approach exploits the miscibility of the polymer precursor surfactant molecule with a perfluorinated fatty acid surfactant in mixed surfactant films at the air-water interface; mixed perfluorocarbon-hydrocarbon systems offer a potentially useful and simple way of patterning surfactant films. PDA is a technologically important polymer and the new method described here requires minimal sample preparation, which has significant possible benefits for applications of these materials. A combination of measurements (π -A compression isotherms, AFM, BAM, fluorescence spectrometry) suggested that orientation in these samples was due to buckling, with the underlying driving force for these effects being the stabilizing PF-PCDA interaction, the rigidity of the resulting photopolymer and the applied compressive stress in the Langmuir trough. While the degree of film order obtained was less than that demonstrated for other polymer film patterning methods, the simplicity of the approach suggests that it holds considerable potential for patterning films of these technologically important photopolymers.

The experimental section for this study is provided in the paper. A detailed description of the experimental techniques used is provided in Chapter 1.

3.2 Description of Candidate's Contribution

For this work, I performed all experimental work, played a major role in interpreting the results, wrote the initial draft of the work and participated in revisions to the manuscript. Dr. Matthew Paige provided extensive guidance throughout the experimental work and was greatly involved in interpretation of results, writing and editing the paper.

3.3 Relation of Contribution to Research Objectives

This contribution was solely performed towards the objectives of the thesis research. The ability to pattern PDA is important for potential applications, but in Chapter 2, there was no real control over the structure of the polymer film. In this chapter, an approach to pattern the mixed, polymerized films in a way that required minimal processing was explored. In this alternative preparation technique, films with a significantly higher PCDA content (1PF:4PCDA) compared with those studied previously were deposited onto glass substrates and photopolymerized at the solid-air interface. Atomic force microscope and *in situ* fluorescence spectrophotometry measurements were also performed on deposited films and directly at the air-water interface, respectively, to provide supporting information on film thicknesses. Use of BAM gave the opportunity to study film behavior directly at the air/water interface. Comparison of the BAM results with those collected from AFM experiments allowed exploration of the effect of the solid substrate on the film. The measurements indicated that the solid substrate did not play a major role in the film morphology. A full discussion of the results as part of the whole study is provided in Chapter 6.

3.4 Reprint of Contribution

The effect of perfluorotetradecanoic acid on the structure of photopolymerized 10,12 pentacosadiynoic acid films at the air-water interface

Hessamaddin Younesi Araghi and Matthew F. Paige

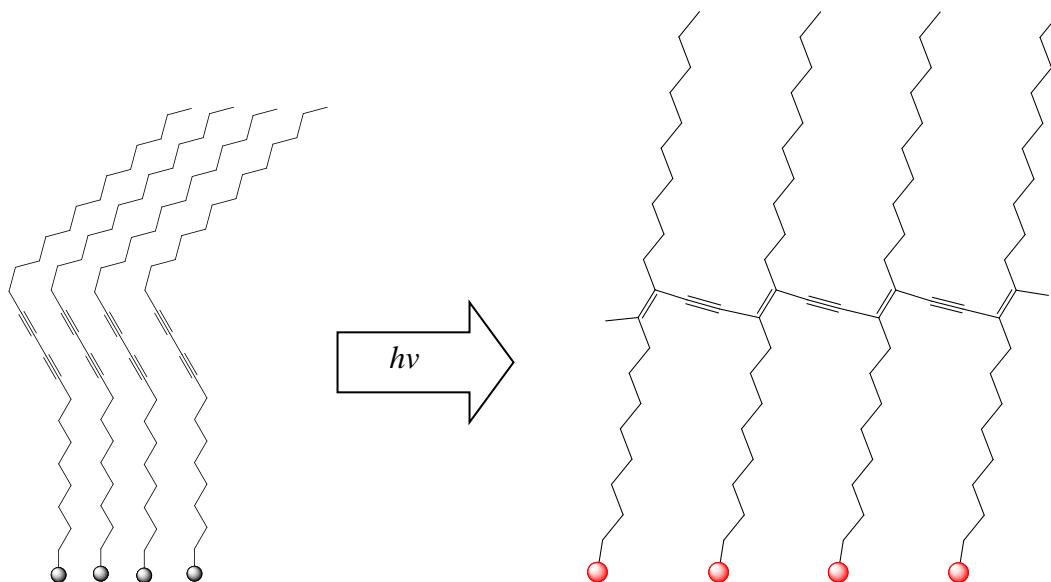
Department of Chemistry, University of Saskatchewan, 110 Science Place,
Saskatoon, SK S7N 5C9
Canada

3.5 Abstract

The influence of the perfluorinated fatty acid perfluorotetradecanoic acid ($\text{CF}_3\text{-(CF}_2\text{)}_{12}\text{-COOH}$; PF) on the structure of films of the photopolymerizable surfactant 10,12 pentacosadiynoic acid (PCDA) has been explored at the air-water interface through a combination of surface pressure-area compression measurements and Brewster angle microscopy imaging during the time course of UV photopolymerization. Addition of the perfluorocarbon to PCDA results in a film structure that differs significantly from the pure PCDA alone, with the most pronounced difference being the formation of photopolymer strands oriented perpendicular to the direction of film compression in a Langmuir trough. Film compression data, supported by *in situ* fluorescence spectrophotometry and Atomic force microscope images of deposited films, suggest that compression-induced stress and accompanying film buckling, enhanced by the strong cohesion between PF and PCDA, contributes to the observed structural differences between the mixed PF – PCDA and pure PCDA photopolymerized films. This approach to forming patterned PDA films is discussed in comparison with other demonstrated methods for structuring this technologically important polymer.

3.6 Introduction

Polydiacetylenes (PDAs), polymers commonly formed through topochemical, UV-induced 1,4 addition of diacetylene functional groups (monomer unit $R-C\equiv C-C\equiv C-R'$; photopolymerization of 10,12 pentacosadynoic acid (PCDA) illustrated in Scheme 3-1) are technologically important materials, having found use in a variety of novel applications ranging from biosensing to non-linear optical device construction¹⁻³. Of particular interest in terms of applications of these materials are their optical properties; PDAs typically exhibit strong absorption and fluorescence in the visible region, with spectroscopic properties being controllable through careful selection of the chemical substituents on the constituent monomers. Further, the optical emission (emission wavelength and efficiency) is a strong function of the mechanical (“mechanochromism”) and thermal (“thermochromism”) states of the polymer, as well as of ligand-binding, with small perturbations to the polymer often resulting in substantial alterations in spectroscopic output. The most widely-exploited of these optical properties for sensing applications is a colorimetric change (transition from a blue, non-fluorescent form to a red, strongly fluorescent form) that occurs upon ligand binding, heating or mechanical perturbation⁴.



Scheme 3-1. Schematic illustration of photopolymerization of PCDA.

Many PDA-based biosensing devices make use of thin polymer films as optical transduction elements and there is considerable interest in patterning films of these materials. A number of PDA patterning approaches have been reported in the literature, including microcontact printing, drop-casting, micromolding in capillaries and 3D replica molding, as well as Langmuir Blodgett (or Langmuir Schaeffer) deposition of mono- and multilayer films⁵⁻¹¹. In terms of Langmuir-based approaches, efforts have largely focused on preparing and characterizing films prepared from the simple fatty acid 10,12 pentacosadiynoic acid (PCDA; Scheme 3-1) and its variants. For example, Carpick et al.⁶ and others have demonstrated that PCDA monolayers (or trilayers upon sufficient film compression) can be formed at the air-water interface, though the films are often unstable in terms of transfer onto solid substrates and inorganic ions (+2 or +3 oxidation numbers) need to be added to aqueous subphases to improve mechanical film stability prior to film deposition. Similar works, observations and applications of these materials are plentiful in the literature, and are described in several reviews on the topic

There have been significant recent advances in the patterning of surfactant films by exploiting miscibility relationships in mixed hydrocarbon-perfluorocarbon surfactant systems (see ¹²⁻¹⁴ and associated publications). This general approach makes use of the lipophobicity of long-chain fluorinated (or perfluorinated) surfactants to yield phase-separated, and under the right conditions, highly-structured mixed films of hydrocarbon-perfluorocarbon surfactant mixtures. In the case of PCDA, recent work in our lab has demonstrated that Langmuir monolayers of PCDA can be significantly stabilized by mixing with perfluorotetradecanoic acid ($\text{CF}_3\text{-(CF}_2\text{)}_{12}\text{-COOH}$; PF) ¹⁵. This enables deposition of LB films onto solid substrates without the use of inorganic ions added to the subphase, and subsequent UV illumination of the films yields micron-scale patches of photopolymer product, albeit with no spatial control over film structure. Under the subphase conditions investigated (pure water subphase, no stabilizing electrolyte), PCDA and PF mix non-ideally at the air-water interface, with a net attractive interaction between components. The resulting LB films are monolayers, with film structure consisting of discrete domains of PCDA surrounded by a continuous matrix of PF (size of the domains could be crudely controlled by adjusting the PF:PCDA mixing ratio). Illumination with UV or visible (532 nm) laser light produces photopolymerized, strongly fluorescent (red) PDA domains with film thicknesses comparable with bilayers (~ 5 nm above the bare underlying substrate). Wang et al. ¹⁶ have investigated a related mixed system (PCDA and a semi-fluorinated tetracosane), but other than a tendency to form an additional half-layer of surfactant at high film compression, noted no particularly remarkable pattern formation in this miscible system.

While useful for film stabilization, this mixed surfactant approach has limited demonstrated capacity for patterning PDAs via Langmuir film approaches. However, there have

been reports of affiliated systems that exhibit significant polymer ordering at the air-water interface; Koga et al.¹⁷ have synthesized a peptide-diacetylene hybrid molecule (based on the pentapeptide Leu-Lys-Leu-Lys-Leu sequence), capable of forming highly-organized β -sheet structures directly at the air-water interface. Tomioka and co-workers¹⁸ have reported the formation of highly-oriented PDA polymers prepared from dibutyl-4,17-dioxo-5,16-dioxa-3,18-diaza-9,11-icosadiynedioate (3BCMUD) that were polymerized directly at the air-water interface, and attributed the orientation effect to packing of the rigid, conjugated polymer backbone in the direction of film compression (large compressive stress) in a Langmuir trough. In our view, the latter effect is of significant potential value for patterning in mixed PF-PCDA films because of the increased stability and rigidity of the mixed films over pure PCDA films alone; one might reasonably expect the high compressive stress accompanying compression of the stabilized film in a Langmuir trough to yield polymer chains oriented normal to the direction of the compression. This approach has the potential to yield patterned surfaces of a technologically useful polymer with minimal processing beyond simple surfactant mixing and film compression. In this investigation, we have explored this possibility through a combination of surface pressure-area compression experiments and Brewster angle microscopy (BAM) imaging experiments on mixed PF-PCDA films before, during and after UV photopolymerization, and as a function of film compression parameters. Atomic force microscope and *in situ* fluorescence spectrophotometry measurements were also performed on deposited films and directly at the air-water interface, respectively, to provide supporting information on film thicknesses. Measurements were focused on 1:4 PF:PCDA mole ratio mixed films; this composition was selected to allow comparison of results with those described previously¹⁵, but also because the

relatively large amount of PCDA in the sample makes detection of the photopolymer relatively easy. Pure PCDA monolayers were also included as simple control samples.

3.7 Experimental section

3.7.1 Chemicals

Perfluorotetradecanoic acid (nominal 97% purity) was purchased from Sigma-Aldrich Corporation while 10,12- pentacosadiynoic acid was purchased from Alfa Aesar. Nakahara et al.¹⁹ have noted that some commercial perfluorocarboxylic acids contain substantial impurities which can affect their surface activity; ¹⁹F-NMR experiments of the commercial product used here showed no detectable impurities, and π -A compression isotherms from multiply-recrystallized PF showed no significant difference from those of the unpurified commercial product indicating that the commercial product was of sufficiently high purity to proceed without additional recrystallization. Similar measurements were carried out with PCDA (purification was carried out by filtration of the commercial product on a silica-gel column), and no significant differences in isotherm behavior (or BAM imaging experiments) were observed between the filtered and stock material. Hence, all experiments were performed with stock materials, without further purification. The solvents hexanes (HPLC grade) and tetrahydrofuran (THF) were purchased from EMD and Merck EM Science, respectively. Stock surfactant solutions were prepared by dissolving the solid hydrocarbon or perfluorocarbon in a 9:1 volume ratio of hexane:THF to a final concentration of 1×10^{-3} M. Microscope cover glass was purchased from VWR International, and was rinsed with absolute ethanol and cleaned for ~20 min in a plasma cleaner (Harrick Plasma, PDC-32G) prior to use. Because of the light sensitivity of PCDA, solution preparation and experiments were performed in the dark wherever possible.

3.7.2 Surface pressure isotherms and Langmuir-Blodgett film preparation

Langmuir film experiments were performed on a KSV 2000 Langmuir trough (KSV Instruments, Helsinki, Finland), at room temperature (22 °C) using ultrapure water (Millipore, resistivity 18.2 M Ω) as a subphase. The water surface was cleaned thoroughly by suction before each experiment and blank runs (compression of the clean surface) showed no appreciable change in surface pressure with compression. For isotherm and deposition experiments, a 100 μ L aliquot of surfactant solution (either the pure component or mixtures as appropriate) was spotted onto the subphase surface, and the solvent was allowed to evaporate for at least 10 minutes. During isotherm measurements, a barrier compression rate of 20 mm.min⁻¹ was used, while for film deposition, the compression rate was 10 mm.min⁻¹. Isotherms were collected in replicate (typically 5-7 samples) and mean molecular areas varied by $\sim \pm 1.5$ %. After the deposition pressure was reached, the film was allowed to stabilize for 20 minutes before the glass substrate was pulled upward through the water-air interface. The film was left to dry at room temperature for one hour before measurement in the AFM.

For polymerization experiments, 100 μ L of a 1:4 PF:PCDA mole ratio mixed solution was spread on the subphase and left for 10 minutes, followed by compression at 10 mm min⁻¹. Upon reaching the desired surface pressure, a short-wavelength UV pen lamp (primary emission output at 254 nm, output power density of 4.5 mW·cm⁻², Edmund Optics) was suspended ~ 10 cm above the subphase surface, turned on and the monolayer was illuminated for ~ 40 minutes. After illumination, the barriers were re-expanded, the polymerized film was given ~ 10 minutes to stabilize and was then compressed at 20 mm min⁻¹ to collect the π -A data.

3.7.3 Atomic force microscope and Brewster angle microscope measurements

AFM measurements were carried out in contact mode in air using a Dimension Hybrid Nanoscope system (Veeco Metrology Group, Santa Barbara, CA). Commercial Si_3N_4 AFM probes (Veeco Metrology Group, Santa Barbara, CA), with spring constant of ~ 0.12 N/m were used for measurements. Control samples of microscope cover glass yielded smooth and featureless images at the nanometer length scale.

BAM measurements were performed on a KSV-NIMA UltraBAM microscope coupled to a Langmuir trough. The microscope used a 50 mW, 658 nm polarized laser for illumination and a CCD detector (collection rate of 20 frames per second). Lateral resolution of the instrument (Rayleigh criterion) was ~ 2 μm and the angle of the incident beam to the air-water interface was fixed at the Brewster angle (53.1°).

3.7.4 In-situ fluorescence spectrophotometry

Fluorescence emission spectra of the polymerized monolayer films were collected using a modified epifluorescence microscope (Nikon Diaphot 200) with laser illumination. The output from a solid-state laser (532 nm, 100 mW, Dragon Lasers) was attenuated to ~ 20 μW (measured at the focal plane) with neutral density filters and focused onto the air-water interface of a Langmuir trough through a quartz window in the bottom of the trough via a microscope objective lens (10x). Fluorescence emission from the polymerized film (“red form”) was collected back through the same objective, passed through an optical emission filter (540LP, Omega Optical), and directed onto a miniature fiber optic-based spectrometer (USB-2000, Ocean Optics). Polymerization was carried out using the UV pen lamp described above. The laser was used to illuminate the sample only during the collection of a fluorescence spectrum and was otherwise blocked to prevent unwanted photopolymerization of the film by the laser.

3.8 Results and Discussion

Compression isotherms (π vs. mean molecular area (MMA)) for the 1PF:4PCDA mixed film were measured before and after illumination at the air-water interface (Figure 3-1). Before illumination, the isotherm consisted of a smoothly increasing curve terminating at a collapse pressure of $\pi_c \sim 32$ mN/m. The limiting area per molecule (A_0), determined by extrapolating the slope of the solid-like region of the isotherm to the x-axis, was $A_0 \sim 26 \text{ \AA}^2$ and was consistent with previous reports for the mixed PCDA-PF system¹⁵. For polymerization measurements, films were compressed to $\pi = 15$ mN/m (optimal pressure for photopolymerization), followed by illumination for ~ 40 minutes, re-expanded and then finally re-compressed. Illumination resulted in the formation of “red” PCDA, which could readily be observed by eye at the air-water interface (Figure 3-2). Isotherms for the polymerized films consisted of a gradual increase in pressure, a plateau at $\pi \sim 34$ mN/m, likely corresponding to the collapse of residual, unpolymerized PCDA, and a final film collapse at $\pi_c \sim 63$ mN/m. Film compressibility (defined as $C_s = -d \ln A / d \pi$) was 5.5×10^{-3} m/mN and 1.7×10^{-2} m/mN for the unpolymerized and polymerized films, respectively, with the former comparable with that expected for liquid-condensed films ($\sim 10^{-3}$ m/mN listed by Petty²⁰).

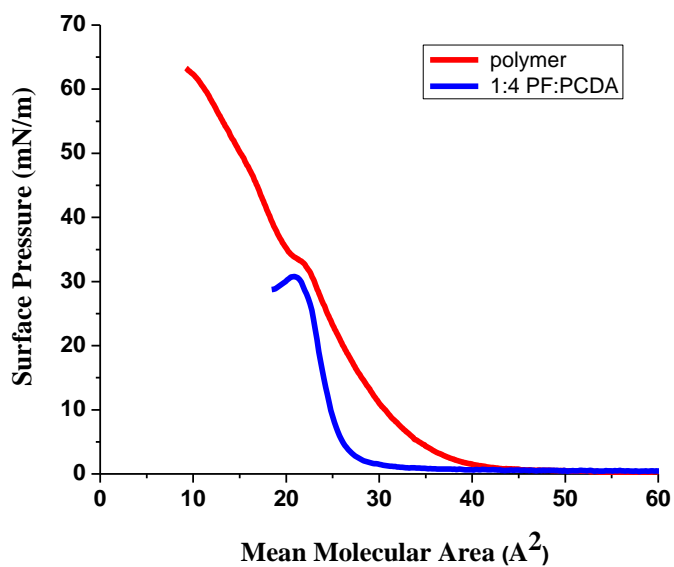


Figure 3-1. π -A compression isotherms for a 1PF:4PCDA mixed monolayer before (blue) and after (red) UV illumination (photopolymerization) on a pure water subphase.



Figure 3-2. Photograph of the experimental apparatus and the air-water interface after ~ 60 minutes of UV illumination. The red PDA photoproduct is readily visible in the image.

The MMA of the mixed film at constant surface pressure (15 mN/m) was monitored as a function of illumination time and was compared with a control film of pure PCDA measured under the same conditions in Figure 3-3. Note, at fixed surface pressure, an increase in MMA corresponds to film expansion, and vice versa. Both the mixed and pure films showed a complex combination of expansions and contractions during illumination. For the mixed film, there was an initial contraction, followed by an expansion and a second contraction (MMA followed a “horizontal s-shape” curve); similar behavior was observed for the pure PCDA film but the rates of expansion and contraction were greater (the pure film reached its minimum area in approximately half the time required for the mixed film to reach the same point) and the initial film area was smaller. The difference in film expansion rates between the pure and mixed film is expected as the effective concentration of the polymerizable surfactant has been lowered by addition of the PF.

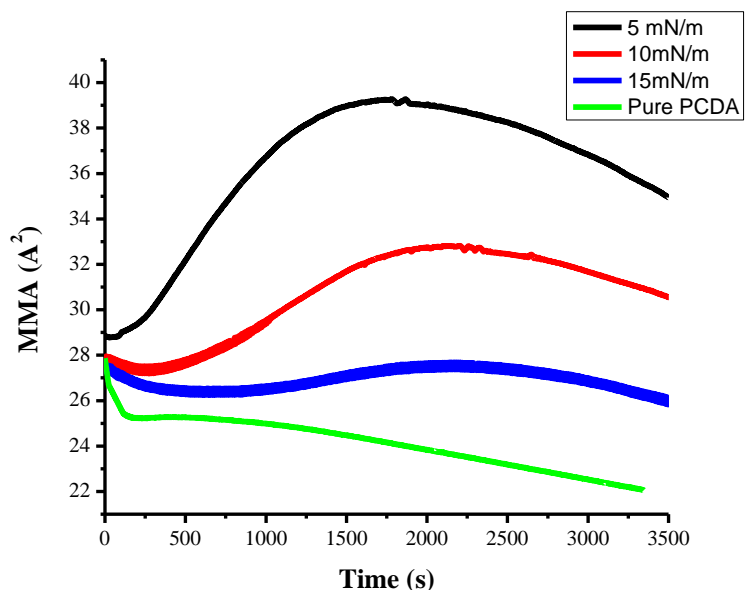


Figure 3-3. Plots showing mean molecular area as a function of illumination time at constant surface pressure for 1PF:4PCDA mixed monolayers at various surface pressures and a pure PCDA monolayer (measured at $\pi = 15$ mN/m).

While numerous authors have reported changes in film areas as a function of PCDA polymerization (see ²¹, for example), comparing results between studies is problematic because the wide range of different experimental conditions used (illumination flux and wavelength, subphase pH and the presence of inorganic ions, the extent of film compression, etc.) will significantly alter film behaviour, and we will not attempt to make a detailed comparison with other studies here. However, we have explored the complex expansions / contractions observed in a systematic way, to rationalize the behavior of the mixed films under our specific experimental conditions.

Results for measurements in which films were compressed to different π values before photopolymerization are shown in Figure 3-3, along with a control experiment in which the MMA was monitored as a function of time both with and without illumination (Figure 3-4). We

re-iterate that in both Figure 3-3 and Figure 3-4, the films were allowed to equilibrate at the air-water interface for ten minutes prior to compression; this is reflected in Figure 3-4 (plot of MMA as a function of total time at the air-water interface) as a break in the time axis. At the lowest surface pressure measured ($\pi = 5$ mN/m), the film expanded to a maximum value until ~ 1750 s of illumination (the net change in MMA was a $\sim 36\%$ increase from the initial film area), after which the film contracted until completion of the experiment (there was a $\sim 20\%$ overall film increase from initial MMA by 3500 s). Curves collected at higher surface pressures ($\pi = 10$ and 15 mN/m) exhibited a smaller initial contraction (by $\sim 1\%$ and $\sim 4\%$, respectively), followed by the expansion and subsequent contraction as was observed at the lower pressure (net change in MMA was $\sim 10\%$ increase and $\sim 5\%$ decrease at 10 and 15 mN/m, respectively). The control measurements shown in Figure 3-4 clearly show that the various film expansions and contractions are not purely photon-driven; measurements without illumination (Figure 3-4, black curve) indicate that a slow film contraction occurs even in the absence of illumination. However, there is a significant influence of illumination. Upon illumination (Figure 3-4, red curve), the rate of film contraction decreases and ultimately reverses, and the subsequent film expansion is clearly photon-driven.

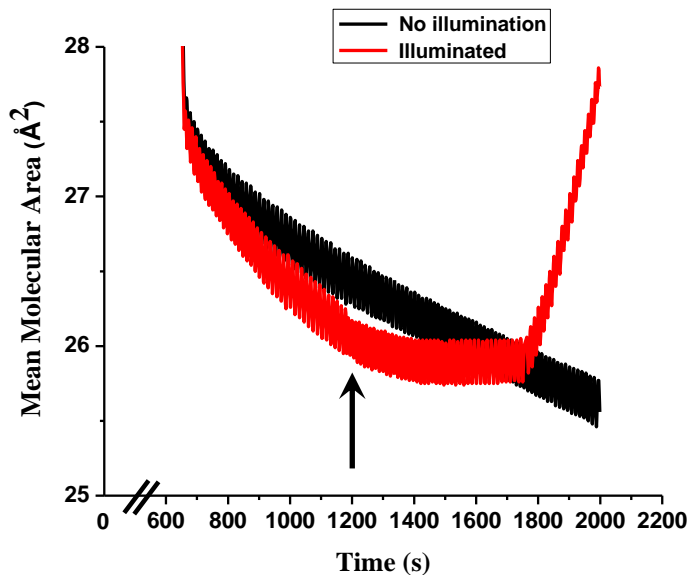


Figure 3-4. Plots showing MMA as a function of time for a 1PF:4PCDA mixed monolayer at the air-water interface. During the initial time period ($t = 0 - 600$ s; data from this region of the curve not shown) the spreading solvent was allowed to evaporate and the film was compressed to the desired pressure ($\pi = 15$ mN/m). The black curve corresponds to a control experiment with no illumination, while the red curve corresponds to an experiment in which illumination commenced at $t = 1200$ s (indicated by an arrow).

Again, while we will not attempt to reconcile these data with all the various studies reported in the literature, some comparison is informative. Huilin et al.²¹ have carried out similar measurements for pure PCDA monolayers on an aqueous Cd^{2+} subphase at 30°C , and observed two different behavior regimes. In their study, monolayers at lower pressures ($\pi = 15$ mN/m) exhibited an initial contraction upon illumination, followed by a gradual expansion ($\sim 31\%$ overall increase) with time. This was proposed to be the consequence of PDA polymers exhibiting continuously flexible Porod-Kratky (worm-like chain) behavior, in which the photopolymer can form loops, stand vertical to the subphase and generally occupy more surface area at the air-water interface than rigid, close-packed polymers. In the high pressure regime ($\pi = 35$ mN/m), Huilin et al.'s films underwent a very brief expansion, followed by a significant contraction ($\sim 50\%$ decrease). The contraction was attributed to the immediate collapse of the

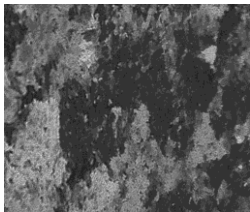
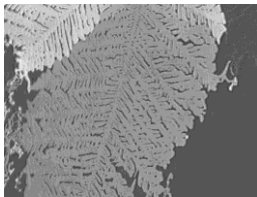
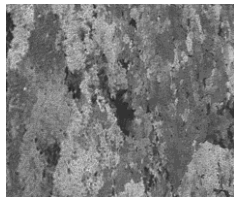

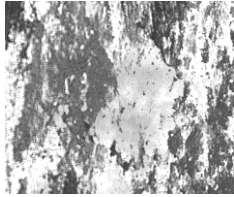
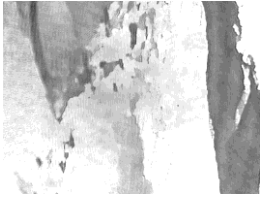

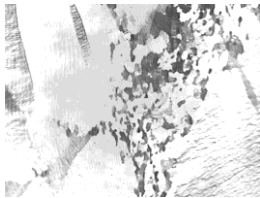

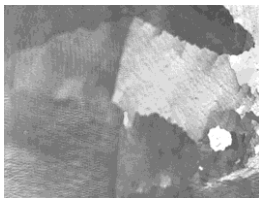
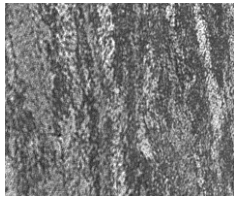
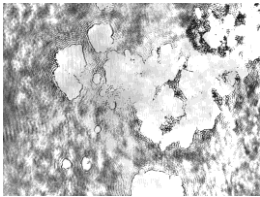
monolayer upon polymerization ($\pi_c = 31$ mN/m for the polymerized film under the subphase conditions used). This mechanism cannot explain our observations for the mixed 1PF:4PCDA films studied here; in addition to an entirely different expansion-contraction behavior, the mixed monolayer collapses at a much higher surface pressure ($\pi_c = 63$ mN/m, consistent with the expected stabilization brought about by the attractive PF-PCDA interaction) and as such the addition of the perfluorinated component to PCDA results in alternative film dynamics at the air-water interface.

To clarify the nature of the diverse expansion and contraction behaviour observed during polymerization, BAM images of mixed and pure surfactant films at the air-water interface were collected and are shown in Table 3-1. For these images, contrast and brightness settings were kept constant throughout, and as such, any differences in the images is the result of actual reflectivity of the films. A representative surface pressure of $\pi = 15$ mN/m was selected in order to study all of the expansion and contraction processes exhibited by the films throughout the polymerization process, but the differences as a function of pressure will also be discussed in subsequent text. Note, perfluorocarbons have refractive indices that are comparable with water (See Skoog et al. ²²; control samples of pure PF films yield no image contrast), and therefore, bright regions in BAM images correspond to the PCDA (or PDA, after polymerization), whereas dark regions are either PF, water or a mixture of both. We further note that BAM contrast is principally controlled by film thickness (albeit with minor contrast variations caused by regions of the film with different molecular tilt azimuths ²³⁻²⁵). Complications can arise when imaging surfactant films comprised of optically absorbing molecules. Gruniger et al. ²⁶ have reported enhanced light reflection from the air-water interface when the adsorbate film can absorb the incident light. The reflection enhancement, which is attributed to constructive interference

between light scattered from the air-water interface and scattered light from the optically absorbing molecules, was reported to scale linearly with optical absorbance. Fortunately, the polymer formed under the conditions used here is exclusively the “red” form of PDA (fluorescence emission spectra for monolayer reported in subsequent figures), and control measurements of monolayer films indicate that the polymer absorption at 658 nm (the wavelength for the BAM light source) is negligible. Further, the relative change in BAM signal upon polymerization is substantial (pixel values increase by almost 200%), and even a small increase in absorbance of the film upon polymerization that is at the detection limit of our spectrometer cannot explain the large change in film reflectivity. Hence, we can reasonably ascribe differences between images to variations in the overall film thickness, and additional independent measurements (AFM and fluorescence spectrometry; *vide infra*) support this assignment.

Upon addition of the surfactant to the subphase and before illumination, numerous highly-reflective patches (assignable to PCDA, as noted above) were observed for the mixed films. The patches formed spontaneously without application of surface pressure (Table 1, Panel A). Surface coverage was not homogeneous; in addition to patches, occasional dendritic structures were also observed, consistent with observations by Volinsky et al.²⁷, and Wang et al.²⁸, and all film structures were highly-mobile, with patches moving (by means of diffusion and convection) rapidly through the focal volume. However, unlike previously reported dendritic structures, those formed with the mixed 1PF:4PCDA did not remain after film compression, indicating they are unstable, transient kinetic structures on the dynamic subphase surface.

Table 3-1. Table of BAM images comparing film structures of 1PF:4PCDA and pure PCDA monolayers as a function of illumination time. Inset BAM images are 520 μm x 380 μm in size. Contrast and brightness in the BAM images was kept fixed throughout the experiment and differences between images are caused by reflectivity differences in the films.

<i>Panel:</i>	<i>Illumination time (s)</i>	<i>Surface Pressure (mN/m)</i>	<i>1PF:4PCDA</i>	<i>PCDA</i>
(A)	Before illumination	0		
(B)	Before illumination	15		
(C)	100	15		
(D)	400	15		
(E)	1500	15		
(F)	3000	15		

During the time interval before illumination (Table 3-1, Panel A, B; this includes the spreading and compression of the mixed film to $\pi = 15$ mN/m), a slow film-reorganization process was observed. Films initially consisted of dispersed, highly reflective patches separated by regions of low-reflectivity. The low-reflectivity regions of the film became smaller in area as a function of time, indicating that unoccupied void regions were being back-filled by PCDA (consistent with the initial film contraction observed in Figure 3-3). Despite this effect, films remained heterogeneous throughout the experiment and consisted of both high- and low-reflectivity regions, likely because there are remaining unoccupied void regions in the films.

Upon illumination, film structures changed markedly, with a significant increase in film reflectivity observed. Films were again non-uniform, but exhibited much greater reflectivity than before illumination, suggesting the co-existence of multiple layers of polymerized PDA. Maximum overall reflectivity was observed after ~ 100 s of illumination (Table 3-1, Panel C), with further illumination resulting in a general decrease in reflectivity (the BAM image in Table 3-1, Panel D is representative, though images collected between 100 – 400 s showed a systematic decrease in reflectivity). Most significantly, after long illumination times, BAM images for the mixed films revealed regions of linear stripes that were hundreds of microns in length, with their long axes oriented perpendicular to the direction of film compression (larger scale image shown in Figure 3-5). This degree of orientation was not observed for the control samples of PCDA alone, as is apparent from Table 3-1 Panel F.

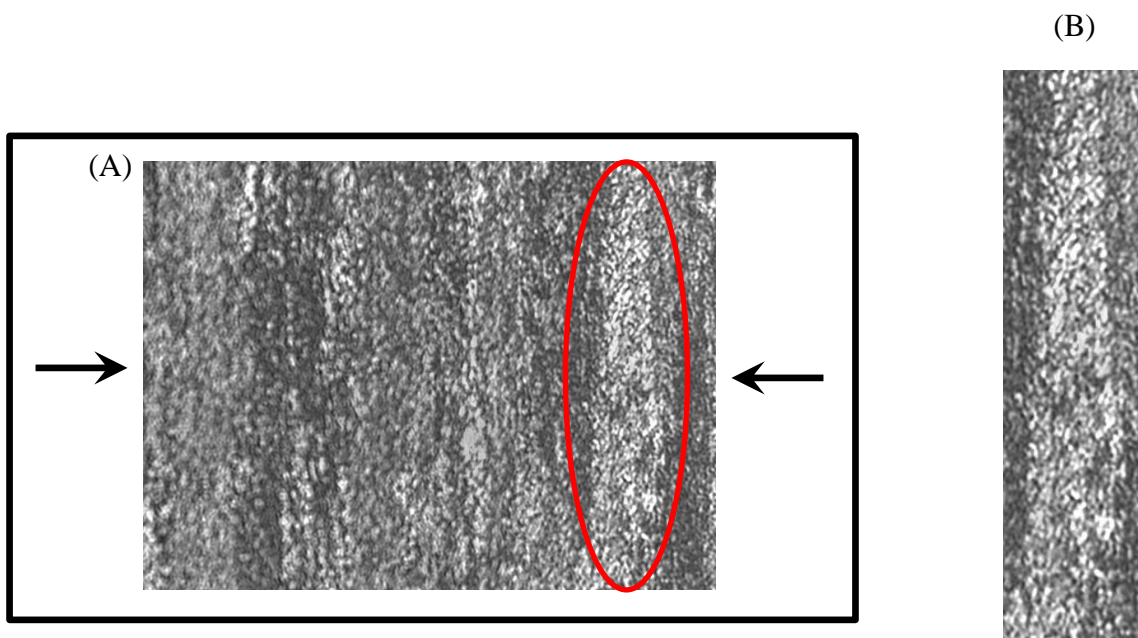


Figure 3-5. A) Expanded view BAM image ($520\ \mu\text{m} \times 380\ \mu\text{m}$) of mixed film at the air-water interface after ~ 60 minutes of illumination time. The direction of film compression by the trough barriers is indicated by the black arrows. B) A zoom-in section of the image (corresponding region indicated by the red ellipse) has been included for closer inspection.

Our interpretation of the cumulative data from Figures 3-3, 3-4 and Table 3-1 is as follows: (i) First, upon reaching the target surface pressure, but before illumination, the mixed film re-structures, with PCDA molecules packing together and filling voids in the monolayer, to form a compact film. This is accompanied by a slow film contraction as observed in the control sample without illumination (Figure 3-4, black curve). We note that this re-structuring is consistent with the pressure-dependence data shown in Figure 3-3. At the lower film pressures, the initial film contraction is not present, as the driving force for re-structuring is negligible. (ii) Upon illumination, three simultaneous and competing processes take place, including continued re-structuring (the film contracts), lateral expansion (the film expands; this effect is well known from pure PCDA polymerization experiments and has been reported previously^{21, 29, 30}) and finally, film “buckling”, in which multimolecular deposits of photopolymer lift up from the

subphase surface to form thick aggregates (the film contracts). The first and last processes are in competition with the second, with the net result being a slow film expansion. Next, (iii), there is a time interval in which the buckling process is largely complete and lateral film expansion dominates. Finally, (iv), a slow relaxation and re-arrangement of the aggregates occurs, leading to a slow film contraction to produce the final, ordered film. After sufficient time for ordering has passed, the compressive force of the trough barriers acting on the film causes the polymers to orient such that extended polymer strands orient perpendicular to the direction of the compressive force (i.e. the long axis of the polymer orient parallel to the trough barriers).

Of particular importance in this proposed interpretation is the competition in regime (ii) between lateral film expansion and “buckling”. Buckling of two-dimensional polymer networks is a well-known phenomenon (for example, see Bourdieu et al.³¹). For polydiacetylene-based phospholipid systems, Morigaki et al.²⁹ have described a similar effect in their investigation of phospholipid bilayers on solid substrates, in which the lateral expansion which accompanied photopolymerization of bilayers constrained to a solid substrate generated internal mechanical stress in the system. The mechanical stress was subsequently relieved by spontaneous detachment of the bilayer from the solid support. While the films measured in our studies are not constrained to a solid substrate, they are maintained at a high surface pressure at the air-water interface and are further stabilized through the cohesive PCDA-PF interaction. As noted above, the resultant photopolymer has very modest C_s values. In effect, the polymer chains are flexible and can “pop up” from the surface to relieve internal film stress. As such, it is reasonable to assume that under these conditions, the driving force for film buckling will be substantial.

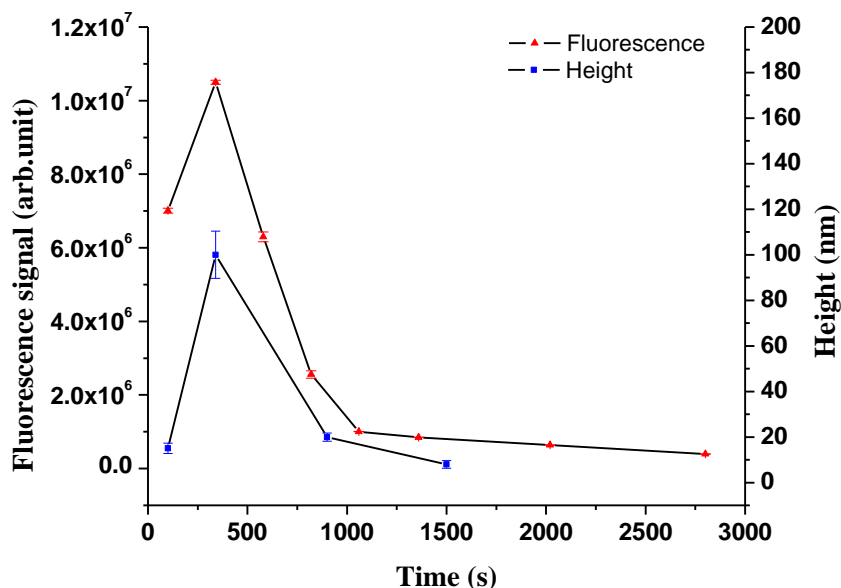


Figure 3-6. Plot showing integrated fluorescence intensity (red; measured by *in situ* fluorescence spectrophotometry) and mean surface feature height (blue; measured by AFM) versus illumination time for the mixed monolayer at the air-water interface. Solid lines are a guide to the eye.

To provide further support for this proposed mechanism, the thickness of the polymer films was measured as a function of polymerization time by AFM imaging of deposited films and by *in situ* fluorescence spectrophotometry directly at the air-water interface. For AFM thickness measurements, samples were deposited at $\pi = 15$ mN/m onto solid glass substrates and imaged with the AFM (representative images for samples measured different illumination times are included as Supporting Information). Film thicknesses were taken as the average height of topographical features over the underlying substrate, and in all cases were found to be greater than the thickness anticipated for a single monolayer (~ 2.5 nm, as reported elsewhere¹⁵). In terms of fluorescence spectrophotometry, the appearance of the strong fluorescence from the red form of the photopolymer provided an easily detectable means of verifying and tracking the polymerization process directly at the air-water interface (upon illumination, fluorescence intensity increased, eventually reaching the saturation limit of the spectrometer, and then

underwent a slow decrease in overall fluorescence intensity; raw spectra are shown as Supporting Information). For these measurements, the total integrated intensity of the red PDA fluorescence emission spectrum was taken as being proportional to the total amount of photopolymer in the illumination volume. The cumulative result of film thickness measurements by both AFM and fluorescence are shown in Figure 3-6. The net integrated fluorescence intensity tracked remarkably well with the film thickness measurements from the AFM. Again, these results are entirely consistent with the proposed air-water film dynamics. The photopolymerization process generates thick multilayers and buckled structures; this compact film contains a large amount of densely packed luminescent material, leading to a strong overall fluorescence signal. As the film undergoes restructuring and expansion, the large, strongly fluorescent aggregates spread and re-integrate to form a more expanded, thin layer, and hence the amount of luminescent material in the collection volume decreases.

The film buckling effect proposed above bears some final, further consideration and exploration. Clearly, if buckling is taking place, the extent to which it occurs should depend strongly upon the surface pressure at which the system is maintained, with more heavily compressed films leading to greater internal stress in the polymer chains, buckling and hence thicker average film structures. Of course, the degree of efficiency of topochemical photopolymerization will depend strongly upon the degree of film packing as well, though from re-inspection of Figure 3-3, it is clear that polymerization still takes place with reasonable efficiency even at $\pi = 5$ and 10 mN/m. These lower pressure curves bear additional consideration. Much of the complexity associated with the high pressure curves (contraction, followed by slow then rapid expansion and a final contraction) becomes less pronounced at lower pressures, and in the case of $\pi = 5$ mN/m, the film simply undergoes an expansion-

contraction cycle. This is precisely the film dynamics that are expected to occur if there is negligible film buckling; that is, predominantly lateral expansion due to photopolymerization, followed by film reorganization. Films that were photopolymerized for 1500 s at these lower surface pressures were deposited onto substrates and imaged in the AFM (Figure 3-7 A, B for $\pi = 5, 10$ mN/m, respectively).

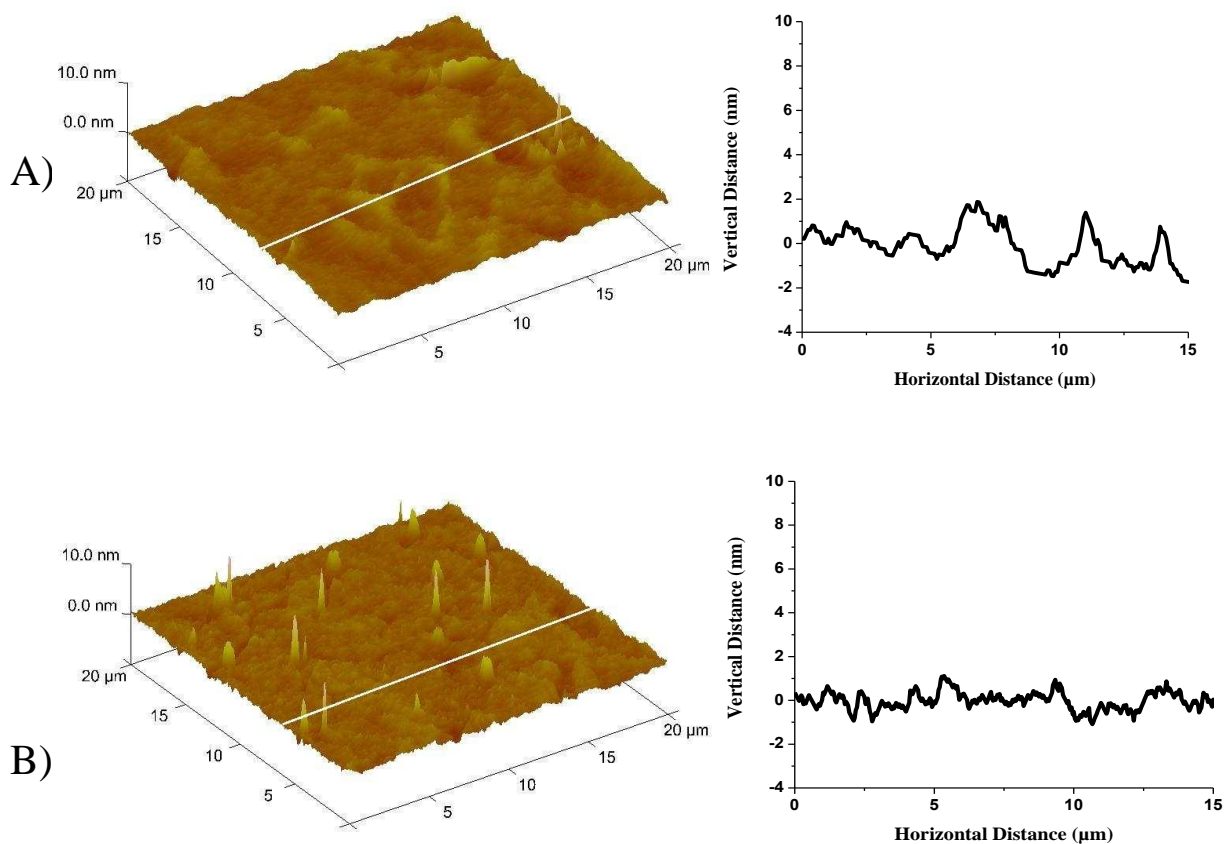


Figure 3-7. AFM height images ($20\ \mu\text{m} \times 20\ \mu\text{m}$) and corresponding cross sectional analysis for 1PF:4PCDA films deposited at A) $\pi = 5\ \text{mN/m}$; and B) $\pi = 10\ \text{mN/m}$ onto mica substrates after 1500 s of UV photopolymerization.

Film features for the $\pi = 5\ \text{mN/m}$ sample were typically on the order of 2 nm in height, suggesting the presence of a PDA, while the $\pi = 10\ \text{mN/m}$ was similar, though a small number of multilayer ($\sim 10\ \text{nm}$) aggregates were also observed. From these measurements, we can reasonably conclude that application of higher surface pressures promotes the buckling process that leads to the formation of multilayers and aggregates in this mixed film system, whereas the effect can be minimized through application of significantly smaller surface pressures.

Finally, we return our attention to the oriented nature of the polymer films after prolonged illumination. While the BAM images indicate there is tendency for the photopolymerized, mixed films to preferentially form into long strands or sheets oriented perpendicular to the direction of applied stress, macroscopic images of the air-water interface (Figure 3-2) clearly show that there is a significant degree of heterogeneity in the films. To measure the extent of film ordering, we have measured the fluorescence anisotropy of the deposited films using a variation of the microscope used for the *in situ* fluorescence microscopy measurements. These measurements exploit the well-defined orientation of the emission transition dipole for PDA, which lies parallel with the long axis of the polymer (eg. along the conjugation length)¹. Briefly, the polarization of the incident laser light was adjusted between vertical and horizontal by using a Berek variable wave plate (New Focus) in conjunction with a linear (excitation) polarizer (Thor Labs). Fluorescence emission was directed through a longpass filter (Omega Filters) to remove residual excitation light and an appropriately oriented linear (analyzer) polarizer was used to select for vertical or horizontal emission. Results from anisotropy measurements are shown in Figure 3-8, with I_{\parallel} and I_{\perp} corresponding to the fluorescence emission spectrum collected with the analyzer oriented parallel and perpendicular to the plane of the incident excitation light, respectively. It should be noted that the sensitivity of the detection system to different polarizations has the potential to distort measured anisotropies, and this must normally be accounted for by an instrument-dependent “G-factor”³². While we will not attempt to interpret the measured data here in a quantitative fashion, and thus forsake introducing a G-factor into the results, we note that these distortion effects are minimal for our setup (anisotropy from light scattered by a solution of colloidal silica gave $r = 0.97$, compared to

an ideal value of $r = 1.00$), and thus differences in measured emission spectra can be attributed to real differences in film orientation.

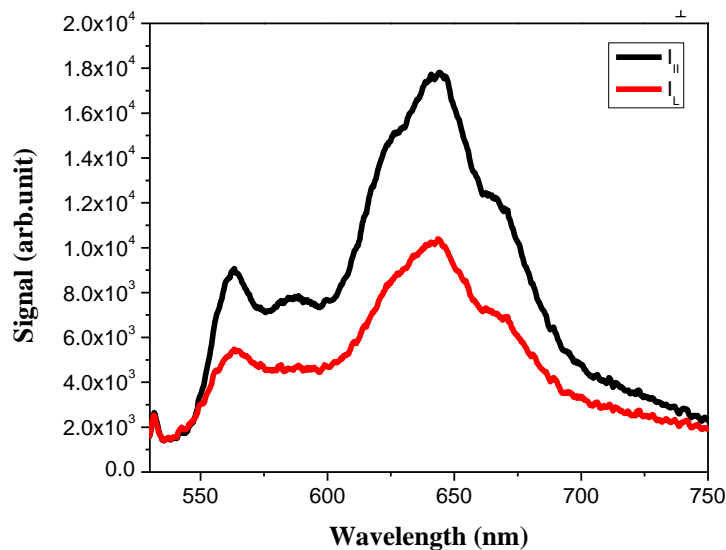


Figure 3-8. Bulk anisotropy measurements for a mixed, photopolymerized 1PF:4PCDA film deposited onto a glass substrate. The black and red curves correspond to parallel and perpendicular orientation of the analyzer, respectively.

The spectra in Figure 3-8 clearly indicate a preferred orientation for the photopolymer in the mixed, polymerized films. As a crude measure of anisotropy, we have calculated $I_{||} / I_{\perp}$, the integrated ratio of fluorescence intensities for the two different analyzer orientations, and obtained a mean value of 1.5 ± 0.3 , measured over $n = 8$ independent samples. While the measured value indicates a modest degree of polymer orientation in the samples, it is significantly lower than that reported for more highly-ordered films (for example, Hao et al.³³ have reported intensity ratios of 1.8 for friction-transferred films of conjugated fluorescent polymers, using a similar microscope-based measurement approach). Further, close inspection of the BAM image in Figure 3-5B reveals that the strands and stripes are comprised of smaller substructures (presumably polymer aggregates) that have various orientations with respect to the

compression axis. Thus, it appears that the polymer films do not consist of perfectly oriented strands of polymer, but rather multiple fragments of polymerized material with a weak tendency to order normal to the compression axis.

At present, the degree of film ordering and long-range homogeneity that can be accomplished using this approach is less than that demonstrated for microcontact printing and variations on molding^{5, 7-11}, the relative simplicity of the sample preparation suggests significant potential utility for further applications, if the process can be further improved. Further attempts to increase the degree of film ordering through refinement of the composition of the mixed films (mole fraction of PF, compression pressure, photoillumination time) is ongoing and will be the topic of future work.

3.9 Conclusions

In this work, we present an important approach for patterning films of the technologically useful luminescent photopolymer PCDA. The approach exploits the miscibility of the polymer precursor surfactant molecule, PDA, with a perfluorinated fatty acid surfactant, PF in mixed surfactant films at the air-water interface; the physical chemical properties of mixed perfluorocarbon-hydrocarbon films has been studied extensively in the literature and these systems offer a potentially useful and simple way of patterning surfactant films^{13, 14, 34}. PCDA is a technologically important polymer, and while there are a number of other demonstrated approaches for patterning PCDA^{5-8, 11}, the approach described here requires minimal sample preparation beyond simple mixing of reagents and film compression. A combination of measurements (π -A compression isotherms, AFM, BAM, fluorescence spectrometry) suggest that orientation in these samples is due to buckling and orientation of the UV-induced photopolymer, with the underlying driving force for these effects being the stabilizing PF-PCDA

interaction, the rigidity of the resulting photopolymer and the applied compressive stress in the Langmuir trough. While the degree of film obtained is less than that demonstrated for other polymer film patterning methods, the simplicity of the approach suggests that it holds considerable potential for patterning films of these technologically important photopolymers.

3.10 Supporting Information

AFM images of mixed films at different photopolymerization times. Raw fluorescence spectra of film at air-water interface during photopolymerization.

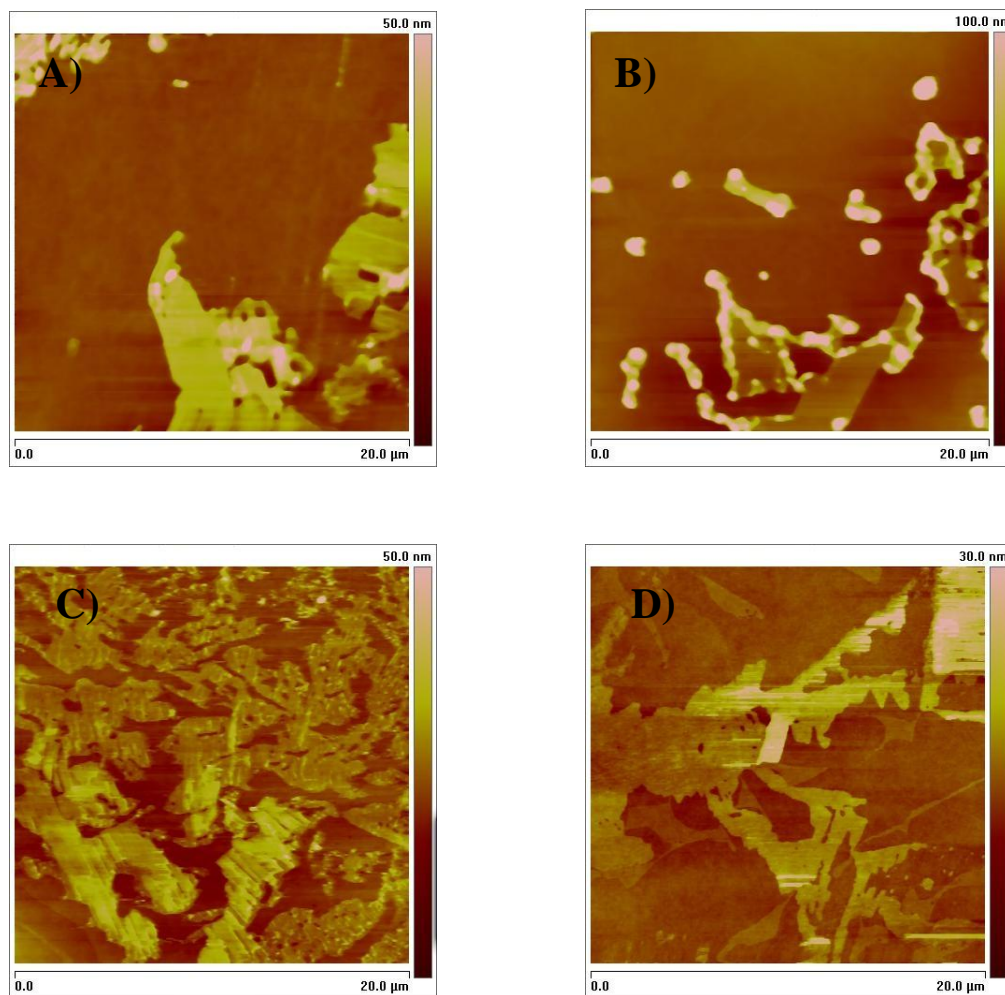


Figure S 3-1. AFM height images (20 μm x 20 μm) for 1PF:4PCDA films deposited at $\pi = 15$ mN/m onto glass substrates after various photopolymerization times. A) 100 s; B) 300 s; C) 900 s; D) 1500 s.

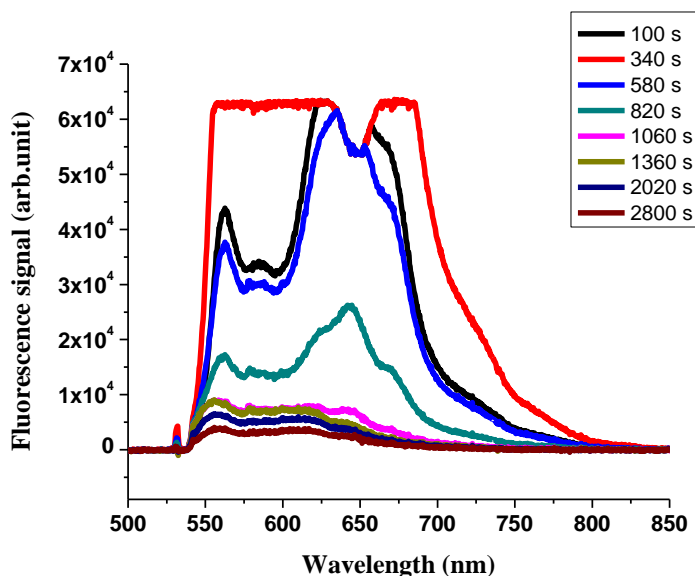


Figure S 3-2. Plot showing time evolution of fluorescence emission spectra for 1PF:4PCDA monolayer at the air-water interface upon photopolymerization with a UV pen-lamp (532 nm excitation).

3.11 Acknowledgments

Funding for this work was provided by the Natural Sciences and Engineering Research Council of Canada (NSERC), the Canada Foundation for Innovation (CFI), the Province of Saskatchewan and by the University of Saskatchewan. Dr. Neeraj Giri is acknowledged for assisting with the polarization anisotropy measurements.

3.12 References

1. Carpick, R. W.; Sasaki, D. Y.; Marcus, M. S.; Eriksson, M. A.; Burns, A. R., Polydiacetylene films: a review of recent investigations into chromogenic transitions and nanomechanical properties. *Journal of Physics: Condensed Matter* **2004**, *16*, R679-R697.
2. Enkelmann, V., Structural aspects of the topochemical polymerization of diacetylenes. *Advances in Polymer Science* **1984**, *63*, (Polydiacetylenes), 91-136.

3. Okada, S.; Peng, S.; Spevak, W.; Charych, D., Color and chromism of polydiacetylene vesicles. *Accounts of Chemical Research* **1998**, 31, (5), 229-239.
4. Ahn, D. J.; Kim, J. M., Fluorogenic polydiacetylene supramolecules: Immobilization, micropatterning, and application to label-free chemosensors. *Accounts of Chemical Research* **2008**, 41, (7), 805-816.
5. Baek, J. H.; Ahn, H.; Yoon, J.; Kim, J.-M., Micro-patterning of polydiacetylene supramolecules using micromolding in capillaries (MIMIC). *Macromolecular Rapid Communications* **2008**, 29, 117-122.
6. Carpick, R. W.; Sasaki, D. Y.; Burns, A. R., First observation of mechanochromism at the nanometer scale. *Langmuir* **2000**, 16, (3), 1270-1278.
7. Choi, J.-M.; Yoon, B.; Choi, K.; Seol, M.-L.; Kim, J.-M.; Choi, Y.-K., Micropatterning polydiacetylene supramolecular vesicles on glass substrates using a pre-patterned hydrophobic thin film. *Macromolecular Chemistry and Physics* **2012**, 213, 610-616.
8. Lee, C. H.; Oh, E.-H.; Kim, J.-M.; Ahn, D. J., Immobilization of polydiacetylene vesicles on cellulose acetate butyrate (CAB)-coated substrates for self-assembled supramolecular sensor arrays. *Colloids and Surfaces A: Physicochemical and Engineering Aspects* **2008**, 313, 500-503.
9. Lee, J.; Yarimaga, O.; Lee, C. H.; Choi, Y.-K.; Kim, J.-M., Network Polydiacetylene Films: Preparation, Patterning, and Sensor Applications. *Advanced Functional Materials* **2011**, 21, (6), 1032-1039.
10. Shim, H. Y.; Lee, S. H.; Ahn, D. J.; Ahn, K.-D.; Kim, J.-M., Micropatterning of diacetylenic liposomes on glass surfaces. *Materials Science and Engineering C* **2004**, 24, 157-161.

11. Yarimaga, O.; Lee, S.; Kim, J.-M.; Choi, Y.-K., Fabrication of patterned polydiacetylene composite films using a replica-molding (REM) technique. *Macromolecular Rapid Communications* **2010**, 31, 270-274.
12. Krafft, M. P.; Riess, J. G., Chemistry, physical chemistry, and uses of molecular fluorocarbon--hydrocarbon diblocks, triblocks, and related compounds--unique "apolar" components for self-assembled colloid and interface engineering. *Chemical Reviews* **2009**, 109, (5), 1714-1792.
13. Matsumoto, M.; Tanaka, K.; Azumi, R.; Kondo, Y.; Yoshino, N., Structure of phase-separated Langmuir-Blodgett films of hydrogenated and perfluorinated carboxylic acids investigated by IR spectroscopy, AFM, and FFM. *Langmuir* **2003**, 19, (7), 2802-2807.
14. Qaqish, S. E.; Paige, M. F., Structural and compositional mapping of a phase-separated Langmuir-Blodgett monolayer by atomic force microscopy. *Langmuir* **2007**, 23, (5), 2582-2587.
15. Younesi Araghi, H.; Paige, M. F., Deposition and photopolymerization of phase-separated perfluorotetradecanoic acid-10,12-pentacosadiynoic acid Langmuir-Blodgett monolayer films. *Langmuir* **2011**, 27, (17), 10657-10665.
16. Wang, S.; Lunn, R.; Krafft, M. P.; Leblanc, R. M., One and a half layers? Mixed Langmuir monolayer of 10,12-pentacosadiynoic acid and a semifluorinated tetracosane. *Langmuir* **2000**, 16, 2882-2886.
17. Koga, T.; Taguchi, T.; Higashi, N., β -sheet peptide-assisted polymerization of diacetylene at the air-water interface and thermochromic property. *Polymer Journal* **2012**, 44, 195-199.
18. Tomioka, Y.; Imazeki, S.; Tanaka, N., Highly oriented polydiacetylene monolayer formed at the air-water interface. *Chemical Physics Letters* **1990**, 174, (5), 433-437.

19. Nakahara, H.; Shibata, O., Langmuir monolayer miscibility of perfluorocarboxylic acids with biomembrane constituents at the air-water interface. *Journal of Oleo Science* **2012**, 61, (4), 197-210.
20. Petty, M. C., *Langmuir-Blodgett Films: An Introduction*. Cambridge University Press: Cambridge, 1996.
21. Huilin, Z.; Weixing, L.; Shufang, Y.; Pingsheng, H., Polymerization of 10,12-pentacosadiynoic acid monolayer at varying surface pressure and temperature. *Langmuir* **2000**, 16, (6), 2797-2801.
22. Skoog, D. A.; Holler, J. F.; Nieman, T. A., *Principles of Instrumental Analysis*. 5 ed.; Nelson Thomson Learning: Toronto, 1998.
23. Henon, S.; Meunier, J., Microscope at the Brewster angle: direct observation of first-order phase transitions in monolayers. *Review of Scientific Instruments* **1991**, 62, (4), 936-9.
24. Tabe, Y.; Yokoyama, H., Fresnel formula for optically anisotropic Langmuir monolayers: an application to Brewster angle microscopy. *Langmuir* **1995**, 11, (3), 699-704.
25. Weidemann, G.; Gehlert, U.; Vollhardt, D., Inner Structure of Condensed Phase Domains in Monolayers at the Air-Water Interface. *Langmuir* **1995**, 11, (3), 864-71.
26. Gruniger, H.; Mobius, D.; Meyer, H., Enhanced light reflection by dye monolayers at the air-water interface. *Journal of Chemical Physics* **1983**, 79, (8), 3701-3710.
27. Volinsky, R.; Gaboriaud, F.; Berman, A.; Jelinek, R., Morphology and Organization of Phospholipid/Diacetylene Langmuir Films Studied by Brewster Angle Microscopy and Fluorescence Microscopy. *J. Phys. Chem. B* **2002**, 106, (36), 9231-9236.

28. Wang, S.; Ramirez, J.; Chen, Y.; Wang, P. G.; Leblanc, R. M., Surface Chemistry, Topography, and Spectroscopy of a Mixed Monolayer of 10,12-Pentacosadiynoic Acid and Its Mannoside Derivative at the Air-Water Interface. *Langmuir* **1999**, 15, (17), 5623-5629.
29. Morigaki, K.; Schoenherr, H.; Okazaki, T., Polymerization of Diacetylene Phospholipid Bilayers on Solid Substrate: Influence of the Film Deposition Temperature. *Langmuir* **2007**, 23, (24), 12254-12260.
30. Pingsheng, H.; Huililn, Z.; Gang, Z., Polymerization kinetics of 10,12-pentacosadiynoic acid monolayer and possible acceleration effect of visible light. *Polymer* **2003**, 44, (11), 3235-3241.
31. Bourdieu, L.; Daillant, J.; Chatenay, D.; Braslau, A.; Colson, D., Buckling of polymerized monomolecular films. *Physical Review Letters* **1994**, 72, (10), 1502-1505.
32. Lakowicz, J. R., *Principles of Fluorescence Spectroscopy*. 3rd ed.; Springer: New York, 2006.
33. Hao, X. T.; Chan, N. Y.; Heck, C.; Tanigaki, N.; Paige, M. F.; Dunstan, D. E.; Smith, T. A., "Log-Rolling" Alignment in Friction-Transferred Light-Emitting Conjugated Polymer Thin Films. *Macromolecules* **2010**, 43, (24), 10475-10480.
34. Krafft, M. P., Large organized surface domains self-assembled from nonpolar amphiphiles. *Accounts of Chemical Research* **2012**, 45, (4), 515-524.

4 CHAPTER 4: POLARIZED FLUORESCENCE MICROSCOPY OF PATTERNED, POLYMERIZED PERFLUOROTETRADECANOIC ACID – PENTACOSADIYNOIC ACID THIN FILMS

4.1 Description

This chapter is a copy of a paper published in *Spectrochimica Acta Part A: Molecular and Biomolecular Spectroscopy*. [Reproduced with permission from: *Spectrochimica Acta Part A: Molecular and Biomolecular Spectroscopy* **2014**, 129, 339-344]

This chapter describes an investigation of the spatial orientation of polymer fibers prepared from the photopolymerization of mixed perfluorotetradecanoic acid and 10, 12-pentacosadiynoic acid films by dual-view polarized fluorescence microscopy. In these polymer systems, fluorescence anisotropy can be used to probe the orientation of the fibers' underlying PCDA polymer backbone because of the correlation between polymer structure and its emission transition dipole moment. Fluorescence anisotropy was measured within individual polymer fibers as well as between different polymer fibers, with experimental results indicating a high degree of orientation in both cases. Results were compared with those obtained from "bulk" anisotropy measurements, which also indicated that the degree of films orientation. Brewster angle microscopy images, collected for polymer films at the air-water interface suggest that the polymer consists of oriented, parallel ribbons at the air-water interface, and that these structures are successfully transferred onto the solid substrates during film deposition.

4.2 Description of Candidate's Contribution

For this contribution, I carried out all experimental works including sample preparation, AFM and BAM measurements. I played the primary role in setting up the fluorescence microscope and carrying out all of the measurements. I played a major role in interpreting the results, wrote the initial draft of the work and participated in the following editing in response to collaborators and editors. Dr. Neeraj Giri helped with the microscope setup, polarization measurements and was involved in interpreting and editing the paper. Dr. Matthew Paige provided extensive guidance throughout the experimental work and was greatly involved in results interpretation, writing and editing the paper.

4.3 Relation of Contribution to Research Objectives

This work was solely performed towards the objectives of the thesis research. In the previous chapters the mixed monolayers of photopolymerizable surfactant - perfluorinated fatty acid was characterized in terms of surfactant miscibility, spectroscopic properties, morphology and potential approaches to pattern it on glass substrates. The ability to pattern the material is important for potential applications. In this chapter, the degree of polymer film ordering was assessed using a novel form of fluorescence microscopy based on polarized emission. Atomic force microscope measurements were performed on deposited films to provide supporting information on film structure and morphology. Brewster angle microscope images provided more information on films behavior at air-water interface. It was concluded from the measurements that individual fibers consisted of multiple photopolymer strands with various orientations, and that there was a preferred orientation for fibers in the film as a whole. A full discussion of the results as part of the whole study is provided in Chapter 6.

4.4 Reprint of Contribution

Polarized fluorescence microscopy analysis of patterned, polymerized perfluorotetradecanoic acid – pentacosadiynoic acid thin films

Hessamaddin Younesi Araghi, Neeraj K. Giri and Matthew F. Paige

Department of Chemistry, University of Saskatchewan, 110 Science Place
Saskatoon, SK., S7N 5C9
Canada

4.5 Abstract

Photoillumination of mixed films comprised of the photopolymerizable fatty acid 10,12 pentacosadiynoic acid and perfluorotetradecanoic acid deposited onto glass substrates gives rise to the formation of oriented polydiacetylene photopolymer fibers. The degree of polymer fiber orientation was investigated using dual-view, polarized fluorescence microscopy of the polydiacetylene, which allowed for characterization of individual fluorescent polymer fibers after photopolymerization, as well as comparison of the orientation of different fibers within the same sample. Measurements indicated that individual fibers consisted of multiple photopolymer strands with various orientations, and that there was a preferred orientation for fibers in the film as a whole. The fibers were preferentially oriented at an angle of approximately 60° to the direction of film compression during deposition from a Langmuir trough, with orientation being the result of mechanical stress exerted by the compression barriers coupled with rotation of the polymer fibers during film draining. These measurements were complemented with conventional “bulk” fluorescence polarization experiments, and compared with mixed film structures described previously for these systems at the air-water interface using Brewster angle microscopy.

4.6 Introduction

Polydiacetylene (PDA) polymers are important technological materials for a variety of applications in biosensing, optical spectroscopy and non-linear optoelectronics^{1, 2}. These materials, typically prepared by topochemical photopolymerization of $R-C\equiv C-C\equiv C-R'$ monomer units, undergo dramatic color changes upon application of heat (“thermochromism”), mechanical stress (“mechanochromism”) and analyte binding, often along with accompanying changes in their fluorescent emission properties. Most notable for the latter are transitions between a non-fluorescent blue polymer and a highly-fluorescent red polymer, believed to be caused by changes to the effective conjugation length of the polymer that accompanies mechanical or thermal perturbation. The luminescent properties of the polymer have been exploited in a wide-variety of applications, typically as a signal transduction mechanism for detection of analyte binding to thin polymer films (see^{3, 4} for reviews).

There is considerable value in preparing patterned films of PDA-based polymers for sensing applications, and there are a number of reports describing novel approaches for creating aligned PDA polymer films. Some of the more successful approaches include microcontact printing, dropcasting, 3D replica molding and Langmuir Blodgett (LB) deposition^{1, 5-9}. Research in our group has focused on the latter; in particular, we are exploring the use of phase-separation of mixed surfactant films comprised of 10, 12 pentacosadiynoic acid ($CH_3(CH_2)_{11}-C\equiv C(CH_2)_8-COOH$; PCDA) and perfluorotetradecanoic acid ($CF_3-(CF_2)_{12}-COOH$; PF), followed by LB deposition onto glass substrates for patterning^{10, 11}. In this approach, PF and PCDA are mixed at the air-water interface and the surfactants undergo phase-separation to give domains of either pure PF or pure PCDA. In addition to segregating the PCDA into well-defined regions of space,

the PF also serves to stabilize the overall film through net attractive interactions between PF and PCDA. The film can then be photopolymerized with UV or laser illumination to yield the red fluorescent photopolymer product. A schematic illustration of the photopolymerization process and the resultant PDA polymer is shown in Figure 4-1.

To date, we have explored several variations of this phase-separation approach for preparing patterned PDA photopolymer. For example, surfactant mixtures of 1:4 mole ratio (PF:PCDA) that were deposited onto glass substrates and subsequently photopolymerized with laser illumination (532 nm) yielded amorphous patches of polymer ¹¹, while compression of the mixed surfactant films at the air-water interface, followed by photopolymerization with UV light at the air-water interface followed by deposition gave rise to the formation of phase-separated stripes of highly-fluorescent red PDA ¹⁰. In this case, the compressive force applied to the films by the barriers of the Langmuir Blodgett trough during photopolymerization caused the resulting PDA regions to organize into stripes oriented parallel to the barriers (perpendicular to the direction of film compression). While this approach did give rise to a generally preferred orientation of the polymer material, the extent of photopolymer ordering was not particularly high and there was considerable organizational heterogeneity in the films.

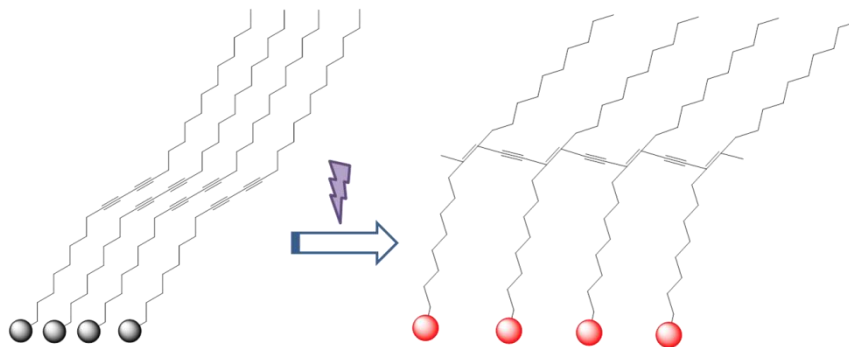


Figure 4-1. Schematic illustration of photopolymerization process of 10, 12 pentacosadiynoic acid films, and the resulting photopolymer film structure.

In this work, we have explored an alternative preparation technique in which films with a significantly higher PF content (2PF:1PCDA) compared with those studied previously are deposited onto glass substrates and photopolymerized at the solid-air interface. We have found that this simple variation in preparation conditions favours the formation of linear aggregates (fibers) of PCDA, and that there is a generally preferred spatial orientation to the fibers. The degree of polymer orientation within a fiber and between individual fibers has been measured using polarized fluorescence microscopy, complemented by conventional fluorescence anisotropy and Brewster angle microscopy. The basis for the polarized fluorescence microscopy measurements is that a single conjugated PDA polymer chain can be reasonably modeled as a single emission transition dipole lying in the plane of the solid glass substrate^{12, 13}, and thus, the fluorescence emission of the photopolymer is highly polarized along the length of the polymer chain. We have employed dual-view polarized fluorescence microscopy imaging in this work¹⁴, in which the fluorescence emission from the sample is split into its constituent vertical and horizontal polarization components, which in turn allows determination of the spatial orientation of the emission transition dipoles in the photopolymer. Measurements have been complemented with conventional bulk polarization measurements on the film along with structural

characterization using atomic force microscope and Brewster angle microscope imaging at the solid-air and air-water interfaces, respectively.

4.7 Materials and Methods

4.7.1 Sample Preparation

Perfluorotetradecanoic acid was purchased from Sigma-Aldrich Corp., and 10,12-pentacosadiynoic acid was purchased from Alfa Aesar. The solvents hexanes and tetrahydrofuran (HPLC grade) were purchased from EMD and Merck EM Science, respectively. All reagents were used as received. Stock solutions of mixed PF – PCDA were prepared by dissolving the solid surfactants in a 9:1 volume ratio of hexanes:THF, to yield a 2:1 mole ratio mixture solution of PF:PCDA. Microscope cover glass (VWR International) was rinsed with absolute ethanol and cleaned in a commercial plasma cleaner (Harrick Plasma) prior to use. Solutions and films were prepared and stored in the dark whenever possible in order to minimize exposure to ambient room light.

Films were prepared using a KSV 2000 Langmuir trough system (KSV-NIMA), at 22 ± 1 °C, with ultrapure water (Millipore, resistivity 18.2 M Ω ·cm) as a sub-phase. The sub-phase surface was cleaned thoroughly by suction before each experiment. The mixed surfactant solution was dotted onto the subphase surface and the solvent was allowed to evaporate for a minimum of ten minutes before compression. Films were compressed at a rate 10 mm·min⁻¹ to a surface pressure of 15 mN·m⁻¹ (measured using a platinum Wilhelmy plate), were allowed to stabilize for ~ 20 minutes and were finally deposited onto a glass substrate using a single vertical upstroke. Films were allowed to dry in a clean environment before further measurements.

Photopolymerization of the films was carried out directly on the fluorescence microscope described below, using the excitation laser as a light source.

4.7.2 Polarized fluorescence microscopy

Polarized fluorescence microscopy measurements were performed on a customized, wide-field epifluorescence microscope (Nikon TE2000, Nikon, Canada), using a 532 nm CW diode laser (100 mW, linear polarization, Dragon Laser Inc.) as an excitation source (Figure 4-2). Polarization of the excitation beam was controlled by first passing it through a linear “clean-up” polarizer (Glan-Thomson) to ensure linearly polarized light, then converting it into circularly polarized light by directing it through a Berek variable wave plate (New Focus). When needed, a second polarizer was placed after the variable wave plate, allowing the excitation light to be linearly polarized in any desired plane. The excitation light was then focused onto the sample using a 60X, 1.4 NA oil immersion objective lens. The emitted fluorescence was collected by the same objective, passed through a band-pass filter (Omega Optical) to attenuate residual excitation light and directed onto a front-illuminated electron multiplying CCD camera (Cascade 512F, Photometrics). A Wollaston prism (Thor Labs) was positioned in front of the CCD camera to split the resulting fluorescence image into its constituent vertically and horizontally polarized images (external dual-view configuration, as described by Kinoshita et al. ¹⁴).

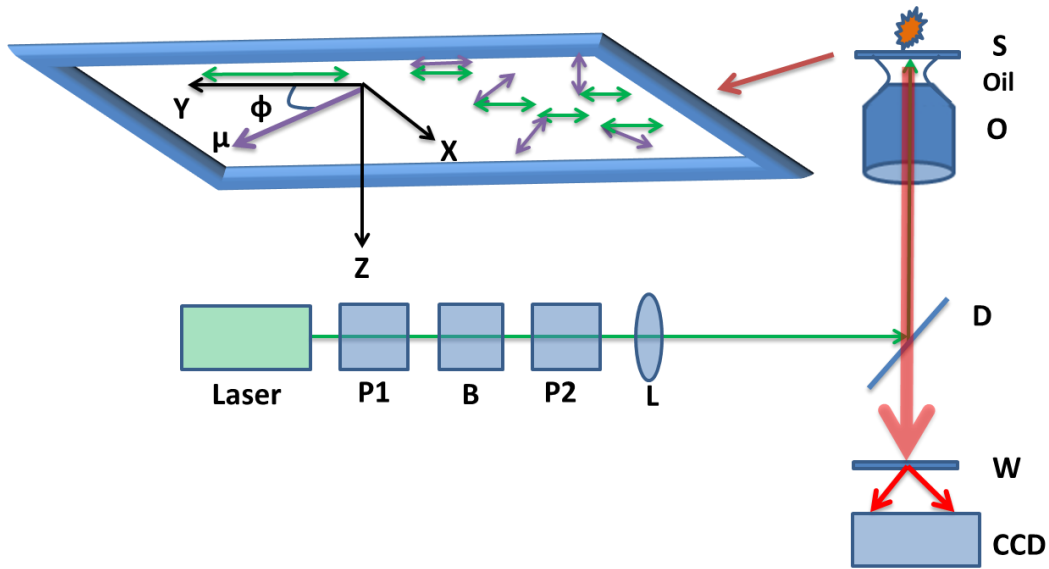


Figure 4-2. Schematic diagram of the dual-view polarized fluorescence microscope (Laser: 532 nm cw diode laser, P1: linear polarizer, B: Berek variable waveplate, P2: linear polarizer (optional) L: focusing lens, D: dichroic mirror, O: objective lens, S: sample, W: Wollaston prism, CCD: electron multiplying CCD detector). The orientation of a single emission transition dipole moment (μ) can be described in the x-y reference plane by using the angle ϕ . The y-axis projection of a variety of oriented transition dipoles are shown in green.

To determine polarization ratios of individual fibers from the fluorescence microscope image data, a region-of-interest (ROI) was drawn around both the horizontal and vertical polarization image for each fiber. Each ROI was background corrected by subtracting the average value of an appropriate number of “dark” pixels from each polarization image. The intensity of each fiber in the horizontal and vertical image (e.g. I_x and I_y in equation (4.1)) was then taken as the sum of background-corrected pixel values in the ROI. Care was taken to ensure that the pixel intensities were well below their saturation threshold.

4.7.3 Atomic Force and Brewster angle microscope imaging

The morphology of deposited films was characterized with a Dimension Hybrid (Bruker / Veeco Metrology) Atomic Force Microscope (AFM) operating in contact mode in air. Samples

could be imaged repeatedly using $0.12 \text{ N}\cdot\text{m}^{-1}$ spring constant probes without causing detectable damage to the surface.

Films were characterized at the air-water interface using an UltraBAM Brewster angle microscope (KSV-NIMA) attached directly to a Langmuir trough. Illumination was provided by a 50 mW, 658 nm polarized laser and images were collected using a charge coupled device detector. The lateral resolution of the instrument was $\sim 2 \mu\text{m}$. Note, the molar absorptivity of PCDA and its polymer PDA is negligible at 658 nm and the BAM imaging laser does not induce photopolymerization¹⁰.

4.7.4 Bulk polarization measurements

Bulk polarization measurements were performed on film using a variation of the dual-view fluorescence microscope. Linearly polarized light from a 532 nm cw diode laser (Dragon Lasers) was used to excite the sample. The plane of polarization of the incident beam could be adjusted through the use of a Berek variable waveplate and linear polarizer (referred to as the excitation polarizer) as described above. Emission was collected through a 10X, 0.25 NA microscope objective, filtered through a 540 nm longpass filter to remove residual excitation light, and directed through a second polarizer (referred to as the emission polarizer). Emission was focused into a fiber-optic based spectrometer (Ocean Optics) to collect an emission spectrum. To correct polarization values from depolarization by the experimental setup, it is necessary to introduce an experimentally measured correction factor (G-factor), defined as $G = I_{\text{HV}} / I_{\text{HH}}$, where I_{ij} is the fluorescence intensity measured with the excitation polarization in the “i” (H – horizontal, V- vertical) orientation and the emission polarizer in the “j” orientation, respectively¹⁵.

4.8 Results and Discussion

The morphologies of 2PF:1PCDA deposited films were measured by AFM imaging before and after photopolymerization and are shown in Figure 4-3A,B. Before polymerization, films consisted of a continuous, elevated matrix with crevices and indentations distributed heterogeneously across the surface; the latter depressions were typically ~ 1.5 nm in depth below the matrix. These structures were similar to those we have reported previously for 1PF:4PCDA mixtures, except that selection of a higher mole fraction of PF in the mixtures favoured the formation of narrow crevices (~ 1 μm wide, ranging in ~ 1 -10 μm in length) instead of the broad amorphous patches observed at lower mole fractions. We have previously ascribed the lower regions in the film to the PCDA component, by means of AFM and fluorescence imaging before and after photopolymerization, and the same assignment holds here. Exposing samples to laser illumination resulted in formation of a luminescent photoproduct in the depressed regions of the film, with the final product projecting out above the underlying matrix by ~ 3 nm. Figure 4-3B shows the results of these measurements, with micron scale “fibers” and amorphous patches of photopolymer product distributed heterogeneously on the substrate. The width of the fibers varied considerably but were typically of the order of ~ 0.8 μm (slightly narrower than the crevices from which they grow), and based upon these dimensions, we can tentatively ascribe them as consisting of bundles of photopolymer product. The fibers were frequently shorter than the entire length of the crevices, indicating that only a fraction of the PCDA is polymerized during light exposure; it is not clear why this is the case, but the result is consistent with earlier observations. We also note that there appeared to be a general orientation to the fibers; while not highly uniform, the long axis of the photopolymer fibers tended to be oriented in approximately

the same direction. For the AFM measurements (as well as subsequent fluorescence microscope measurements), samples were positioned in the microscope such that the x-axis in the images was the same as the direction of film compression in the trough. With this positioning, the fibers were generally oriented at a $\sim 60^\circ$ angle to the x-axis; that is, the long axis of the fibers was generally at an angle of $\sim 60^\circ$ to the direction of compression in the Langmuir trough. The orientation of the photopolymer, both within a fiber and between different fibers, was further explored through the use of polarized fluorescence microscopy and anisotropy measurements.

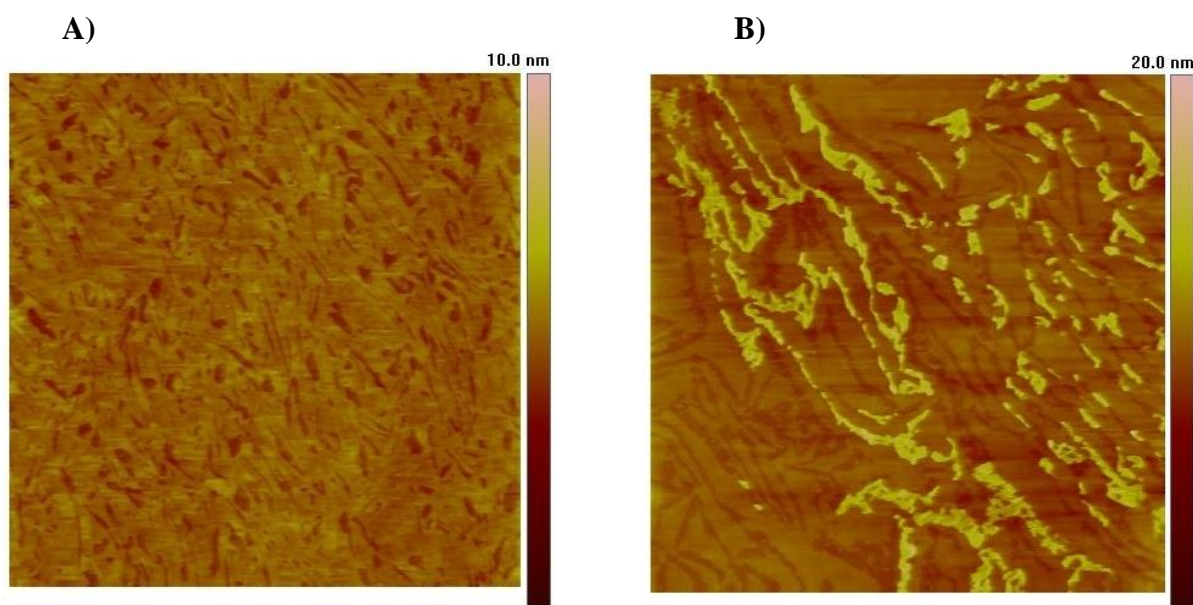


Figure 4-3. AFM height mode images of a 2PF:1PCDA mixed surfactant film A) before, and B) after photopolymerization with a 532 nm diode laser. Samples are positioned such that the x-axis is the direction of film compression in the Langmuir trough.

Dual-view polarized fluorescence microscope images of several different fibers in 2PF:1PCDA samples are shown in Figure 4-4. In these measurements, samples were excited with circularly polarized incident light to ensure that fibers of all orientations were excited with equal probability, and the resulting fluorescence emission was split into its corresponding x- and y-polarization components through the use of a polarizing Wollaston prism. The resulting

polarized images were simultaneously imaged onto a single CCD camera, ensuring detector-based noise and amplification gain was the same for both images. For stationary emission transition dipoles such as those here, the ratio of fluorescence emission intensities in the two images will be independent of incident excitation polarization, and reflect the orientation of the emission transition dipole (e.g. the angle ϕ in Figure 4-2) in the sample plane ¹⁶.

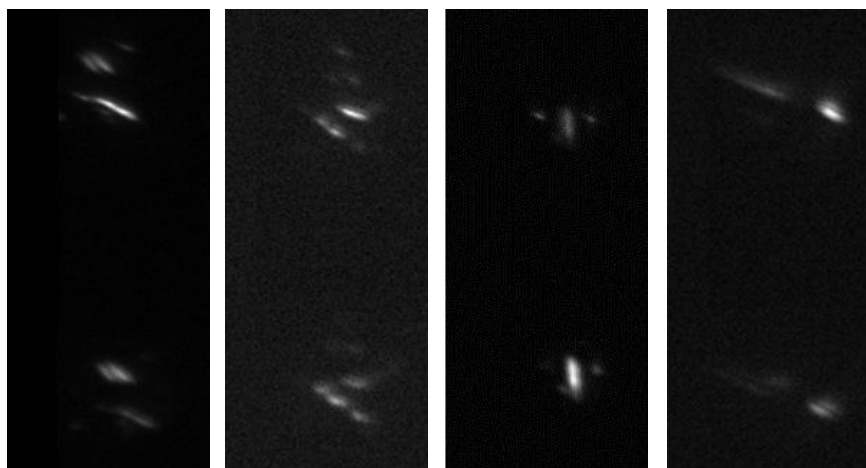


Figure 4-4. Dual-view polarized fluorescence microscope images of various 2PF:1PCDA samples imaged using circularly polarized incident light. Images are $30\ \mu\text{m} \times 12\ \mu\text{m}$ in size. The top portion of the image is herein referred to as the x-polarization component of the image, and the bottom portion, the y-polarization component. Note the general tendency for the fibers to orient themselves at $\sim 60^\circ$ to the field of view.

In an idealized case, a PCDA polymer molecule behaves as a single quantum emitter and can be modeled as a single emission transition dipole aligned along the main axis of the polymer chain (e.g. the conjugation length of the polymer). When imaged using a high-numerical aperture objective lens, the expected fluorescence intensity polarization ratio (P) for a single emitter can be defined and calculated according to equation (4.1) ¹⁶:

$$P \equiv \frac{I_x - I_y}{I_x + I_y} = \frac{(C_1 - C_2)(\sin^2 \phi - \cos^2 \phi)}{(C_1 + C_2) + 2C_3 \cot^2 \theta} \quad (4.1)$$

where I_x , I_y are the measured fluorescence intensities in the horizontal (x) and vertical (y) channel, respectively, C_n are coefficients that reflect the light collection capacity of high NA objective lenses ($C_1=0.742$, $C_2= 0.016$, $C_3=0.243$ for 1.4 NA lenses), the angle ϕ is defined in Figure 4-2, and θ is the angle between the z-axis and the emission transition dipole moment. For transition dipole moments oriented in the x-y plane, the expected result for the deposited film system measured here, $\theta = 90^\circ$, and equation (4.1) simplifies to:

$$P(\phi) = 0.958 \times (2 \sin^2 \phi - 1) \quad (4.2)$$

We note that the function $P(\phi)$ (plotted in Supplemental Figure S4-1) approaches values of ± 0.958 for a number of orientations, which corresponds to nearly exclusive projection of the emission transition dipole onto the x- or y-planes, respectively (e.g. fully polarized emission).

Photopolymer fibers were imaged and the polarization ratio for individual fibers was calculated by using the definition in equation (4.1) and the background-corrected fluorescence intensities in the x- and y-channels. For all photopolymer fibers excited with circularly polarized light, the measured polarization ratio was always significantly different from ± 0.958 limiting values; that is, under no circumstances did we observe fibers in which the emission was fully polarized in either the x- or y-plane. For the $n = 114$ fibers observed, we measured a mean value of $P = 0.41 \pm 0.05$. We take these measurements to mean that the fibers did not consist of an individual strand of PCDA (single emitters), as is consistent with the dimension of the fibers

measured from the AFM images, nor of many strands of rigid photopolymer that were aligned parallel (similar to that reported by Putman et al.¹⁶ for crystalline LB films), but rather bundles of photopolymer strands of slightly different orientations grouped together. We note, of course, that many of the fibers formed in samples are not perfectly linear and as such, we would not anticipate observing entirely polarized emission. However, as seen in Figure 4-4, many of the fibers are highly linear, and even in these cases, the emission was not entirely polarized. Having a range of polymer strand orientations within a fiber is consistent with the phase-separation process that gives rise to the structures. While the mutual immiscibility of PF and PCDA results in phase-separation of the two surfactant components, the resulting phase-separated structures are not highly-ordered or homogeneous. A number of closely-related systems lipid monolayer systems, including binary mixtures of saturated fatty-acids with perfluorocarboxylic acids, as well as fluorocarbon / hydrocarbon diblock molecules do form highly-ordered and in some cases semi-crystalline, self-assembled structured films¹⁷⁻¹⁹. In such cases, highly-ordered films and hence emission transition dipoles might reasonably be expected. In the case of PF-PCDA mixtures, however, the phase-separated films are significantly less organized and as such, the resulting photopolymer will be less orderly.

As noted above, there was a preferred general orientation for the fibers observed, approximately 60° to the x-direction (film compression direction). The standard deviation in $P(\phi)$ values (± 0.05) indicates a strong degree of orientation inhomogeneity between fibers, and on the basis of the relative error of this value, we can crudely estimate that this angle varies, on average, by around $\pm 6^\circ$. Nonetheless, the measurements do suggest that the bulk films themselves are oriented should exhibit an overall polarized emission. We have tested this by

measuring polarization-dependent fluorescence emission spectra as described in section 4.4.3, above. Results are shown in Figure 4-5.

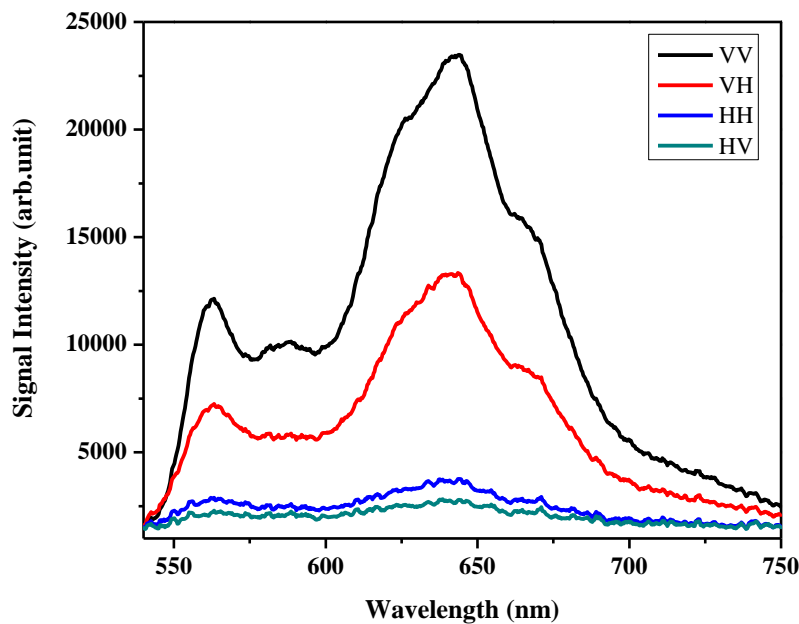


Figure 4-5. Polarized fluorescence emission spectra for mixed film after photopolymerization. Spectra were collected with various orientations of the excitation and emission polarizers as detailed in section 4.4.3.

The fluorescence emission spectra for the films consisted of two primary emission peaks (centered at 560 nm and 645 nm, consistent with the formation of the “red” form of photopolymer¹¹) and were highly polarized, as evidenced by their dependence on the excitation and emission polarizer orientations. The polarization ratio of the bulk films was calculated using a combination of equation (4.3) and equation (4.4):

$$P = \frac{3r}{2 + r} \quad (4.3)$$

$$r = \frac{I_{VV} - GI_{VH}}{I_{VV} + 2GI_{VH}} \quad (4.4)$$

where the values I_{ij} were the integrated peak areas for the appropriate fluorescence emission spectra. After correcting for the instrumental depolarization “G-factor”, a polarization of 0.39 ± 0.05 was measured, which was in good agreement with the average result obtained from measuring multiple photopolymer fibers. We note that while the photopolymerized films are quite heterogeneous, and consist of both crudely aligned fibers and patches of material, the good correlation in polarization values for the fiber and bulk film measurements suggest that the amorphous patches of material consist of randomly oriented photopolymer and that they contribute little to the polarized emission of the film as a whole.

A final question that must be considered is the underlying mechanism which leads to the net fiber orientation. Mixed PF-PCDA surfactant films that are photopolymerized directly at the air-water interface have previously been shown to form stripes that were oriented perpendicular to the direction of film compression in the Langmuir trough¹⁰, as have closely-related single-component PDA monolayer systems²⁰. We carried out similar measurements for unpolymerized films, with BAM images for typical mixed films shown in Figure 4-6 A-C for three different surface pressures. Note, the refractive index of the perfluorocarbon is comparable with that of water, meaning the PF component is undetectable; bright (highly-reflective) patches in the BAM images therefore consist of the hydrogenated surfactant only. Further, the diffraction-limited optical spatial resolution of the microscope was $\sim 2 \mu\text{m}$, meaning that for highly compressed films; individual fibers will not be resolvable.

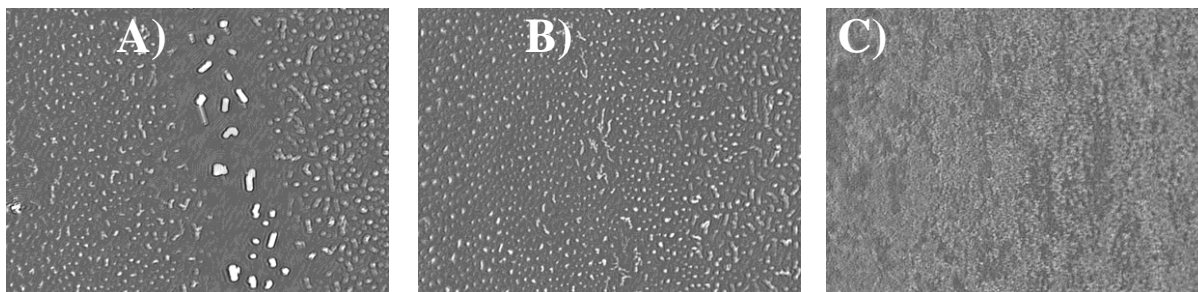


Figure 4-6. BAM images ($520\ \mu\text{m} \times 380\ \mu\text{m}$) of mixed films at the air-water interface taken at several different surface pressures (A: $\pi = 1\ \text{mN}\cdot\text{m}^{-1}$, B: $8\ \text{mN}\cdot\text{m}^{-1}$, C: $15\ \text{mN}\cdot\text{m}^{-1}$) before photopolymerization. The x-axis (long axis) of the images is the direction of film compression.

For the low compression pressures (Figure 4-6A, B; $1\ \text{mN}\cdot\text{m}^{-1} < \pi < 8\ \text{mN}\cdot\text{m}^{-1}$), images consisted of highly-reflective structures interspersed with extended regions of low reflectivity. As expected, the highly-reflective structures were heterogeneous, consisting of a mixture of amorphous aggregates along with fibers that were aligned approximately perpendicular to the direction of film compression. This is consistent with the fluorescence and AFM observations of the phase-separated films described above. In addition to the preferential alignment of fibers, there were also occasional stripes of low-reflectivity that spanned the width of the images, and again, these were oriented perpendicular to the direction of film compression. As with the solid-deposited films by AFM and by fluorescence, the degree of ordering at the air-water interface was neither extensive nor long range, but it was clearly detectable in the BAM. At higher compression pressures (Figure 4-6C; $15\ \text{mN}\cdot\text{m}^{-1}$), the spacing between individual fibers and aggregates was largely unresolvable, as expected. However, there were still readily-detectable regions of low-reflectivity that were tens of microns in length, and again, were oriented perpendicular to the direction of film compression, suggesting that while the constituent fibers may not be resolvable, the overall tendency for orientation within the film remained.

We interpret these results to mean that upon deposition onto solid substrates, the phase-separated films retain a reasonable net degree of fiber orientation. Previous studies of phase-separated arachidic acid-PF monolayers have reported that perfluorocarbon-hydrocarbon mixed films show minimal structural perturbations upon deposition from the air-water to solid-air interface²¹, and the results obtained here with the PF-PCDA mixtures are consistent with this observation. Further, the $\sim 60^\circ$ orientation of fibers with respect to the solid substrates can also be reasonably rationalized. Based on the arguments presented above, we might reasonably expect the fibers imaged in the AFM and BAM measurements to be oriented at an angle of 0° (i.e. pointing in the x-direction in Figure 4-3 and Figure 4-4). However, as has been reported for a variety of affiliated systems²²⁻²⁴, including phase-separated arachidic acid-PF monolayers, hydrodynamic flow of liquid out of the draining films after deposition can result in orientation of anisotropic structures in the direction of liquid flow. That is, elongated structures, such as fibers, will tend to turn towards the direction that fluid drains off the drying film. Hence, the fibers will be oriented at an angle greater than 0° with respect to the substrate because of this liquid flow.

As a final note, we do acknowledge that the degree of PCDA film orientation (and resulting fluorescence emission polarization) that can be achieved using the phase-separation approach is still inferior in comparison with other demonstrated methods of patterning PCDA (see⁵⁻⁸ for example), and for polymer patterning in general. Not only does the deposition process result in a wide range of polymer fiber orientations within the films, but additionally, a significant fraction of photopolymer material forms amorphous patches and does not appear to make a net contribution to the overall polarization of emission. Both of these effects need to be improved in order to enhance the degree of ordering in these systems. Enhancements may be

possible through further refinement of the film composition in order to “tune” the structure of the phase-separated films; for example, in mixed stearic acid - PF systems, highly-ordered stripes of hydrocarbon were observed at the solid-air interface, with the overall film structure being strongly influenced by the interplay between surface tension and dipole-dipole repulsion between the two film components, which in turn, is a strong function of the length (and molecular weight) of the constituent film components. We will explore this effect in greater detail in future investigations.

4.9 Conclusions

We have devised a simple method for preparing oriented solid films of PCDA through the use of phase-separation with a perfluorinated surfactant, followed by deposition onto solid substrates. Orientation in these films is driven by a combination of phase-separation of the two immiscible surfactant components, in combination with the mechanical force exerted by mechanical barriers during the deposition process. The resulting film structures are highly heterogeneous, consisting of both oriented fibers as well as amorphous patches of photopolymer. Fluorescence emission of the resulting photopolymer films is significantly polarized, with the polarization resulting from the preferred orientation of the fibers. This polarization dependence can be extracted through both bulk anisotropy measurements as well as through selective polarized imaging of individual fibers. While the films do show a reasonable degree of fiber orientation, the overall polarization and alignment is not as extensive as is observed using alternative preparation techniques, and further development is required in order to improve the overall homogeneity of the films.

4.10 Acknowledgements

Financial support for this research has been provided by the Natural Sciences and Engineering Research Council (NSERC) of Canada, the Canada Foundation for Innovation (CFI) and by the University of Saskatchewan.

4.11 Supplemental Figures

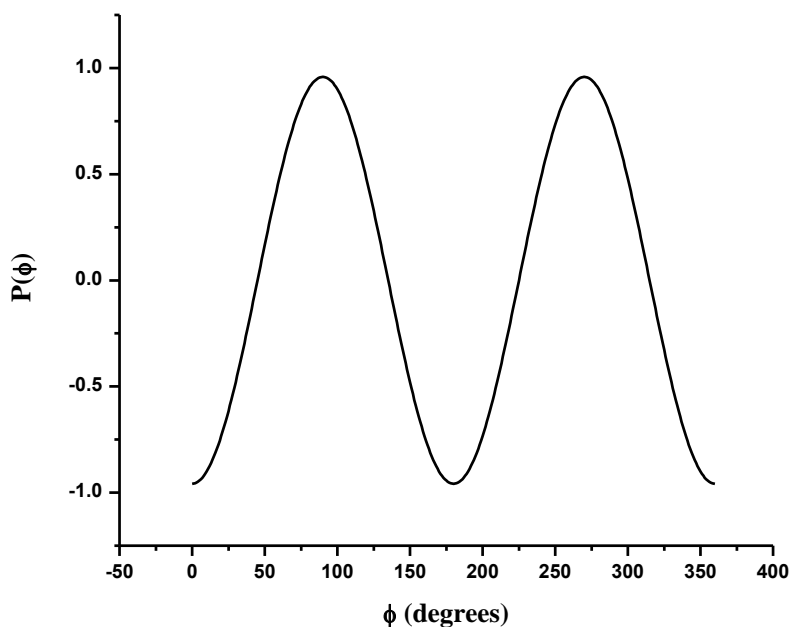


Figure S 4-1. Plot showing calculated value of polarization ratio ($P(\Phi)$) as defined in equation (4.2)) as a function of in-plane angle Φ .

4.12 References

1. Carpick, R. W.; Sasaki, D. Y.; Marcus, M. S.; Eriksson, M. A.; Burns, A. R., Polydiacetylene films: a review of recent investigations into chromogenic transitions and nanomechanical properties. *Journal of Physics: Condensed Matter* **2004**, 16, R679-R697.

2. Enkelmann, V., Structural aspects of the topochemical polymerization of diacetylenes. *Advances in Polymer Science* **1984**, 63, (Polydiacetylenes), 91-136.
3. Ahn, D. J.; Kim, J. M., Fluorogenic polydiacetylene supramolecules: Immobilization, micropatterning, and application to label-free chemosensors. *Accounts of Chemical Research* **2008**, 41, (7), 805-816.
4. Okada, S.; Peng, S.; Spevak, W.; Charych, D., Color and chromism of polydiacetylene vesicles. *Accounts of Chemical Research* **1998**, 31, (5), 229-239.
5. Baek, J. H.; Ahn, H.; Yoon, J.; Kim, J.-M., Micro-patterning of polydiacetylene supramolecules using micromolding in capillaries (MIMIC). *Macromolecular Rapid Communications* **2008**, 29, 117-122.
6. Choi, J.-M.; Yoon, B.; Choi, K.; Seol, M.-L.; Kim, J.-M.; Choi, Y.-K., Micropatterning polydiacetylene supramolecular vesicles on glass substrates using a pre-patterned hydrophobic thin film. *Macromolecular Chemistry and Physics* **2012**, 213, 610-616.
7. Lee, J.; Yarimaga, O.; Lee, C. H.; Choi, Y.-K.; Kim, J.-M., Network Polydiacetylene Films: Preparation, Patterning, and Sensor Applications. *Advanced Functional Materials* **2011**, 21, (6), 1032-1039.
8. Shim, H. Y.; Lee, S. H.; Ahn, D. J.; Ahn, K.-D.; Kim, J.-M., Micropatterning of diacetylenic liposomes on glass surfaces. *Materials Science and Engineering C* **2004**, 24, 157-161.
9. Yarimaga, O.; Lee, S.; Kim, J.-M.; Choi, Y.-K., Fabrication of patterned polydiacetylene composite films using a replica-molding (REM) technique. *Macromolecular Rapid Communications* **2010**, 31, 270-274.

10. Araghi, H. Y.; Paige, M. F., The effect of perfluorotetradecanoic acid on the structure of photopolymerized 10,12-pentacosadiynoic acid films at the air-water interface. *Can. J. Chem.* **2013**, 91, (11), 1130-1138.
11. Younesi Araghi, H.; Paige, M. F., Deposition and photopolymerization of phase-separated perfluorotetradecanoic acid-10,12-pentacosadiynoic acid Langmuir-Blodgett monolayer films. *Langmuir* **2011**, 27, (17), 10657-10665.
12. Goettgens, B. M.; Tillmann, R. W.; Radmacher, M.; Gaub, H. E., Molecular order in polymerizable Langmuir-Blodgett films probed by microfluorescence and scanning force microscopy. *Langmuir* **1992**, 8, (7), 1768-74.
13. Putman, C. A. J.; Hansma, H. G.; Gaub, H. E.; Hansma, P. K., Polymerized LB films imaged with a combined atomic force microscope-fluorescence microscope. *Langmuir* **1992**, 8, (12), 3014-19.
14. Kinoshita, K.; Itoh, H.; Ishiwata, S.; Hirano, K.; Nishizaka, T.; Hayakawa, T., Dual-View Microscopy with a Single Camera - Real-Time Imaging of Molecular Orientations and Calcium. *Journal of Cell Biology* **1991**, 115, (1), 67-73.
15. Lakowicz, J. R., *Principles of Fluorescence Spectroscopy*. 3rd ed.; Springer: New York, 2006.
16. Forkey, J. N.; Quinlan, M. E.; Goldman, Y. E., Protein structural dynamics by single-molecule fluorescence polarization. *Progress in Biophysics & Molecular Biology* **2000**, 74, (1-2), 1-35.

17. Kimura, H.; Watanabe, S.; Shibata, H.; Azumi, R.; Sakai, H.; Abe, M.; Matsumoto, M., Phase-Separated Structures of Mixed Langmuir-Blodgett Films of Fatty Acid and Hybrid Carboxylic Acid. *Journal of Physical Chemistry B* **2008**, 112, (48), 15313-15319.
18. Krafft, M. P., Large organized surface domains self-assembled from nonpolar amphiphiles. *Accounts of Chemical Research* **2012**, 45, (4), 515-524.
19. Qaqish, S. E.; Paige, M. F., Structural and compositional mapping of a phase-separated Langmuir-Blodgett monolayer by atomic force microscopy. *Langmuir* **2007**, 23, (5), 2582-2587.
20. Tomioka, Y.; Imazeki, S.; Tanaka, N., Highly oriented polydiacetylene monolayer formed at the air-water interface. *Chemical Physics Letters* **1990**, 174, (5), 433-437.
21. Eftaiha, A. F.; Paige, M. F., Phase-separation of mixed surfactant monolayers: A comparison of film morphology at the solid-air and liquid-air interfaces. *Journal of Colloid and Interface Science* **2012**, 380, (1), 105-112.
22. Jeffery, G. B., The motion of ellipsoidal particles in a viscous fluid. *Proceedings of the Royal Society of London Series a-Containing Papers of a Mathematical and Physical Character* **1922**, 102, (715), 161-179.
23. Okagawa, A.; Cox, R. G.; Mason, S. G., Kinetics of Flowing Dispersions .6. Transient Orientation and Rheological Phenomena of Rods and Disks in Shear-Flow. *Journal of Colloid and Interface Science* **1973**, 45, (2), 303-329.
24. Qaqish, S. E.; Paige, M. F., Mechanistic insight into domain formation and growth in a phase-separated langmuir-blodgett monolayer. *Langmuir* **2007**, 23, (20), 10088-10094.

5 CHAPTER 5: SIMULTANEOUS ATOMIC FORCE MICROSCOPY AND FLUORESCENCE MICROSCOPY IMAGING OF POLYMERIZED PERFLUOROTETRADECANOIC ACID – 10, 12- PENTACOSADIYNOIC ACID LANGMUIR-BLODGETT FILMS

5.1 Description

This chapter describes the development and application of a microscope that is capable of both atomic force microscope imaging and fluorescence imaging for characterizing mixed PCDA-PF films. The microscope allowed AFM images to be acquired while simultaneously monitoring the fluorescence of the sample. By applying simultaneous AFM and fluorescence imaging measurements, the correlation between film morphology and fluorescence properties of PDAs was obtained. As noted in previous chapters, the product of PCDA photopolymerization has two phases, a red phase with strong fluorescence and a blue phase with no fluorescence. With the help of the dual AFM-fluorescence microscope, it was found that both the red and blue polymer phases were produced in the same sample from photoillumination. This is in agreement with affiliated systems¹ reported in the literature, though the ability to carry out this simultaneous characterization with a single microscope is both novel and important. Further, the importance of intrinsic mechanical stress in the films is discussed in terms of its influence on selectivity for the red polymer phase.

5.2 Description of the Candidate's contribution

For this contribution, I carried out all experimental works including construction and modification of the microscope, sample preparation and imaging. I played the principal role in interpreting the results. Dr. Neeraj Giri provided minor assistance with the microscope setup and laser alignment. Dr. Matthew Paige provided extensive guidance throughout the experimental work and was greatly involved in results interpretation.

5.3 Relation of Contribution to Research Objectives

This work was exclusively performed towards the objectives of the thesis research. In the previous chapters, mixed monolayers of photopolymerizable surfactant - perfluorinated fatty acid were characterized in terms of surfactant miscibility, spectroscopic properties and film morphology. Further, potential approaches to pattern the material on glass substrates and the orientation of the photopolymer fibers were explored. An important question which remains, however, is to determine how selective the photopolymerization process was in terms of ability to generate the red (fluorescent) versus blue (non-fluorescent) photopolymer. In this chapter, the degree of product selectivity was assessed using a novel microscope that consisted of a combination of a fluorescence microscope and an Atomic Force Microscope, allowing correlated structure-fluorescence imaging. After the instrument was constructed and tested, it was applied to a typical mixed PCDA-PF film. Atomic force microscope images were collected on deposited films to provide correlated information on film morphology and fluorescence output. By correlating AFM and fluorescence images, it was concluded that individual fibers, as described in Chapter 4, consisted of multiple phases of photopolymer, and that there was a preferred

production of the red phase of polymer under the illumination conditions used. A full discussion of the results as part of the whole study is provided in Chapter 6.

5.4 Introduction

New insights into the structure and function of a wide variety of different materials have been provided by atomic force microscopy (AFM) and optical microscopy. Since its invention in 1986 by Binnig, Quate and Gerber^{2,3}, the AFM has evolved into a technique capable of resolving molecular-level details of surfaces under ambient or in liquid conditions. The AFM quickly gained recognition for its high spatial resolution, with sub-nanometer axial resolution and nanometer-scale lateral resolution. The relatively simple and label-free preparation of most samples has also contributed to the success of the AFM when compared with other microscopy methods, particularly electron microscopy which requires extensive sample preparation and measurement in vacuum. Because of these benefits, AFM is widely-available as a bench-top commercial instrument and is used by researchers at the borders between disciplines.

Although the first commercially available AFMs were manufactured in the late 1980s, the beginnings of optical microscopy are much less clear, but are alleged to lay with simple magnifying glasses in the 9th century with further advances in the 16th century. Nevertheless, it wasn't until the 17th century that first scientific observations were recorded. Early experiments were carried out by Hooke and van Leeuwenhoek⁴ with simple microscopes, generally in the field of biology. In most modern applications, optical microscopy resolution is on the order of 200-300 nm laterally, and 500 nm in depth. The resolving power of optical imaging is fundamentally limited by diffraction to approximately half the wavelength of the light used⁵. However, its ability to image through the entire depth of certain samples with chemical

specificity (usually a sample is labeled with a fluorescent tag and fluorescence optical microscopy is used) allows researchers to identify specific structures or molecules within a sample. Optical microscopy's chemical specificity and ability to image live processes within the depth of a sample is well-complemented by the higher resolution capabilities of the AFM.

An interesting and promising area of advance for AFM has been in its combination with optical microscopy, particularly fluorescence microscopy^{1, 6}. A more complete understanding of structure-function relationships in complex materials can be obtained with a combined AFM/fluorescence microscope system over either AFM imaging or fluorescence imaging alone. When fluorescence imaging is coupled with AFM's ability to measure high-resolution topographical images, forces, and/or elasticity on a sample, there are many advantages over AFM imaging alone. Consequently, both techniques complement each other in that AFM has excellent spatial resolution but lacks identification capabilities, whereas fluorescence microscopy offers poor resolution but excellent identification properties. Combined, correlated microscopy has proven itself useful for characterizing a number of challenging samples of the past decade⁷⁻⁹.

An important illustration of combined AFM-fluorescence imaging in the area of PCDA films has been reported by Putman and coworkers¹. In this work, pure PCDA films were prepared and polymerized using an Hg lamp and imaged in a combined microscope setup. In terms of instrumentation, the authors used an inverted, sample-scanning AFM coupled with a fluorescence microscope on top. Their measurements showed a direct correlation between the cracks seen in polymerized PCDA LB films with the fluorescence microscope and the molecular arrangement of polymer strands in the crystalline polymer as revealed by the AFM. These results indicated that the LB film breaks along the direction of the polymer backbone. They also

repeated the work by Goettgens¹⁰ which showed that the fluorescence from polymerized PCDA LB films is highly polarized (polarization degree > 0.95) at high surface pressures.

In this study, the combined AFM / fluorescence microscope was used to image LB films comprised of mixed PF-PCDA surfactants, as described in Chapter 2. As demonstrated in previous chapters, these mixed surfactants are amenable to AFM imaging as they adhere well to a solid support, in this work, microscope cover glass. In addition, PCDA shows a 0.8 nm lower profile than PF, which is easily detectable by AFM, and when it is illuminated and eventually polymerized, the product is several nanometers in height. As discussed in the previous chapters, PCDA films can be polymerized upon exposure to a laser beam or UV-lamp illumination. By using AFM and polarized fluorescence microscopy individually, fibers of polymer strands were characterized in topography images and analyzed for orientation in Chapter 4. In Chapters 2 and 3 fluorescence images and the emission spectrum of polymerized samples were reported. An important remaining question is if the entire photopolymer film is in the red phase, the blue phase, or a mixture of the two. Previous chapters indicate that a substantial amount of red phase product is formed, but further investigation and quantification of this is required. Further, it is of interest to determine conditions of sample preparation and polymerization approaches, if any, that can selectively produce red phase polymer. Efforts to address these questions are described in this chapter.

First, the feasibility of combining two techniques for simultaneous imaging was demonstrated. AFM and FM on standard fluorescent 1.0 μm diameter fluorophore spheres control samples were used to test the system, and finally, simultaneous imaging of a mixed PF-PCDA film was performed. Fluorescence microscopy allowed for detection of structures of red

PDA while simultaneous AFM scanning revealed a high-resolution image of all film components including PF, PCDA, red PDA and blue PDA. Fluorescence microscopy gave a detailed image of the distribution of red PDAs that could be correlated with AFM topography images.

5.5 Materials and Methods

5.5.1 Sample Preparation

Perfluorotetradecanoic acid was purchased from Sigma-Aldrich Corp., and 10,12-pentacosadiynoic acid was purchased from Alfa Aesar. Hexanes and tetrahydrofuran (HPLC grade) were purchased from EMD and Merck EM Science, respectively and used as surfactant solvent. No further purification was applied and all reagents were used as received. A 9:1 volume ratio of hexanes:THF were mixed and used as solvent to prepare stock solutions of mixed PF – PCDA, to yield a 2:1 mole ratio mixture solution of PF:PCDA. Microscope cover glass (VWR International) was rinsed with absolute ethanol and cleaned in a commercial plasma cleaner (Harrick Plasma) prior to use. Solutions and films were stored in a dark room, and films were prepared with minimal exposure to ambient room light.

Langmuir film experiments were performed on a KSV 2000 Langmuir trough (KSV Instruments) at room temperature (22 °C) using ultrapure water (Millipore, resistivity 18.2 MΩ) as a subphase. The water surface was cleaned thoroughly before each experiment. For deposition, a 100 μL aliquot of the mixed surfactant solution was spotted onto the subphase surface, and the solvent was allowed to evaporate for at least 10 minutes. For film deposition a barrier compression rate of 10 mm min⁻¹ was used. After the deposition pressure was reached,

the film was allowed to stabilize for 20 minutes before the glass substrate was pulled upward through the water/air interface. The film was left to dry at room temperature for one hour before further measurement in the AFM. For combined microscope measurements, one side of the glass slide was washed thoroughly with Millipore water and followed by rinsing with chloroform, in order to remove the deposited film from one side of the cover glass. The slides were left for an hour to dry completely.

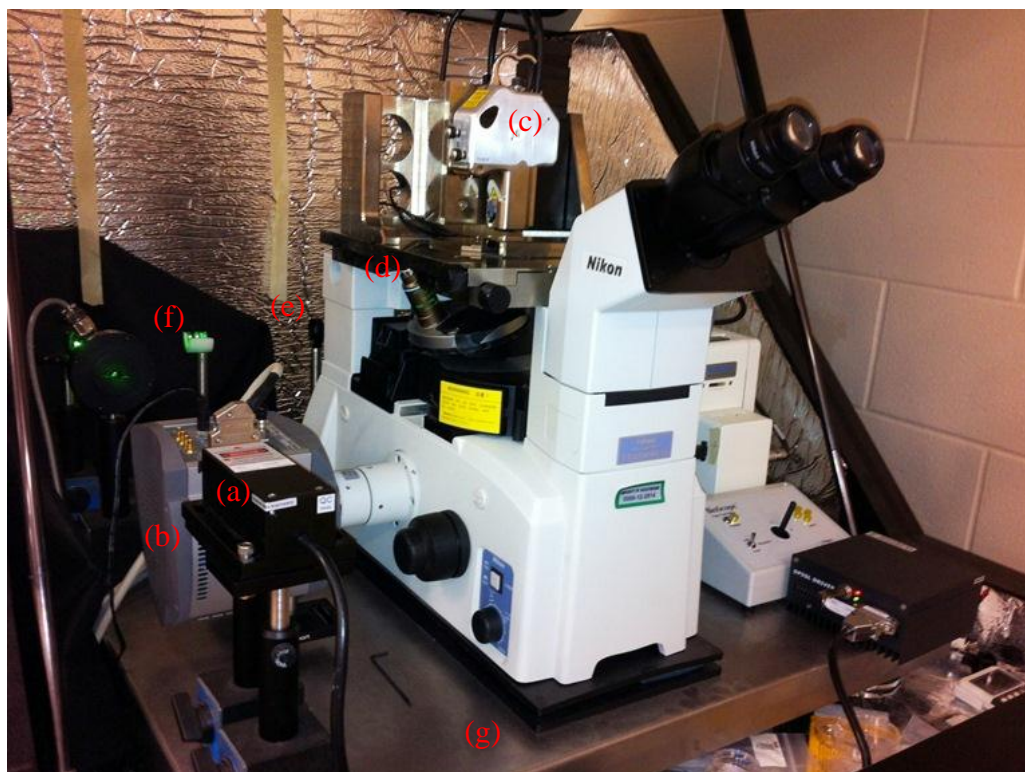


Figure 5-1. Photograph of the combined AFM-fluorescence microscope system; (a) laser diode (532 nm emission), (b) CCD camera, (c) AFM head, (d) microscope objective, (e) focusing lens, (f) neutral density filters, (g) vibration isolation table equipped with an air cushion underneath it.

5.5.2 Instrumentation

The combined instrument was based on an AFM (Dimension Hybrid, Bruker), mounted on an optical microscope (TE2000, Nikon) that used a 532 nm diode laser (100 mW, Dragon

Laser Inc.) as an excitation source (Figure 5-1). For AFM imaging, the microscope was operated in contact mode in air. Samples could be imaged repeatedly using $0.12 \text{ N}\cdot\text{m}^{-1}$ spring constant probes without causing detectable damage to the surface. For fluorescence imaging, the excitation light was focused onto the sample using a 40X objective lens. The emitted fluorescence was collected by the same objective, passed through a series of optical filters (further detail provided later in the text) to attenuate residual excitation light as well as light from the AFM feedback laser and directed onto a CCD camera (iXon, Andor). The instrument was mounted on an anti-vibration table equipped with an air cushion and acoustic shielding (Figure 5-2).

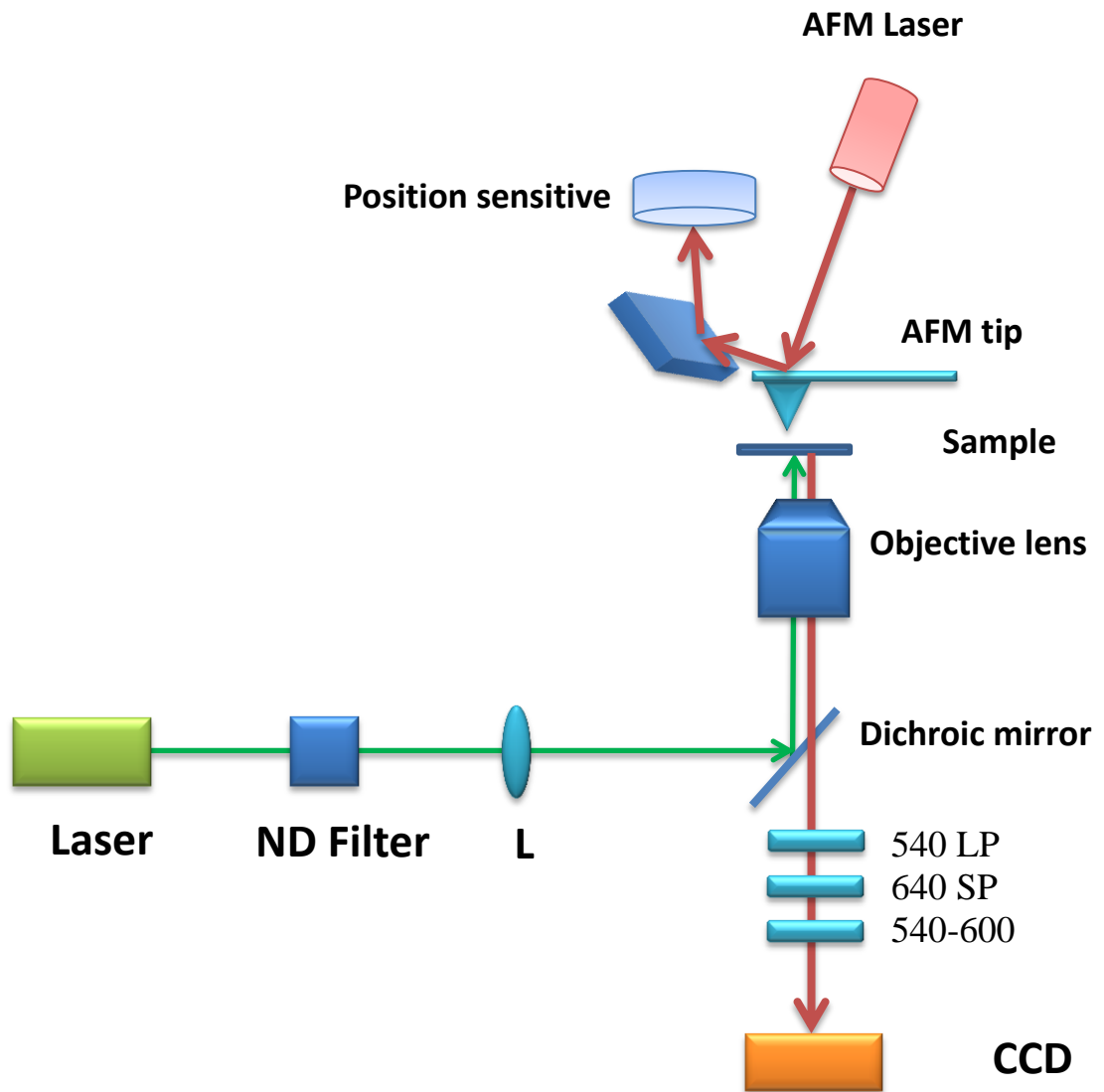


Figure 5-2. Schematic illustration of combined AFM/fluorescence microscope system, Neutral density filters (ND), Lens (L).

Integrating these two technologies is challenging, and different design criteria must be met to ensure success. In terms of general optical design, it was deemed preferable to illuminate the sample through an optical microscope condenser (the objective lens), and align the laser through a series of mirrors and lenses. This would allow the optical path to be on the opposite

side of the microscope from the AFM head, and allow the objective lens to be used as both a condenser for transmitted light as well as a viewing means for aligning the AFM feedback laser onto the optical lever (Figure 5-1 and 5-2).

Because the AFM uses a laser to track deflection of the cantilever, there must be several considerations in the selection of optical filters in order to minimize interference and crosstalk in the desired fluorescence data (Figure 5-3). AFM uses a red laser diode (650-690 nm) for optical lever tracking. The red laser is challenging; it would be seen in images taken on the optical microscope and obscure fluorophores that excite or emit within the wavelength range of the diode. Addition of a filter under the microscope objective could block these signals from saturating the camera electronics and obscuring the fluorescence of the sample. The key challenge here was that the emission of the AFM laser falls in the middle of PDA's emission spectrum. To solve this problem, an additional cut-off filter was added before the CCD camera, in order to remove emission of the AFM laser (Figure 5-3). To assess the efficiency of this, the CCD camera (shown in Figure 5-2) was replaced with a spectrophotometer (Ocean Optics). First, the AFM probe (which holds the cantilever) was removed from AFM head to ensure that the maximum possible amount of light from the AFM diode laser was reaching the detector. No sample was used in this trial. The resulting spectra, both with and without the use of optical filters, are shown in Figure 5-3 and Figure 5-4. Before addition of the optical filters, strong red region emission from the AFM diode laser between 650 nm – 700 nm was measured. The 540 long pass filter was already in place to remove scattered 532 nm excitation laser. The next filter added was a 640 short pass filter to remove residual laser light reaching the detector from the AFM. As is clear from Figure 5-4, there was still a strong peak at 685 nm and at 645 nm which

would interfere with PDA fluorescence measurements, indicating the optical filtering was not yet sufficient. An additional 540-600 nm band pass filter was added, and the results are shown in Figure 5-4 (red curve).

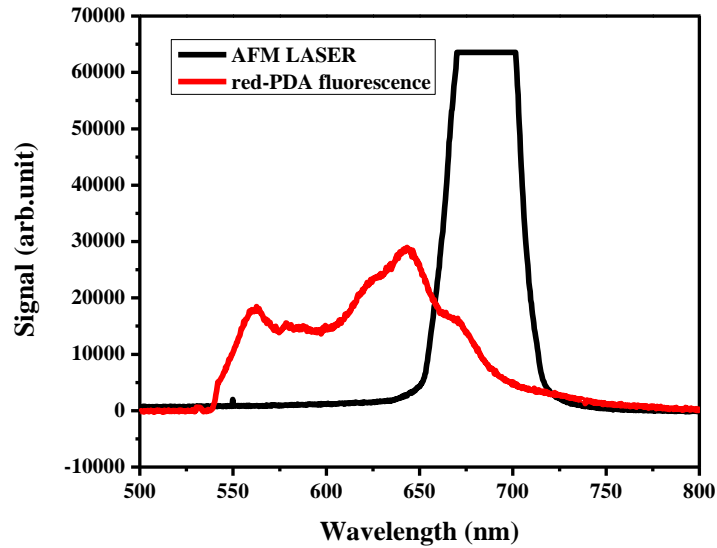


Figure 5-3. Optical signals measured in the combined microscope. The black curve shows the laser output from the AFM laser diode (signal is cut off because of detector saturation); and the red curve shows the two 550 and 640 nm characteristic fluorescence emission peaks of red-PDA.

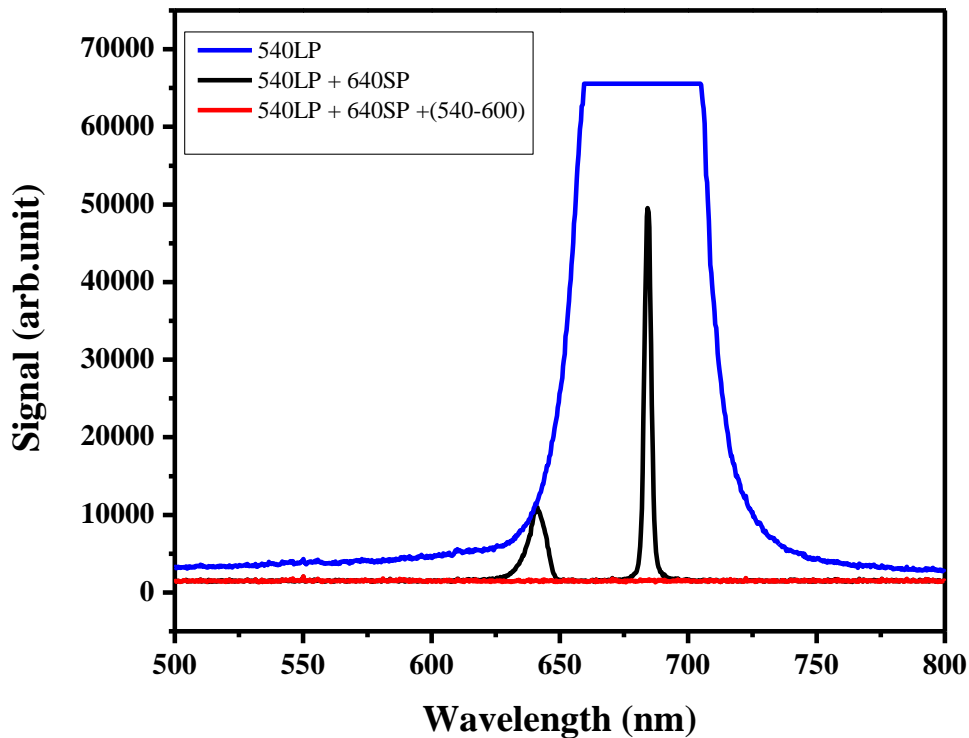


Figure 5-4. Optical signals in the combined microscope, showing the effect of adding optical filters. The filters that were added were a 540 Long Pass (LP), a 640 Short Pass (SP) and finally a 540-600 band pass filter. This resulted in the blue, black and red curves, cumulatively.

After solving the problem caused by the AFM diode laser, the next challenge to be solved was optical alignment. The AFM probe tip and the laser excitation beam from the fluorescence microscope needed to be aligned so the same sample region was being measured using both AFM and fluorescence imaging. For coarse alignment, the AFM cantilever and AFM feedback laser which positions the cantilever movements were aligned with the help of a 10x objective lens which was then replaced by a 40x objective lens. The complete AFM head was then moved using the alignment features available on the AFM sample stage until the excitation source (532 nm green beam) was positioned close to the AFM tip. When the alignment was close, scattered

green light and AFM feedback laser backscattered spots were readily visible through the microscope eyepiece (Figure 5-5 (A)). For fine alignment, the AFM cantilever with its tip was imaged with FM and alignment was continued until a clear image of the AFM tip appeared on the CCD camera screen (Figure 5-5 (B)).

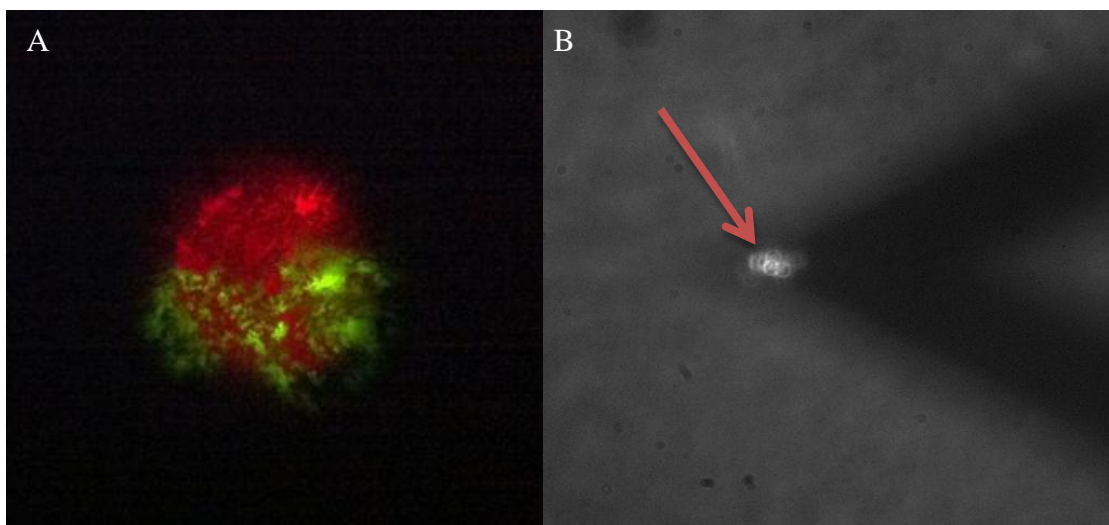


Figure 5-5. Images collected using the combined microscope. A) Fluorescence image of standard fluorophore spheres sample, viewed through the microscope eyepiece. Green emission is from the 532 nm excitation laser beam, and the red emission is fluorescence emission of the sample in combination with the scattered laser light from AFM red laser beam. The image was taken with a camera through the microscope eyepiece, and was intended to show the alignment of two lasers light. Image size is approximately $100\ \mu\text{m} \times 100\ \mu\text{m}$, B) CCD camera perspective of the same sample. The red arrow indicates fluorescence emitted from sample because of the 532 nm laser illumination. For these measurements, the AFM noise canceling box was left open, and the background is due to ambient light. An out-of-focus outline of the triangular AFM cantilever is visible above the glass substrate. Image size is approximately $400\ \mu\text{m} \times 400\ \mu\text{m}$.

The final step to adjust the fluorescence microscope was to calibrate the size-scale of the image collected by the FM. This was carried out using a USAF resolution test target. The original image produced by the FM was rotated and inverted relative to the AFM image (Figure 5-6, left image), so a 90° clockwise image rotation and horizontal inversion of the image was performed using the CCD camera software to produce the final image (Figure 5-6, right image).

In this way the image appearing on the AFM screen and FM screen had the same orientation (Figure 5-7).

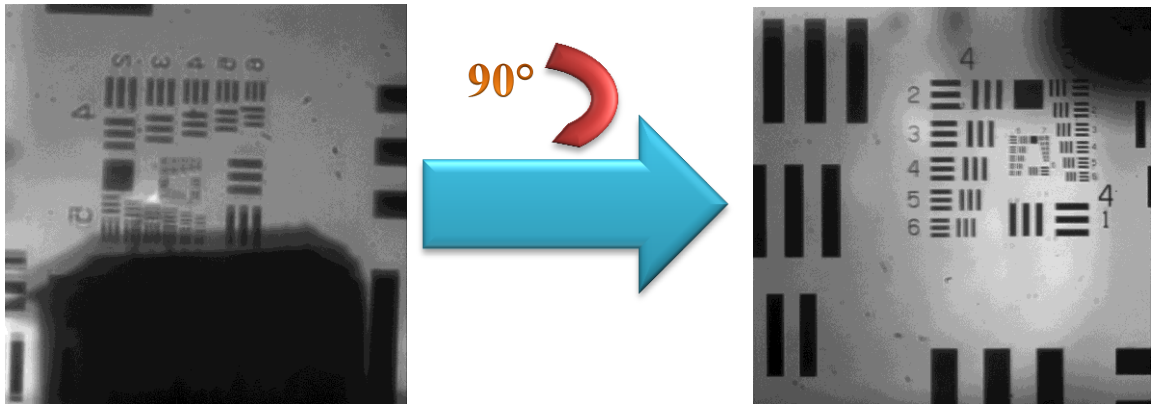


Figure 5-6. Optical image of USAF test target imaged using ambient light and the CCD detector. The out-of-focus rectangular object in the lower field of view is the AFM probe. Image size is $1000\ \mu\text{m} \times 1000\ \mu\text{m}$. To obtain the final image, the image was rotated 90 degrees clockwise and horizontally inverted (mirror image).

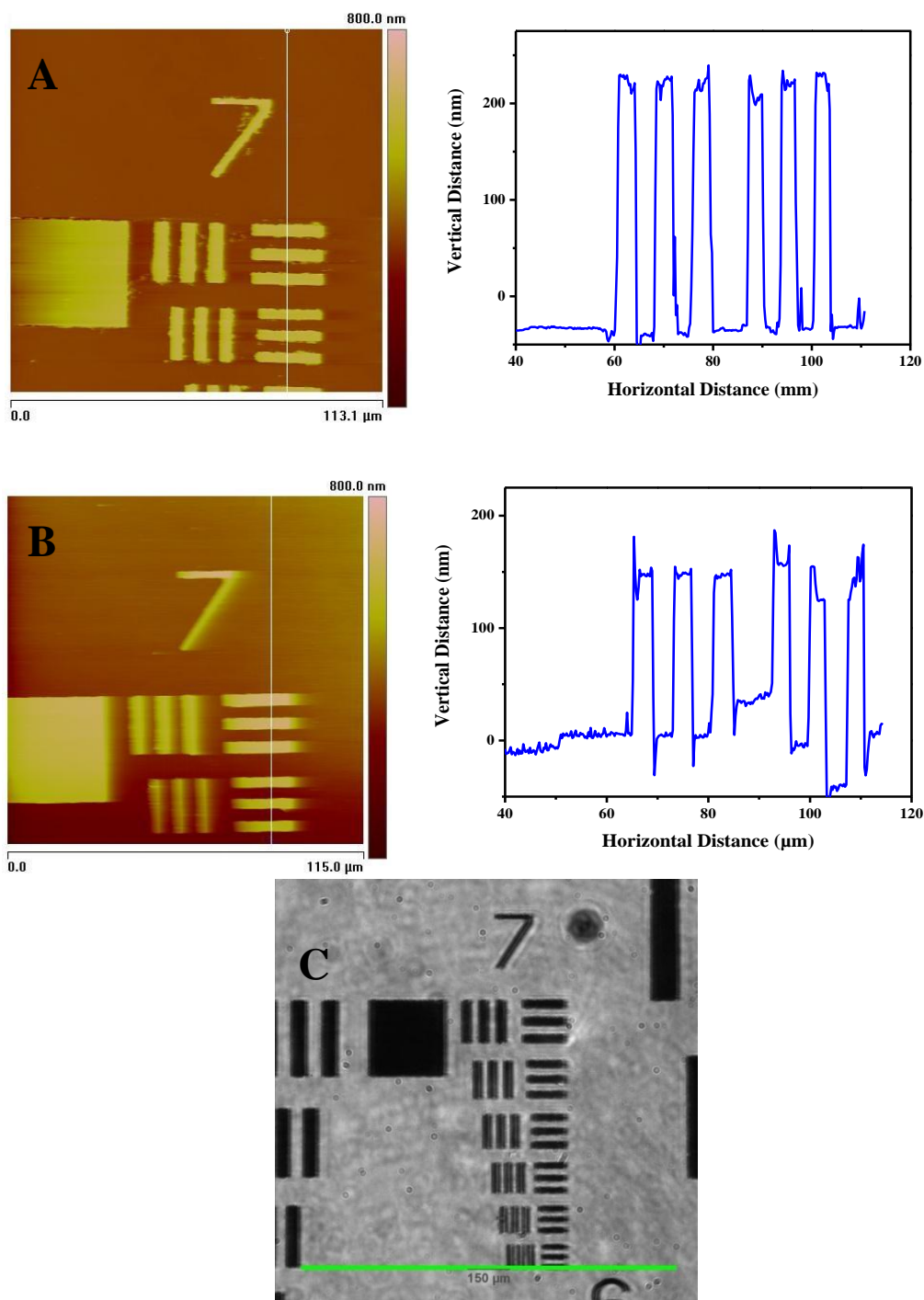


Figure 5-7. (A) Atomic force topography image (image size 113 μm x 113 μm) captured when all the additional equipment was powered off; (B) Atomic force topography image (image size 115 μm); (C) optical microscope image (reflected light) with 150 μm \times 150 μm size, (B) and (C) were collected simultaneously with the combined microscope.

Figure 5-7 shows images of the USAF test target collected simultaneously by AFM and FM from the same sample region. To test the effect, if any, of the various components used in the fluorescence microscope on the performance of the AFM, images of the USAF test target were taken with and without the fluorescence microscope turned on. Figure 5-7 (A) is an AFM image of a USAF test target captured while the FM instrument components (including CCD camera, laser and power supply for shutter) were kept powered off whereas images in Figure 5-7 (B) and (C) were collected simultaneously. A cross sectional analysis of the AFM topographical images also is provided for comparison between two situations. The RMS noise calculated from the AFM images was 2.79 nm and 3.96 nm for images (A) and (B) in Figure 5-7 respectively. RMS noise is the standard deviation of the height values within the selected area of the image. There was a very small difference observed in the noise when the fluorescence microscope components were operating concurrently with AFM, indicating fluorescence microscope operation did not substantially affect AFM performance. Combining the AFM with the fluorescence microscope does not negatively impact the performance of either instrument.

A sample of standard fluorophore spheres was prepared by drop casting a solution of 1.0 μm sized standard spheres on a glass coverslip, and imaged in order to test alignment of the setup before using the real sample of PF-PCDA. The main concern was to determine if the two microscopes, the AFM and the FM, were well-aligned and imaging the same region of the sample. Figure 5-8 shows the AFM topography image and fluorescence image collected from same sample at same spot, with the instruments operating concurrently. There are common features in both images, proving the same spot has been located by the both microscope and again the quality of the AFM image remains unaffected by the FM.

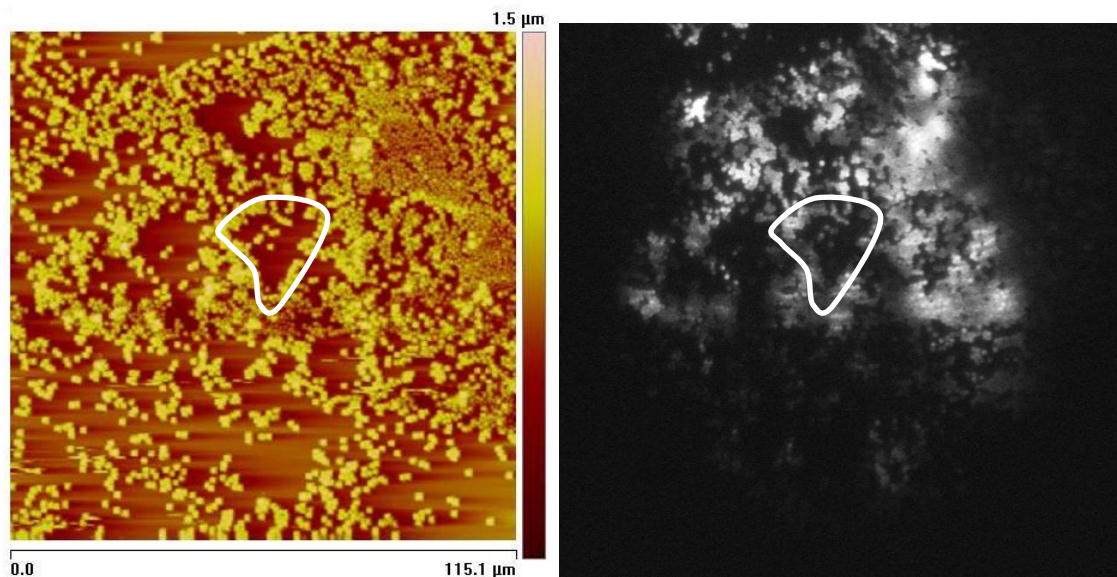


Figure 5-8. Standard 1.0 μm diameter fluorescent spheres. (A) AFM deflection image of standard fluorophore; (B) fluorescence image of standard fluorophore (120 μm \times 120 μm); the 532 nm excitation laser power density used here was 5.0 $\text{mW}\cdot\text{cm}^{-2}$ with 1.0 second integration time. A unique region of the sample has been highlighted in both images as a reference marker.

5.6 Results and Discussion

An AFM topography image of a polymerized sample is shown in Figure 5-9(A). As reported in previous chapters, the appearance of tall features is evidence of photopolymerization of PCDA. As noted above, red phase PDA and blue phase PDA are the two main phases reported¹¹⁻¹⁴. The difference between these two is the ability of the red phase to emit fluorescence upon excitation. In Figure 5-9(C) the simultaneous fluorescence image of the spot shown in Figure 5-9(A) is presented. The red phase PDAs appear as bright spots on the image. Comparing the fluorescence features with the AFM topography image reveals differences between the two. In this experiment, the 532 nm laser beam was used as an illumination source to photopolymerize the sample as well as an excitation source for generating fluorescence. During these experiments, a significant challenge was noticed. In order to polymerize the sample with the laser beam, the

power needed to be kept high ($5.0 \text{ mW}\cdot\text{cm}^{-2}$). However, the high power density that was needed for polymerization caused the cantilever to heat up and the temperature was high enough to melt and permanently bend the cantilever. This resulted in a gradual increase in imaging noise, followed by a sudden disappearance of the AFM feedback laser signal on the AFM detector and finally, a complete loss of the AFM image. AFM cantilever deformation was clearly visible through the microscope eyepiece, and damage was irreversible. The issue was addressed by placing a small piece of aluminum foil between the AFM tip and the sample during photopolymerization to block the strong radiation of the laser reaching the cantilever. For FM imaging, a lower laser power was used ($0.5 \text{ mW}\cdot\text{cm}^{-2}$), which was strong enough to excite the sample and produce easily detectable fluorescence, but not to damage the AFM tip. This resulted in some limitations to the experiment; we are unable to dynamically image the photopolymerization process, but were rather restricted to measuring “snapshots” of the sample after high-power illumination.

Similar experiments were carried out using a UV-pen lamp (254 nm light) as a source of irradiation. The UV lamp was suspended approximately 5 cm above the sample, and illuminated the sample for a period of ~30 seconds. After illumination, the sample was placed in the microscope setup for imaging. For fluorescence excitation light, the green 532 nm laser was used.

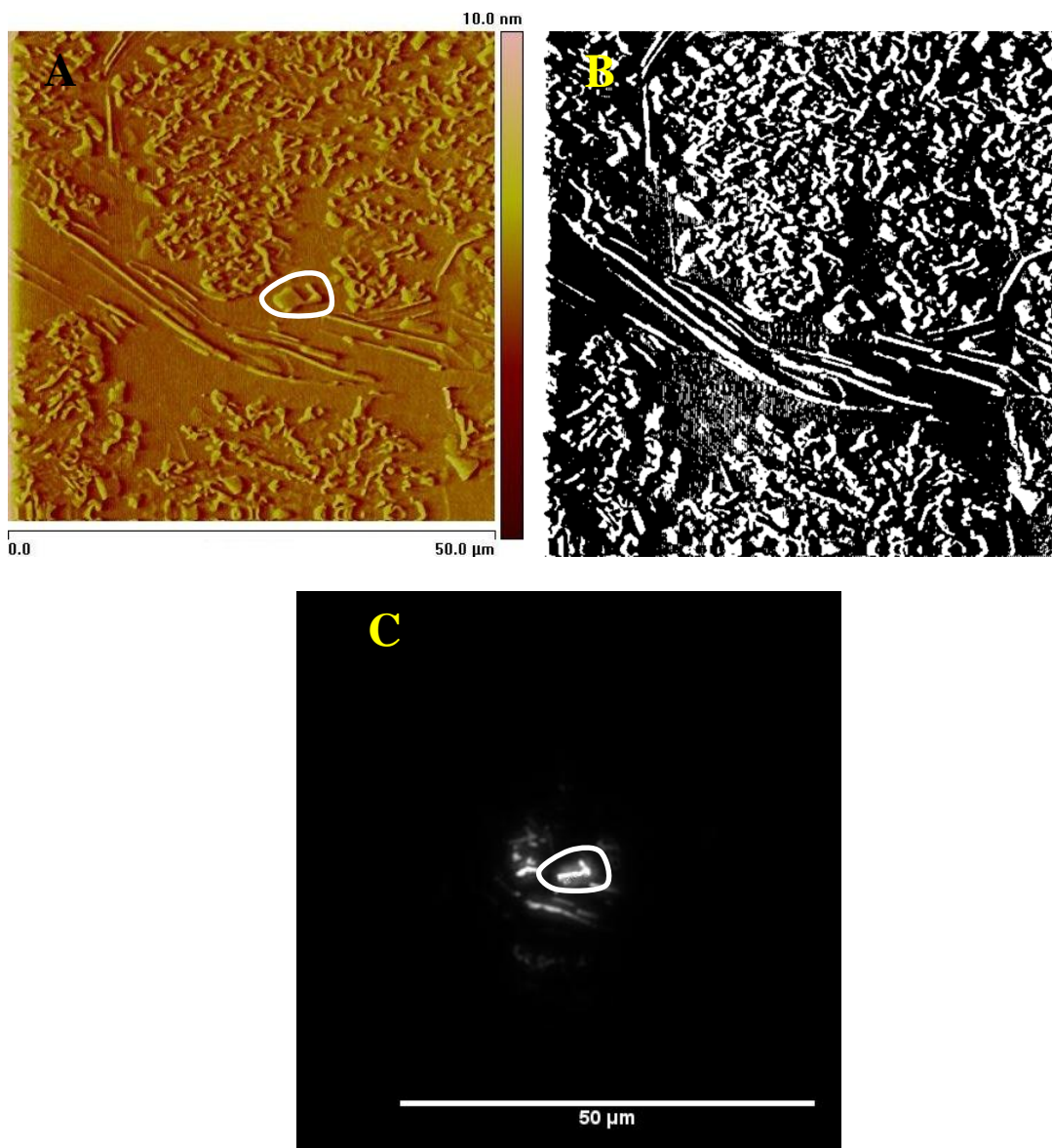


Figure 5-9. AFM image (A) and (B) is the binary image reproduced by ImageJ software from the AFM image (A) for ease of image analysis and (C) is the fluorescence image of 2:1 PF:PCDA film; Laser light $\lambda=532$ nm induced polymerization. (A) and (C) were collected simultaneously using combined microscope.

The combined images were analyzed to determine the extent of sample polymerization and the relative fraction of red versus blue phase. Using the software “ImageJ”¹⁵ the AFM images were converted into binary images (an example can be found in Figure 5-9(B)) and subjected to further analysis. A selected area of interest in the fluorescence image was superimposed on the AFM binary image and subjected to the same analysis. In this analysis, a histogram of pixel values was calculated for the selected area. The histograms were then background corrected and finally the pixels with positive values were assigned as PDA in the AFM images and red phase PDA in the corresponding fluorescence image. All illumination products, (blue and red PDA) appeared as tall features in the AFM images and when the AFM image was converted to their binary counterpart, they appeared as white pixels with a positive value whereas the positive pixel values in the fluorescence image only came from the red phase photopolymer. The difference between the number of pixels in the fluorescence image and the AFM image was taken to be the amount of polymer in the blue phase. A summary of the image analysis of both types of samples, those which were polymerized by the 532 nm green laser beam and those polymerized by the UV-pen lamp with effective 254 nm wavelength are presented in Table 5-1.

Table 5-1. Summary of results collected from photopolymerization of 2:1 PF:PCDA sample with two different light sources.

2:1 PF:PCDA	Green laser (532 nm)	UV pen lamp (254 nm)
Power density ($mW.cm^{-2}$)	5.0	4.5
Illumination time (sec)	30	30
Polymerized area (%) [*]	32	32
Blue-Phase PDA (%) [†]	20 ± 4	18 ± 3
Red-Phase PDA (%) [†]	80 ± 4	82 ± 3

^{*}Calculated from AFM topography image, [†] Calculated from FM image difference with AFM image.

More than 10 images were analyzed to produce Table 5-1 for each set of illumination conditions. All other conditions of experiments were kept constant for each set of illumination conditions. The percentage area that was polymerized for both sets of conditions was approximately 32%, which is close to the PCDA percentage content in the mixture, 2:1 PF:PCDA, used to prepare the films. This indicates that almost all of the PCDAs were polymerized upon irradiation. In addition to this information, the coupled AFM-FM microscope also revealed that the product of illumination was primarily the red phase polymer though there was a sizable fraction (~ 20%) of the blue phase polymer.

The photopolymerization mechanism of PCDA has been studied extensively and is reviewed elsewhere¹⁶. It follows a radical mechanism initiated by light followed by a 1,4-addition. It is a topochemical reaction. The principles of topochemical reactions indicate that the monomer functional groups (reactive sites) must be at the right distance and optimum angle for the reaction to occur. The monomers are arranged in a stack so that one monomer unit can react with its two neighbors. In the case of PCDA, the optimum distance of 5.9Å and 45° orientation should be met for successful polymerization¹⁷. These parameters were met during sample

preparation and reported elsewhere^{18, 19}. Generally the illumination product is blue and upon application of an stimuli like mechanical stress, heat or chemical recognition²⁰, it turns red. The change in the polymer phase is associated with a twisting of the polymer backbone, and it has been shown that the polymer goes from fully conjugated system in its backbone (blue phase) to partially conjugated backbone (red phase)^{21, 22}. The difference between the samples that were used in this project and works by others in the field is that for our studies, pure PCDA wasn't used but rather a 2:1 mixture of PF:PCDA. It is believed that the presence of PF in the sample induces mechanical stress in the film. To re-iterate from Chapter 2 in Figure 2-2, where the isotherm of pure PCDA was compared with the isotherm of mixtures of PF and PCDA with different ratios, the mean molecular area of the film is decreased from mixing with PF. In the case of pure PCDA and 2:1 PF:PCDA mixture, there is a 1.0 Å² reduction in the overall MMA. As discussed, this reduction helps to stabilize the monolayer on the water and there is no need to add excess of divalent cations to the subphase.

However, as reported in Chapter 3, the addition of PF and compression on the trough also introduces mechanical stress into the film. We propose that the intrinsic mechanical stress that is in the film ultimately results in preferential formation of the red phase polymer upon illumination. Previous measurements described in Chapter 3 have illustrated the connection between film “buckling”, mechanical stress and photopolymerization, and mechanical stress (“mechanochromism”) in these systems is well known. This proposed source of selectivity was supported by additional experiments carried out under different illumination conditions, which failed to show substantial differences from those shown in Table 5-1. Other authors have reported production of blue phase with lower illumination source power and irradiation time^{21, 23}

in films that did not contain PF, which further suggests that the ability to produce blue product is related to intrinsic stress inside the film. We further note that mechanical stress from PF is not homogenous across the film. The result of this inhomogeneity yields the results summarized in Table 5-1.

Despite all of the previous attempts to run both microscopes simultaneously, only a small number of studies can be truly considered successful^{8, 9, 24-26}. In addition, in all of the previous reports on PCDA LB film photo-polymerization^{16, 20, 27-32}, no one has quantitatively determined the extent of polymerization of the film and selectivity of the process. It has been claimed that the films were polymerized and under different illumination conditions blue or red products were attained, but no quantitative discussion about how much monomer remained unpolymerized or to what extent the polymer product was in the blue (or red) phase. To the best of the author's knowledge, this is the first report of simultaneous AFM-FM imaging of PF:PCDA samples and also the first report in which the degree of selectivity of the polymerization process has been quantified.

In this project, AFM and fluorescence microscope were simultaneously operated without negatively compromising the functionality of either technique. Coupling these two microscopes has made the quantitative analysis of this photopolymerization process possible. A systematic study is still required to fully determine conditions to increase the degree of selectivity of photopolymerization over the 82% described here. However, the instrumental tools and procedures are now in place to allow measurement and quantification of the process.

5.7 Conclusions

The results collected using a combination of two microscopes are of particular importance in connection with the research results discussed in the previous manuscripts, as it allowed for correlation of structural and spectroscopic features in the PF:PCDA system. As discussed earlier, PCDA undergoes photopolymerization upon illumination and produce the blue phase or red phase polymer. To determine the relative amounts of these two phases, measurements that that allowed for collection of both the fluorescence image and the atomic force micrographs of the same region of the sample were performed. This approach, comprised of combined AFM and fluorescence imaging, provided *in situ* topographic images and fluorescence images of the sample. The correlation of topographic images provided by the AFM and spectroscopic measurements allowed for better understanding of the system after polymerization. The result of photopolymerization under the conditions explored was a combination of blue (non-fluorescent) product and red (fluorescent) product, with the majority of product existing in the red form. This was postulated to be the result of intrinsic mechanical stress inherent to the film, caused by mixing PCDA with PF and mechanical compression of the film, as detailed in a previous chapter.

5.8 Acknowledgments

Financial support for this research has been provided by the Natural Sciences and Engineering Research Council (NSERC) of Canada, the Canada Foundation for Innovation (CFI) and by the University of Saskatchewan.

5.9 References

1. Putman, C. A. J.; Hansma, H. G.; Gaub, H. E.; Hansma, P. K., Polymerized LB Films Imaged With A Combined Atomic Force Microscope Fluorescence Microscope. *Langmuir* **1992**, 8, (12), 3014-3019.
2. Binnig, G.; Quate, C. F.; Gerber, C., Atomic Force Microscope *Physical Review Letters* **1986**, 56, (9), 930-933.
3. Binnig, G.; Gerber, C.; Stoll, E.; Albrecht, T. R.; Quate, C. F., Atomic resolution with atomic force microscope. *Europhys. Lett.* **1987**, 3, (12), 1281-6.
4. Benitez Bribiesca, L., The role of the optic microscope in biomedical discoveries. *Revista Medica del Instituto Mexicano del Seguro Social* **2000**, 38, (1), 77-80.
5. Esposito, A.; Popleteeva, M.; Venkitaraman, A. R., Maximizing the Biochemical Resolving Power of Fluorescence Microscopy. *PLoS One* **2013**, 8, (10), 13.
6. Flores, S. M.; Toca-Herrera, J. L., The new future of scanning probe microscopy: Combining atomic force microscopy with other surface-sensitive techniques, optical and microscopy fluorescence techniques. *Nanoscale* **2009**, 1, (1), 40-49.
7. Gaiduk, A.; Kuhnemuth, R.; Antonik, M.; Seidel, C. A. M., Optical characteristics of atomic force microscopy tips for single-molecule fluorescence applications. *Chemphyschem* **2005**, 6, (5), 976-983.
8. Kassies, R.; Van der Werf, K. O.; Lenferink, A.; Hunter, C. N.; Olsen, J. D.; Subramaniam, V.; Otto, C., Combined AFM and confocal fluorescence microscope for applications in bio-nanotechnology. *Journal of Microscopy-Oxford* **2005**, 217, 109-116.

9. Madl, J.; Rhode, S.; Stangl, H.; Stockinger, H.; Hinterdorfer, P.; Schutz, G. J.; Kada, G., A combined optical and atomic force microscope for live cell investigations. *Ultramicroscopy* **2006**, 106, (8-9), 645-651.
10. Goettgens, B. M.; Tillmann, R. W.; Radmacher, M.; Gaub, H. E., Molecular Order In Polymerizable Langmuir-Blodgett Films Probed By Microfluorescence And Scanning Force Microscopy. *Langmuir* **1992**, 8, (7), 1768-1774.
11. Menzel, H.; Horstmann, S.; Mowery, M. D.; Cai, M.; Evans, C. E., Diacetylene polymerization in self-assembled monolayers: influence of the odd/even nature of the methylene spacer. *Polymer* **2000**, 41, (22), 8113-8119.
12. Lio, A.; Reichert, A.; Ahn, D. J.; Nagy, J. O.; Salmeron, M.; Charych, D. H., Molecular imaging of thermochromic carbohydrate-modified polydiacetylene thin films. *Langmuir* **1997**, 13, (24), 6524-6532.
13. Carpick, R. W.; Sasaki, D. Y.; Marcus, M. S.; Eriksson, M. A.; Burns, A. R., Polydiacetylene films: a review of recent investigations into chromogenic transitions and nanomechanical properties. *Journal of Physics: Condensed Matter* **2004**, 16, R679-R697.
14. Reichert, A.; Nagy, J. O.; Spevak, W.; Charych, D., Polydiacetylene Liposomes Functionalized With Sialic-Acid Bind And Colorimetrically Detect Influenza-Virus. *Journal of the American Chemical Society* **1995**, 117, (2), 829-830.
15. Rasband, W. S. *ImageJ*, 1.37v; U.S. National Institute of Health: Bethesda, Maryland, USA, 1997-2005.
16. Enkelmann, V., Structural aspects of the topochemical polymerization of diacetylenes. *Advances in Polymer Science* **1984**, 63, (Polydiacetylenes), 91-136.

17. Ogawa, K.; Tamura, H.; Hatada, M.; Ishihara, T., Study of Photoreaction Processes of PDA Langmuir Films. *Langmuir* **1988**, 4, (4), 903-906.
18. Younesi Araghi, H.; Paige, M. F., Deposition and photopolymerization of phase-separated perfluorotetradecanoic acid-10,12-pentacosadiynoic acid Langmuir-Blodgett monolayer films. *Langmuir* **2011**, 27, (17), 10657-10665.
19. Younesi Araghi, H.; Paige, M. F., The effect of perfluorotetradecanoic acid on the structure of photopolymerized 10,12-pentacosadiynoic acid films at the air-water interface. *Canadian Journal of Chemistry-Revue Canadienne De Chimie* **2013**, 91, (11), 1130-1138.
20. Ahn, D. J.; Kim, J. M., Fluorogenic polydiacetylene supramolecules: Immobilization, micropatterning, and application to label-free chemosensors. *Accounts of Chemical Research* **2008**, 41, (7), 805-816.
21. Carpick, R. W.; Sasaki, D. Y.; Burns, A. R., First observation of mechanochromism at the nanometer scale. *Langmuir* **2000**, 16, (3), 1270-1278.
22. Pingsheng, H.; Huililn, Z.; Gang, Z., Polymerization kinetics of 10,12-pentacosadiynoic acid monolayer and possible acceleration effect of visible light. *Polymer* **2003**, 44, (11), 3235-3241.
23. Sasaki, D. Y.; Carpick, R. W.; Burns, A. R., High molecular orientation in mono- and trilayer polydiacetylene films imaged by atomic force microscopy. *Journal of Colloid and Interface Science* **2000**, 229, (2), 490-496.
24. Kim, J. M.; Ohtani, T.; Sugiyama, S.; Hirose, T.; Muramatsu, H., Simultaneous topographic and fluorescence imaging of single DNA molecules for DNA analysis with a

scanning near-field optical/atomic force microscope. *Analytical Chemistry* **2001**, 73, (24), 5984-5991.

25. Fukuda, S.; Uchihashi, T.; Iino, R.; Okazaki, Y.; Yoshida, M.; Igarashi, K.; Ando, T., High-speed atomic force microscope combined with single-molecule fluorescence microscope. *Review of Scientific Instruments* **2013**, 84, (7), 8.

26. Hards, A.; Zhou, C. Q.; Seitz, M.; Brauchle, C.; Zumbusch, A., Simultaneous AFM manipulation and fluorescence imaging of single DNA strands. *Chemphyschem* **2005**, 6, (3), 534-540.

27. Okada, S.; Peng, S.; Spevak, W.; Charych, D., Color and chromism of polydiacetylene vesicles. *Accounts of Chemical Research* **1998**, 31, (5), 229-239.

28. Hofmann, U. G.; Peltonen, J., Color transitions in monolayers of a polymerizable single-chain diacetylenic lipid. *Langmuir* **2001**, 17, (5), 1518-1524.

29. Ahn, D. J.; Chae, E. H.; Lee, G. S.; Shim, H. Y.; Chang, T. E.; Ahn, K. D.; Kim, J. M., Colorimetric reversibility of polydiacetylene supramolecules having enhanced hydrogen-bonding under thermal and pH stimuli. *Journal of the American Chemical Society* **2003**, 125, (30), 8976-8977.

30. Charych, D. H.; Nagy, J. O.; Spevak, W.; Bednarski, M. D., Direct Colorimetric Detection Of A Receptor-ligand Interaction By A Polymerized Bilayer Assembly. *Science* **1993**, 261, (5121), 585-588.

31. Kim, J. M.; Lee, Y. B.; Yang, D. H.; Lee, J. S.; Lee, G. S.; Ahn, D. J., A polydiacetylene-based fluorescent sensor chip. *Journal of the American Chemical Society* **2005**, 127, (50), 17580-17581.

32. Huilin, Z.; Weixing, L.; Shufang, Y.; Pingsheng, H., Polymerization of 10,12-pentacosadiynoic acid monolayer at varying surface pressure and temperature. *Langmuir* **2000**, 16, (6), 2797-2801.

6 CHAPTER 6: DISCUSSION, CONCLUSIONS AND FUTURE WORK

6.1 Discussion

Significant progress in the field of photopolymerizable surfactant films has been reported in this thesis to clarify the relationships that exist between film structure, mechanical properties and spectroscopic properties.

An important accomplishment of this thesis work is demonstrating that structures of PCDA films can be manipulated through phase-separation with PF. Previous works in the literature have shown that the interaction between perfluorinated and hydrogenated surfactants can be exploited for patterning two dimensional structures with a high level of control ¹, and we have demonstrated that this approach can be extended to the photopolymerizable systems. Further, this thesis has demonstrated that some degree of control over the spectroscopic properties of the photopolymer can be obtained by using these approaches.

In the first study² (Chapter 2), the interaction between a perfluorinated fatty acid PF and a diacetylene molecule PCDA was explored in Langmuir monolayers and LB films to understand the interfacial behavior of the mixed film components. This research was important in order to understand the elementary interactions between the surfactant pairs and to establish a basis for future research, as it may ultimately enable control of the surface patterns in perfluorinated carboxylic acid- pentacosadiynoic acid mixed films. The collected data were reproducible and were in good agreement with previously reported measurements of PCDA. Carpick³ et al reported that addition of Cd²⁺ to the subphase helped with PCDA monolayer stabilization. One of

the major findings in this thesis was that the head group attractive interaction between PCDA and PF provided significant film stabilization without further divalent cation addition to subphase or before UV-illumination which lead to polymerization of PCDA. The pure *Millipore* water used as a subphase at 22.5 °C has pH=5.5 which makes PF deprotonated and keeps PCDA protonated. This initial work established both the importance and benefit of using PF for controlling photopolymer film structure and mechanical properties.

To our knowledge, this is the first reported example of forming mechanically stable, structured PCDA LB films on pure water, and this was a novel, important accomplishment in light of related systems in the literature.

Although the interfacial behavior of hydrocarbon-fluorocarbon mixed monolayer films have been widely studied, further research in this area is necessary because none of these studies could explain the appearance of unique features after laser-light induced polymerization. Tomioka⁴ has reported highly-oriented PDA polymer formation that was prepared at the air/water interface. The packing of conjugated polymer backbone in the direction of film compression in Langmuir trough was considered as a driving force for polymer orientation. In our view, the latter effect is of significant potential value for patterning in mixed PF-PCDA films because of the increased stability and rigidity of the mixed films over pure PCDA films alone. Therefore, measurements with higher portion of PCDA in PF: PCDA mixtures were carried out in Chapter 3⁵ to collect information on basic thermodynamics, structural and performance properties of mixed PF-PCDA monolayers. It was found that the orientation of the photopolymer product in these samples was due to buckling, with the underlying driving force for these effects being the stabilizing PF-PCDA interaction, the rigidity of the resulting photopolymer and the

applied compressive stress in the Langmuir trough. The simplicity of the method suggests significant potential in these systems for patterning films, and the important relationship between mechanical properties of films and their structure has been elaborated.

As shown in the previous studies, the mixed surfactant monolayers provided a simple model system to investigate interfacial behavior of PF-PCDA and helped to provide a better understanding of photopolymerization in these systems. Upon photopolymerization in 2D, it was found that the film undergoes buckling and oriented polymer ribbons (strands) formed, suggesting a potential approach for patterning organic films. Chapter 4⁶ introduced a simple technique to pattern PCDA through the use of phase-separation with a perfluorinated surfactant, followed by deposition onto solid substrates via Langmuir-Blodgett techniques. The main purpose of Chapter 4 was to compare the effect of deposition process on the morphology of phase-separated monolayer films of PF-PCDA at the solid/air and water/air interfaces using AFM and BAM measurements and quantitatively measure the orientation of the polymer strands. The fluorescence emission of the resulting photopolymer films was significantly polarized, with the polarization resulting from the preferred orientation of the fibers. This polarization dependence can be extracted through both bulk anisotropy measurements as well as through selective polarized imaging of individual fibers⁶. It should be noted that the degree of PCDA film orientation that could be achieved using the phase-separation approach was mediocre in compare to the work previously reported by Baek⁷. It is worth putting greater effort into developing this technique and improving the resulting product in regard to a better alignment as this approach offers fast, easy and reliable means of film preparation.

The novel accomplishment in this part of the thesis is that an important and simple approach for patterning photopolymer has been devised. The LB technique for patterning has been expanded into the area of an important technological material by depositing a mixture of 2:1 PF:PCDA on micro cover glass slide.

In the last study of this thesis (Chapter 5), the impact of PF on the phase behavior of PCDA and its photopolymerization behavior was characterized. This is of particular importance in connection with the research results discussed in the previous manuscripts, as it allowed for correlation of structural and spectroscopic features in this system. As discussed earlier, PCDA undergoes photopolymerization upon illumination and produce the blue phase or red phase polymer. To collect an informative data on this matter a sets of measurement that allows collecting both the fluorescence image and the atomic force micrographs of the same spot in the sample was configured. This technique comprised AFM and fluorescence microscope provided *in situ* topographic image and fluorescence image of the sample. The correlation of topographic image provided by the AFM and spectroscopic measurements allowed for better understanding of the system after polymerization. It was clear the result of photopolymerization under the conditions explored was a combination of blue (non-fluorescent) product and red (fluorescent) with the majority of product being in the red form. It explains PCDA monomers surrounding condition is not homogeneous throughout the sample. The surprising result was that photoillumination produced both forms of polymer and although the red phase polymer was the major product, the blue product was also produced and the approach was not 100% selective for the red form. The unique approach that has been developed here provides a useful and

straightforward approach for measuring the extent of film polymerization, which can be used in the future to help optimize conditions for selective polymerization.

This work is important because it is the first time anyone has measured and quantified the relative amounts of polymer in these systems. This will allow us to optimize conditions to improve selectivity for the red polymer, which in turn, will lead to biosensors that give larger signals and are therefore more sensitive.

6.2 Future Work

It is important to understand the physical characteristics of mixed PCDA-hydrogenated surfactants monolayers in order to tailor the structure, composition and mechanical properties of surfactant films at the solid/air and liquid/air interfaces. This will help in accomplishing an ultimate goal of patterning PCDA films for applications of interest. To attain this goal, it is necessary to screen a wide range of simple fatty acids and fluorinated surfactants. I suggest to explore the impact of a series of longer PF molecules (for instance $C_n = 16$ and 18) on the interfacial behavior of PCDA monolayers. They (longer C chain PF) are anticipated to obey the general demixing properties with hydrocarbons (PCDA)^{1, 8-10}. Generally, it is proposed to carry out a systematic study and explore a wide range of different fluorinated surfactant mixed with PCDA. It might be possible to establish a general set of rules which dictate when a system will phase-separate, and what patterns it will form. On the other hand, simple fatty acid such as arachidic acid¹¹ ($C_{19}H_{39}COOH$) mixing with PCDA is predicted to be a miscible system (both have hydrocarbon tail with carboxylic head) and the result film expected to reveal interesting information on film structure and mechanical properties and particularly the photopolymerisation behavior.

Organic photovoltaic solar cells based on conjugated polymers have been reported in the literature^{12, 13}. The conductivity of un-doped PDA thin films is estimated to be around 5×10^{-6} S/cm¹⁴ which is in the range of semiconductors like Ge or Si and much larger than polypyrrole, making it a potentially useful material for these applications¹⁴. Because of this, it is important to collect information regarding the conductivity of the PDAs in thin films. It is proposed that the methods of PDA film preparation used in this thesis be explored from the perspective of conductivity. Blue phase of PDA is conductive¹⁵ as it was predicted from the planar and long fully conjugated backbone rather than short and twisted back bone in red phase. On this basis, it is proposed to use double tip scanning tunneling microscopy¹⁵ to prepare a conductivity map of sample, which in turn would allow determination of the phase distribution (blue/ red) of PDA throughout the sample upon polymerization.

Having produced two phases of PDAs (red and/or blue) under the conditions described in this thesis, another valuable accomplishment would be to improve the control over polymerization to selectively produce one phase of PDA^{3, 16}. As seen in the Chapter 5 through the polymerization of mixed PF: PCDA, the majority of the product is red, but a substantial fraction of blue polymer is also being produced. Considering the applications of PDAs, it is important to have a better control over the selectivity of method applied for polymerization to get better yield of desired phase of PDA. It is recommended to study the effect of different types of fatty acids, subphase pH and condition of polymerization such as different source of irradiation effect and to investigate how these factors contribute to phase selectivity.

6.3 References

1. Nakahara, H.; Shibata, O., Langmuir monolayer miscibility of perfluorocarboxylic acids with biomembrane constituents at the air-water interface. *Journal of Oleo Science* **2012**, 61, (4), 197-210.
2. Younesi Araghi, H.; Paige, M. F., Deposition and photopolymerization of phase-separated perfluorotetradecanoic acid-10,12-pentacosadiynoic acid Langmuir-Blodgett monolayer films. *Langmuir* **2011**, 27, (17), 10657-10665.
3. Carpick, R. W.; Sasaki, D. Y.; Marcus, M. S.; Eriksson, M. A.; Burns, A. R., Polydiacetylene films: a review of recent investigations into chromogenic transitions and nanomechanical properties. *Journal of Physics: Condensed Matter* **2004**, 16, R679-R697.
4. Tomioka, Y.; Imazeki, S.; Tanaka, N., Highly oriented polydiacetylene monolayer formed at the air-water interface. *Chemical Physics Letters* **1990**, 174, (5), 433-437.
5. Younesi Araghi, H.; Paige, M. F., The effect of perfluorotetradecanoic acid on the structure of photopolymerized 10,12-pentacosadiynoic acid films at the air-water interface. *Canadian Journal of Chemistry-Revue Canadienne De Chimie* **2013**, 91, (11), 1130-1138.
6. Younesi Araghi, H.; Giri, N.; Paige, M. F., Polarized fluorescence microscopy analysis of patterned, polymerized perfluorotetradecanoic acid-pentacosadiynoic acid thin films. *Spectrochimica Acta Part A: Molecular and Biomolecular Spectroscopy* **2014**, 129, 339-344.
7. Baek, J. H.; Ahn, H.; Yoon, J.; Kim, J.-M., Micro-patterning of polydiacetylene supramolecules using micromolding in capillaries (MIMIC). *Macromolecular Rapid Communications* **2008**, 29, 117-122.

8. Qaqish, S. E.; Paige, M. F., Rippled domain formation in phase-separated mixed Langmuir-Blodgett films. *Langmuir* **2008**, 24, (12), 6146-6153.
9. Nakahara, H.; Lee, S.; Krafft, M. P.; Shibata, O., Fluorocarbon-hybrid pulmonary surfactants for replacement therapy - A Langmuir monolayer study. *Langmuir* **2010**, 26, (23), 18256-18265.
10. Nakahara, H.; Tsuji, M.; Sato, Y.; Krafft, M. P.; Shibata, O., Langmuir monolayer miscibility of single-chain partially fluorinated amphiphiles with tetradecanoic acid. *Journal of Colloid and Interface Science* **2009**, 337, (1), 201-210.
11. Qaqish, S. E.; Paige, M. F., Characterization of domain growth kinetics in a mixed perfluorocarbon-hydrocarbon Langmuir-Blodgett monolayer. *Journal of Colloid and Interface Science* **2008**, 325, (1), 290-293.
12. Strein, E.; deQuilettes, D. W.; Hsieh, S. T.; Colbert, A. E.; Ginger, D. S., Hot Hole Transfer Increasing Polaron Yields in Hybrid Conjugated Polymer/PbS Blends. *Journal of Physical Chemistry Letters* **2013**, 5, (1), 208-211.
13. Knesting, K. M.; Ju, H. X.; Schlenker, C. W.; Giordano, A. J.; Garcia, A.; Smith, O. L.; Olson, D. C.; Marder, S. R.; Ginger, D. S., ITO Interface Modifiers Can Improve V-OC in Polymer Solar Cells and Suppress Surface Recombination. *Journal of Physical Chemistry Letters* **2013**, 4, (23), 4038-4044.
14. Day, D. R.; Lando, J. B., Conduction In Polydiacetylene Bilayers. *Journal of Applied Polymer Science* **1981**, 26, (5), 1605-1612.

15. Takami, K.; Mizuno, J.; Akai-Kasaya, M.; Saito, A.; Aono, M.; Kuwahara, Y., Conductivity measurement of polydiacetylene thin films by double-tip scanning tunneling microscopy. *Journal of Physical Chemistry B* **2004**, 108, (42), 16353-16356.
16. Tachibana, H.; Yamanaka, Y.; Sakai, H.; Abe, M.; Matsumoto, M., In situ AFM study on the morphological change of the Langmuir-Blodgett film of cadmium 10,12-pentacosadiynoate during polymerization. *Langmuir* **2000**, 16, (6), 2975-2977.